HIGH-QUALITY SCREENING BY CAPILLARY ELECTROPHORESIS

New Advances in High-quality Screening by Capillary Electrophoresis: A Unified

Platform for Thermodynamic and Kinetic Characterization of Protein-Small

Molecule Interactions

By

JENNILEE M. A. GAVINA, B.Sc.Honours

A Thesis

Submitted to the School of Graduate Studies

In Partial Fulfillment of the Requirements

for the Degree

Doctorate of Philosophy

McMaster University

DOCTORATE OF PHILOSOPHY (2009)   McMaster University

(Chemistry and Chemical Biology)   Hamilton, Ontario

TITLE: New Advances in High-quality Screening by Capillary

Electrophoresis: A Unified Platform for Thermodynamic and

Kinetic Characterization of Protein-Small Molecule Interactions

AUTHOR: Jennilee M.A. Gavina, B.Sc.Honours (University of Winnipeg)

SUPERVISOR: Dr. Philip Britz-McKibbin

NUMBER OF PAGES: xxxii, 206

Abstract

The development of high-quality screening assays for the identification of biologically active ligands is critical in drug discovery. This thesis is aimed at developing new advances in capillary electrophoresis (CE) for the characterization of the conformational stability and enzymatic activity of protein targets with small molecules. CE provides a convenient platform for unbiased assessment of multiple thermodynamic and kinetic parameters associated with biomolecular interactions involving regulatory protein or isomerase enzymes, where various sample pretreatment steps can be integrated directly in-capillary during analysis. The first two chapters of the thesis (**Chapters II, III**) outline the development of dynamic ligand exchange-affinity capillary electrophoresis (DLE-ACE) as a novel strategy for the screening of allosteric ligands based on the differential stability of urea-induced unfolding of various *apo/holo*-protein states of cAMP receptor protein constructs. This work introduced a label-free and multivariate approach for ligand selection based on complementary thermodynamic parameters that allowed for determination of the dissociation constant of protein-ligand interactions over a wide dynamic range ($> 10^4$, $K_d \approx$ nM-mM). The subsequent two chapters of the thesis (**Chapters IV, V**) describe the development of a novel kinetic assay for unbiased characterization of isomerase activity associated with *D/L*-amino acid metabolism using hydroxyproline epimerase as a model system. Stereoselective resolution of various hydroxyproline isomers was accomplished via *off-line* or *on-line* chemical

derivatization with dynamic complexation using chiral selector(s) in order to screen potential inhibitors for putative epimerase and racemase activity. The integration of both thermodynamic and kinetic strategies for differentiation of mutant from wild-type enzymes was important for revealing the function of a catalytic acid/base cysteine pair in the epimerase active site. Overall, this thesis outlines an integrative framework based on CE for high-quality screening, which is relevant in reducing the high attrition rate of lead candidates in drug development.

v

Acknowledgements

The work embodied in this thesis would never have been possible without the support of many people. I would like to first acknowledge my supervisor, Dr. Philip Britz-McKibbin, for his guidance and support during the course of this thesis. I am thankful for the opportunity to learn and grow under his tutelage and for his boundless optimism, "chemical intuition" and faith – in both the research and myself. I would like to thank present (Meera Shanmuganathan, Naomi Janson, Lisa D'Agostino) and past (Adam Ptolemy, Richard Lee, Kenneth Chalcraft, Giselle Segui-Lines, Solenne Despax, Elyse Bernard, Jason D'Amaral, Claire Kaiser) for their assistance and friendship over the years. I also gratefully acknowledge my PhD Advisory Committee Members, Dr. Guiseppe Melacini and Dr. Yingfu Li, for their guidance and support. I am thankful to my collaborators; Dr. Melacini, Dr. Rahul Das, Mohammad Mazhab-Jarafi; Dr. Turlough Finan and Dr. Catharine White for their contributions aiding in the scientific advancements achieved in this thesis. NSERC is thanked for financial support.

Last, but not least, I would like to thank family and friends (too many to mention by name) for their patience and support during my time at McMaster University. Most of all, I thank my husband, Erik, for faithfully supporting me through both the high and the low times. It has been said that, *"No man is an island."* (John Donne, 1624) Thus I am grateful each and every one of you for your assistance. Thank you.

The following material has been previously published and is reprinted with written permission:

Chapter I:

-Reprinted in part from: *CAC*, **3**, J. M. A. Gavina and P. Britz-McKibbin, *Protein Unfolding and Conformational Studies by Capillary Electrophoresis*, 17-31. Copyright (2007) with permission from Bentham Science Publishers.

Chapter II:

-Reprinted from: *Electrophoresis*, **27**, Gavina, J. M. A., Das, R. and P. Britz-McKibbin, *Dynamic unfolding of a regulatory subunit of cAMP-dependent protein kinase by capillary electrophoresis: Impact of cAMP dissociation on protein stability*, 4196-4204. Copyright (2006) with permission from Wiley InterScience.

Chapter III:

-Reprinted from: *Biochemistry*, **48**, Gavina, J. M. A, Mazhab-Jafari, M. T. and P. Britz-McKibbin, *Label-Free Assay for Thermodynamic Analysis of Protein-Ligand Interactions: A Multivariate Strategy for Allosteric Ligand Screening*, 223-225. Copyright (2009) with permission from the American Chemical Society.

Chapter IV:

-Reprinted from: submitted work, *The Analyst,* Gavina, J. M. A., White, C. E., Finan, T. M., and P. Britz-McKibbin, *A Stereoselective Platform for Kinetic Studies of Isomerase Enzymes: Evaluation of 4-Hydroxyproline-2-Epimerase Activity by Capillary Electrophoresis.*

Statement of Contribution

The previously published material within this thesis contains multiple authored work. The following contributions are acknowledged:

Chapter II:

R. Das and G. Melacini are credited for preparation and purification of the RIα-APK construct. The use of this construct is by permission of S.S. Taylor. Mass spectrometry was performed with the assistance of R. Lee. The author contributed all experimental other procedures and data analysis. The author assisted P. Britz-McKibbin in preparation of the manuscript.

Chapter III:

M. Mazhab-Jafari and G. Melacini are credited for preparation and purification of the Epac construct. The author contributed all other experimental procedures and data analysis. The author assisted P. Britz-McKibbin in preparation of the manuscript.

Chapter IV:

C. E. White and T. M. Finan are credited for preparation and purification of the HyPRE enzyme. The plasmid containing the gene for HyPRE expression was kindly donated by P. Minoprio. C. E. White is acknowledged for performing the off-line enzyme assays used for data analysis as well as for previous work

determining optimum buffer composition and pH for activity. The author contributed preliminary enzyme assays for optimization of enzyme and substrate concentrations as well as protocol for derivatization. All other experimental procedures and data analysis where contributed by the author. The author assisted P. Britz-McKibbin in preparation of the manuscript.

Chapter V:

C. E. White and T. M. Finan are credited for preparation and purification of the HyPRE enzymes. The plasmid containing the gene for HyPRE expression was kindly donated by P. Minoprio. The *S. meliloti* mutants were made by C. E. White who is also acknowledged for performing the off-line enzyme assays used for data analysis. The author contributed preliminary enzyme assays for optimization of enzyme and substrate concentrations as well as protocol for derivatization. All other experimental procedures and data analysis where contributed by the author.

Table of Contents

I. Introduction to Separation Science and Characterization of Biomolecule Interactions by Capillary Electrophoresis

II. Dynamic unfolding of a regulatory subunit of cAMP-dependent protein kinase by capillary electrophoresis: Impact of cAMP dissociation on protein stability

III. Label-free Assay for Thermodynamic Analysis of Protein-Ligand Interactions: A Multivariate Strategy for Allosteric Ligand Screening

List of Figures and Schemes

List of Tables

List of Abbreviations

α	Selectivity Factor
β-ME	β-Mercaptoethanol
ΔG	Gibbs Free Energy
ΔG_U^0	Standard Free Energy of Unfolding
ε	Dielectric Constant
η	Viscosity
μ_{eo}	Electroosmotic Mobility
μ_{ep}	Electrophoretic Mobility
$\mu_{ep,}^{A}$	Apparent Electrophoretic Mobility
$\mu_{ep,AC}$	Complexed Electrophoretic Mobility
v	Viscosity Correction Factor
σ^2	Variation
ζ	Zeta Potential
3-*L*-Hyp	*Trans*-3-Hydroxy-*L*-Proline
4-*D*-Hyp	*Cis*-4-Hydroxy-*D*-Proline
4-*L*-Hyp	*Trans*-4-Hydroxy-*L*-Proline
8-Br-cAMP	8-Bromo Adenosine 3′,5′-Cyclic Monophosphate

8-pCPT-2-OMe-cAMP	8-(*para*-Chlorophenylthio)-2′-O-Methyladenosine 3′,5′-Cyclic Monophosphate
8-pCPT-cAMP	8-(*para*-Chlorophenylthio)adenosine 3′,5′-Cyclic Monophosphate
A	Adenosine
ACN	Acetonitrile
ACE	Affinity Capillary Electrophoresis
AcP	Acylphosphatase
ADME	Adsorption, Distribution, Metabolism, Excretion
Ala	Alanine
AMP	Adenosine Monophosphate
Asp	Asparagine
β-CD	Beta-Cyclodextrin
β-GC	β-Glucoceramidase
BGE	Background Electrolyte
cAMP	Cyclic Adenosine Monophosphate
cAPK	Cyclic Adenosine Monophosphate Dependent Protein Kinase A

CD	Cyclodextrin
CE	Capillary Electrophoresis
CEC	Capillary Electrchromatography
CGE	Capillary Gel Electrophoresis
cGMP	Guanosine $3',5'$-Cyclic Monophosphate
CHES	N-Cyclohexyl-2-Aminoethanesulfonic Acid
CIEF	Capillary Isoelectric Focusing
cIMP	Inosine $3',5'$-Cyclic Monophosphate
C_M	Concentration at Midpoint of Denaturation
cmc	Critical Micelle Concentration
cNT	Cyclic Nucleotide
Cp	Heat Capacity
CTAB	Cetyl Trimethylammonium Bromide
CV	Coefficient of Variation
CYP	Cytochrome P450
Cys	Cysteine
cyt. c	Cytochrome C
CZE	Capillary Zone Electrophoresis

D	Diffusion Constant
DAP	Diaminopimelic Acid
DLE-ACE	Dynamic Ligand Exchange-Affinity Capillary Electrophoresis
DTAB	Dodecyltrimethylammonium Bromide
DTT	Dithiothreitol
E	Electric Field
E	Enzyme
EDTA	Ethylenediaminetetraacetic Acid
EGTA	Ethylene glycol-bis(2-aminoethylether)-N,N,N`,N`-tetraacetic acid
ELISA	Enzyme-Linked Immunosorbant Assay
EMMA	Electrophoretically Mediated Microanalysis
EOF	Electroosmotic Flow
Epac	Exchange Protein Directly Activated by cAMP
ES	Enzyme-Substrate Complex
ESI	Electrospray Ionization
EtOH	Ethanol
F	Folded

F_{el}	Electric Force
F_f	Frictional Force
f_F	Fraction Folded
Fmoc-Cl	9-Fluoroenylmethyloxycarbonyl Chloride
f_U	Fraction Unfolded
GC	Gas Chromatogaphy
GdnHCl	Guanidine Hydrochloride
GE	Gel Electrophoresis
Glu	Glutamine
GPCR	G-protein Coupled Receptor
GTP	Guanidine Triphosphate
HCS	High Content Screening
HEPES	N-(2-Hydroxyethyl)piperazine-N'-2-ethanesulfonic acid
HTS	High Throughput Screening
HyPRE	Hydroxyproline-2-Epimerase
I	Inhibitor
IBMX	3-Isobutyl-1-Methylxanthine
IC50	Half-Maximal Inhibition Concentration

ID	Instrinsically Disordered Domain
IS	Internal Standard
ITP	Isotachophoresis
K	Partition Coefficient
$k^`$	Retention Factor
k_{cat}	Turnover Number
KCE	Kinetic Capillary Electrophoresis
KCl	Potassium Chloride
K_d	Dissociation Constant
KH_2PO_4	Potassium Phosphate Monobasic
K_M	Michaelis-Menten Constant
k_{off}	Off Rate (Rate of Dissociation)
K_U	Unfolding Constant
LB	Luria Bertani
LC	Liquid Chromatography
L_d	Length to Detector
LINF	Laser-Induced Native Fluorescence
L_t	Total Length

m	Cooperativity Coefficient
MEKC	Micellar Electrokinetic Chromatography
MeOH	Methanol
MES	Morpholineethanesulfonic Acid
MLR	Multilinear Regression
MS	Mass Spectrometry
μTAS	Micro Total Analysis System
N	Separation Efficiency
Na_2HPO_4	Sodium Phosphate Dibasic
NaCl	Sodium Chloride
NaN_3	Sodium Azide
NaOH	Sodium Hydroxide
NECEEM	Non-Equilibrium Capillary Electrophoresis of Equilibrium Mixtures
NH_2OH	Ethanolamine
NH_4Cl	Ammonium Chloride
NH_4CO_3	Ammonium Carbonate
$\nu\mu^A_{ep}$	Viscosity Corrected Apparent Electrophoretic Mobility

NMR	Nuclear Magnetic Resonance
P	Product
P5C	Pyrrolidone-5-Carboxylic Acid
Pa	*Pseudomonas aeruginosa*
PAO	Plasma Amine Oxidase
PCA	Principle Component Analysis
PEO	Polyethylene Oxide
pI	Isoelectric Point
PRAC	Proline Pacemase
Pro	Proline
PTE	Phosphotriesterase
PVP	Polyvinyl Pyrrolidone
PYC	Pyrrole 2-Carboxylic Acid
q	Charge
Q_{eff}	Effective Charge
R	Gas Constant
R_H	Radius, hydratred
RIα	Type Iα Regulatory Subunit

RNaseA	Ribonuclease A
Rp-cAMPS	Rp-Adenosine 3′,5′-Cyclic Monophosphorothioate
Rs	Resolution
S	Substrate
SC	Sodium Cholate
SDC	Sodium Deoxycholate
SDS	Sodium Dodecylsulfate
Ser	Serine
Sm	*Sinorhizobium meliloti*
Sp-cAMPS	Sp-Adenosine 3′,5′-Cyclic Monophosphorothioate
STC	Sodium Taurocholate
T	Temperature
t^A	Apparent Migration Time
TCEP	Tris(2-Carboxyethyl)phosphine Hydrochloride
TDC	Taurodeoxycholate
t_{eo}	Migration time of the Electroosomotic Flow
TLCK	1-Chloro-3-(Tosylamino)-7-Amino-L-2-Heptanone
TPCK	L-1-(Tosylamino)-2-Phenylethyl Chloromethyl Ketone

Tris-HCl	Tris(hydroxymethyl)aminomethane Hydrochloride
U	Unfolded
UV	Ultraviolet
v	Velocity
V	Voltage
V_0	Initial Velocity
V_{max}	Maximum Velocity
$W_{1/2}$	Width at Half Peak Height
wt	Wild-Type

Chapter I

Introduction to Separation Science and Characterization of Biomolecular

Interactions by Capillary Electrophoresis

I. Introduction to Separation Science and the Characterization of Biomolecular Interactions by Capillary Electrophoresis

1.1. Capillary Electrophoresis in Bioanalysis

Capillary electrophoresis (CE) is a high efficiency microseparation technique used for the resolution of complex mixtures of ions that is increasingly being recognized as a versatile biophysical technique for the characterization of non-covalent interactions in free solution. For instance, affinity CE (ACE)[1-3] and kinetic CE (KCE)[4] represent two useful methods for the determination of thermodynamic and kinetic parameters associated with biomolecular interactions, such as receptor-ligand binding. In addition, new methods have recently been developed in CE to probe ligand interactions involving groups of cells,[5] single cells,[6, 7] as well as sub-cellular organelles.[8] The ability to tune the electromigration behaviour of various classes of charged solutes (*e.g.,* metals, metabolites, protein, cells *etc.*) using small amounts of sample (< 10 nL) in complex sample matrices, renders CE a useful platform for drug screening. High-throughput screening (HTS) of biomolecular interactions can also be realized by CE when using multiplexed capillary array instruments, which is a format widely used in DNA sequencing.[9] In addition, CE provides a convenient format for integration of several time-consuming *off-line* sample pre-treatment steps during analysis, such as desalting, chemical derivatization and protein preparation. In fact, techniques for HTS rarely address the many "front-end" labour-intensive

protein preparative steps that are often a major bottleneck in drug screening. Moreover, recent evidence suggests that despite increasing investment in HTS technologies, a large fraction of putative ligand "hits" identified as potential lead drugs often fail at later stages of clinical trials, which is extremely inefficient and costly.[10] Future analytical platforms that provide quality high-content screening (HCS)[11] benefits, in terms of functionally relevant information that link *in-vitro* ligand binding with *in-vivo* protein activity, are highly desired to reduce late-stage attrition rates common with conventional primary screening assays. Also, new methods that utilize label-free strategies that minimize the extent of sample work-up while allowing for the characterization of impure or partially fractionated protein samples are urgently needed. New advances in separation-based techniques that can thus provide multiple thermodynamic and kinetic parameters for characterizing biomolecular interactions are required for improving the quality of candidate selection during primary screening, such as orthosteric or allosteric modulators of protein activity.[12, 13]

The separation of a sample mixture into discrete analyte zones represents a significant challenge when analyzing complex biological samples and/or solutes possessing similar intrinsic properties (*e.g.*, stereoisomers). In order to achieve effective resolution, each analyte must possess unique physicochemical properties to allow their differential migration from other constituents in the sample matrix. In general, there are two distinct mechanisms that control resolution in separation systems, namely separative and dispersive transport.[14] Separative transport refers

to the differential movement of analytes that is dependent on their specific interactions in a local environment. These interactions are related to the fundamental physicochemical properties associated with analytes, such as molecular size, polarity and effective charge, which can be exploited to induce differences in energetic and/or kinetic processes allowing for their separation. In contrast, dispersive transport occurs as a result of random solute diffusion, resistance to mass transfer and/or convection leading to what is more commonly referred to as band broadening. A fundamental understanding of these mechanisms is thus necessary to maximize separative transport in a manner that minimizes dispersion in order to achieve optimal resolution within a short analysis time.

Analysis of biomolecules spans a wide range of techniques with most low-molecular weight analytes being characterized by separation formats such as gas chromatography with mass spectrometry detection (GC/MS). Larger non-volatile biomolecules such as peptides, proteins, DNA, polysaccharides, as well as low molecular weight polar metabolites often require alternative methods. For instance, high resolution protein analysis rely predominantly on several complementary methods, including gel electrophoresis, size-exclusion liquid chromatography (LC) and electrospray ionization (ESI)-MS. However, analysis of protein structure and conformation require alternative spectroscopic techniques based on fluorescence and circular dichroism, as well as more powerful atomic-resolution methods, including nuclear magnetic resonance (NMR) and X-ray

crystallography. Although one cannot hope to replace the plethora of techniques available with a single format, CE represents a versatile platform applicable for the characterization of a wide range of biomolecules as compared to traditional methods. Separations in CE are often performed using narrow-bore fused-silica capillaries for effective dissipation of Joule heating due to ion conduction which would otherwise lead to band broadening. Moreover, fluid transport in CE arises from the generation of an electroosmotic flow (EOF) as a natural electrokinetic pumping mechanism. This mode of fluid transport contributes to high separation efficiency and is advantageous to the pressure-driven system common in liquid chromatography (LC) due to the flat flow profile which minimizes axial diffusion. This unique transport mechanism is highly sensitive to electrolyte composition and capillary surface properties, which allows for the tuning of separations based on several operating parameters. CE is further amenable to the integration of a number of sample pre-treatment steps, including *on-line* sample preconcentration with chemical derivatization, in order to minimize sample handling and improve sample throughput while improving detection limits. The flexibility of CE makes it an ideal platform for analysis of a wide range of analytes, ranging from the resolution of amino acid enantiomers to the characterization of whole cells.[5, 15-18] The fundamental principles governing the operation of CE will be discussed in the following sections. These principles will then be applied in method development for investigations involving protein conformational studies, protein-ligand interactions, and enzyme kinetics. Relevant background will be presented in the

remaining sections of this chapter of the thesis in the context of major research contributions presented in the subsequent chapters of this thesis.

1.2. Capillary Electrophoresis

Early achievements in electrolysis, electroosmosis and solution conductivity by Faraday, Ruess, Hittorf and Helmholtz[19] pre-date the first description of electrophoresis. The principles of electrophoresis were first introduced in 1897 by Kohlrausch[20] based on the differential movement of ions under an electric field. However, it was Kohlrausch's student Tiselius[21] who was first able to experimentally demonstrate these principles as applied to separation of a protein mixture using an electrophoresis apparatus. Within the same research group, Svedberg[22] recognized the significance of the work for protein characterization, notably for the determination of the isoelectric point (*pI*) of proteins. Further contributions were made by Tiselius's students Svensson, Longsworth and Dole for their development of optics for moving boundary electrophoresis and fundamental equations to describe electrophoresis.[23-25] Despite the early promises of the technique, electrophoresis suffered from significant band broadening due to Joule heating, which was caused by resistive heating of the electrolyte solution during ion migration thereby resulting in thermal dispersion of analyte bands. Continued advances in support materials for dissipating heat led to the use of paper, sucrose density gradients and the modern polymer gel support medium for electrophoresis. The use of density gradients

from density centrifugation for density gradient electrophoresis was initially developed by Svennson[26] and later became the basis for isoelectric focusing (IEF) electrophoresis. Hjertén,[27] another student of Tiselius, introduced anticonductive polymer media (*e.g.* agarose, polyacrylamide *etc.*) which greatly reduced Joule heating associated with the use of electrolyte solutions. Gel electrophoresis (GE) using polymer-based support media remains today a valuable means of characterization of complex mixtures of biopolymers, such as protein and DNA, where the matrix serves both to dissipate heat and act as a sieving device to separate polymer ions based on their effective size.

Free zone electrophoresis was not performed until 1967, when Hjertén[28] carried out free solution electrophoresis using narrow (1-3 mm) longitudinally-rotated quartz tubes to enhance dissipation of Joule heating. Mikkers later improved the format by applying Hjertén's technique to Teflon tubes which were able to dissipate heat more efficiently based on its superior thermal conductive properties.[29] The birth of CE, however, is associated with the pioneering work of Jorgensen and Lukacs[30, 31] for adaptation of free zone electrophoresis using fused-silica capillaries with microscale inner diameters (75 μm). Their studies demonstrated high efficiency electrophoretic separations of fluorescently labelled amino acids, peptides and amines using laser-induced fluorescence detection for improved concentration sensitivity. The narrow capillary dimensions allowed for effective dissipation of resistive heating, even under high applied voltages (30 kV), due to the large surface-to-volume ratio of the capillary. This breakthrough

research set the stage for later commercial development of automated CE instrumentation, the first of which was released by Beckman in 1989. Since this time, much effort has been directed towards improvements in sensitivity, selectivity, robustness and reliability with significant achievements in chiral amino acid analysis,[18, 32] high resolution protein separation,[33-35] and DNA sequencing.[36] To date, CE has been used as a high efficiency microseparation technique in various applications ranging from detection of biomarkers for clinical diagnostics,[37] doping control,[38] and most noteworthy, for high-throughput DNA sequencing in the Human Genome Project.[9] More recent work in CE has been directed at developing new forensic,[39] environmental[40, 41] and clinical applications,[37, 42] fsuch as identification of chemical chaperones.[43] It is anticipated that CE-based research will continue to grow with recent interest directed towards miniaturization based upon chip-based formats, such as micro total analysis systems (μTAS).[44, 45]

1.2.1. Set-Up and Apparatus

The typical apparatus used in CE is depicted in **Figure 1.1.** A fused-silica capillary is suspended between two level buffer-filled reservoirs. Each reservoir also contains platinum or stainless steel electrodes which are connected to a high voltage power supply. In order to detect analyte bands photometrically during electromigration, a portion of the polyimide coating on the fused-silica capillary is
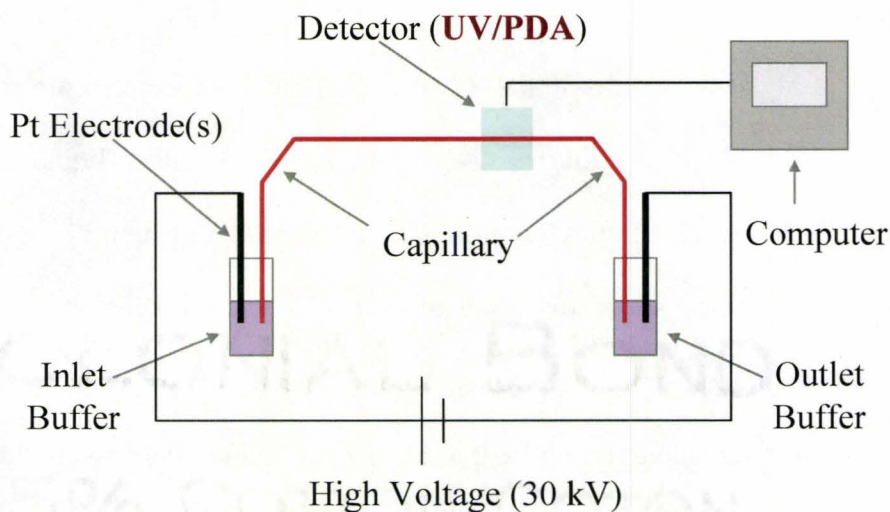
Figure 1.1. Schematic of typical instrument set-up for CE with on-line photometric detection.

burned to reveal a transparent detector window for UV absorbance or fluorescence detection. Prior to use, the capillary is first conditioned with various solvents and then rinsed with an aqueous buffer solution. Buffers used in CE make up the background electrolyte (BGE) which is required to perform separations. These solutions are typically composed of buffer salts which possess low conductivity to reduce Joule heating while having high buffering capacity to resist changes in solution pH caused by electrolysis. The use of low amounts of aqueous buffers makes CE highly compatible for the analysis for most biological molecules. The composition of the BGE plays an essential role in tuning the selectivity in CE for separation of weakly ionic analytes. Samples are introduced into the capillary via hydrodynamic or electrokinetic injection which is performed by placing the sample reservoir at the inlet side of the capillary and applying a positive pressure or voltage for a specific time interval. Following sample

injection, the inlet is returned the buffer reservoir and separation is initiated by the application of high voltage (10-30 kV). Modern commercial instruments employ narrow-bore, fused-silica capillaries (2-100 µm i.d.) with either liquid or air-cooled cartridges for temperature control. The combination of high voltages and narrow-bore capillaries allow for rapid and high efficiency separations while minimizing sample consumption. Typical sample injection volumes are less than 10 nL with buffer consumption under 0.5 mL per run. Upon voltage application, an electric field is established and solutes are separated on the basis of their effective charge to size ratio. Overall, there are two fundamental electrokinetic parameters which influence the migration of analytes in CE, namely the EOF and the electrophoretic mobility (μ_{ep}) of the analyte.

1.2.2. Electroosmotic Flow

The EOF represents a natural electrokinetic pumping mechanism that serves to move bulk solution from the inlet to outlet reservoirs. The magnitude and direction of the EOF depends mainly on the composition of the BGE and the properties of the capillary wall. The use of aqueous buffers ionizes the weakly acidic silanol groups ($pK_a \sim 6.5$),[46] resulting in a net negative charge on the capillary wall. It is at this surface that an electric double layer is formed in accordance with the Debye-Huckle-Stern model[47] shown in **Figure 1.2**. The electric double layer consists of the Stern layer, a rigid layer of cations
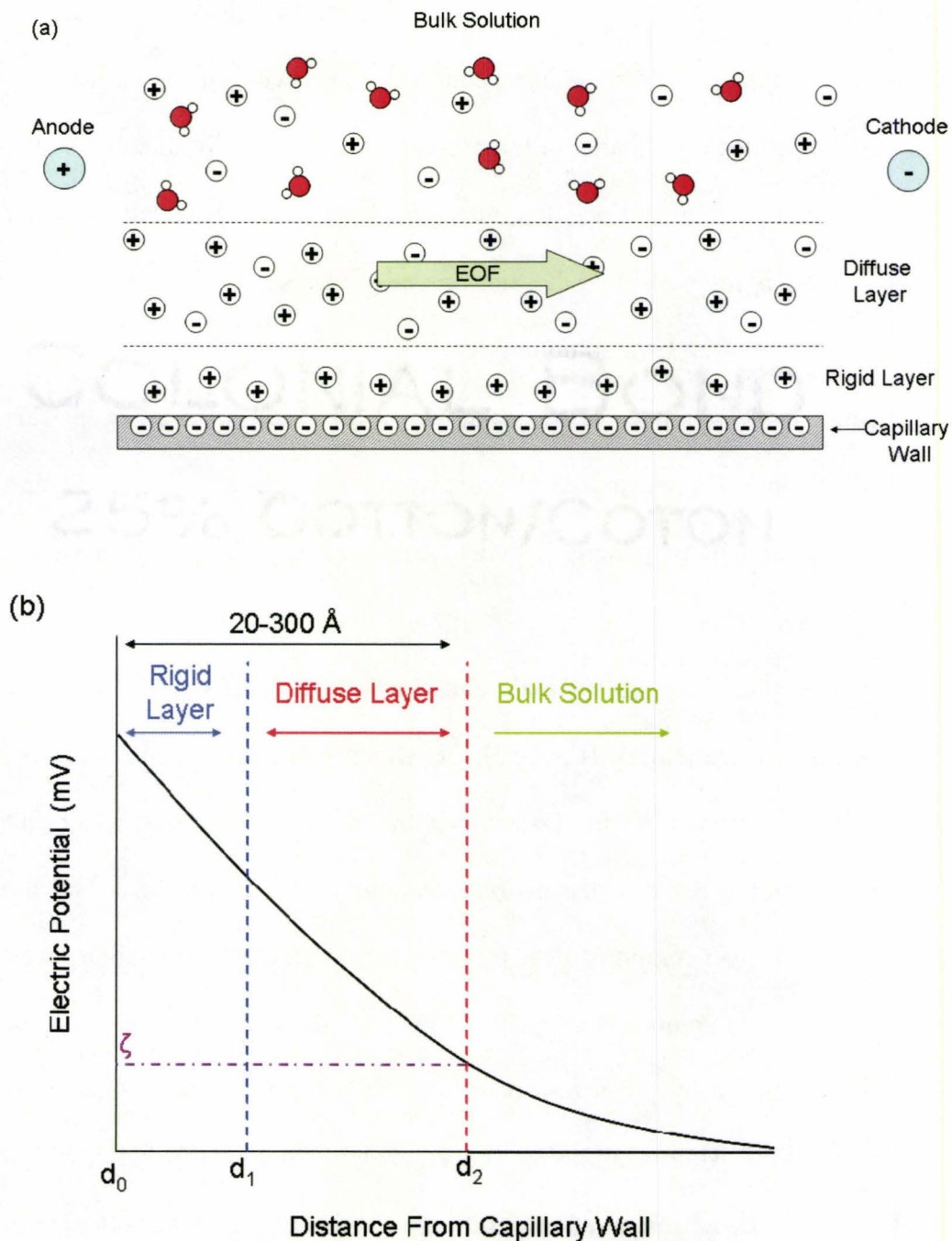
Figure 1.2. Debye-Huckle-Stern model of the electric double layer showing (a) the rigid and diffuse layers and (b) zeta potential (ζ) that generates the EOF at the capillary wall (d_0) under an external voltage due to migration of solvated cations in the electrical double layer where d_1 is the Stern plane and d_2 represents the slipping plane.

which are tightly adsorbed to the negative capillary wall, followed by a diffuse electric double layer. The diffuse layer consists of an excess of mobile cations, however since the negative charge of the capillary wall is partially shielded by the Stern layer, both positive and negative ions are present. The boundary between these two layers is referred to as the Stern plane whereas the boundary between the diffuse layer and the bulk solution is generally defined as the slipping plane. The potential at the slipping plane is known as the zeta potential (ζ). This potential is directly related to the charge density near the capillary wall and decreases exponentially with increasing distance from the capillary wall, as shown in **Figure 1.2(b).**

Upon application of an external voltage across the capillary cations within the diffuse layer migrate towards the cathode, which is typically the outlet in the normal mode of operation in CE. Transport of the bulk solution occurs as a result of hydrogen bonding between the hydrated cations in the diffuse layer and the bulk solution. The generation of flow from near the surface of the capillary wall is responsible for the uniquely flat profile of the EOF as compared to the laminar flow profile produced by pressure-driven flows (**Figure 1.3**). This linear flow minimizes axial diffusion resulting in reduced analyte band broadening and high separation efficiency as compared to traditional pressure driven transport used in LC.

The magnitude and direction of the EOF is governed by the following equation:[30]

(a)

(b)
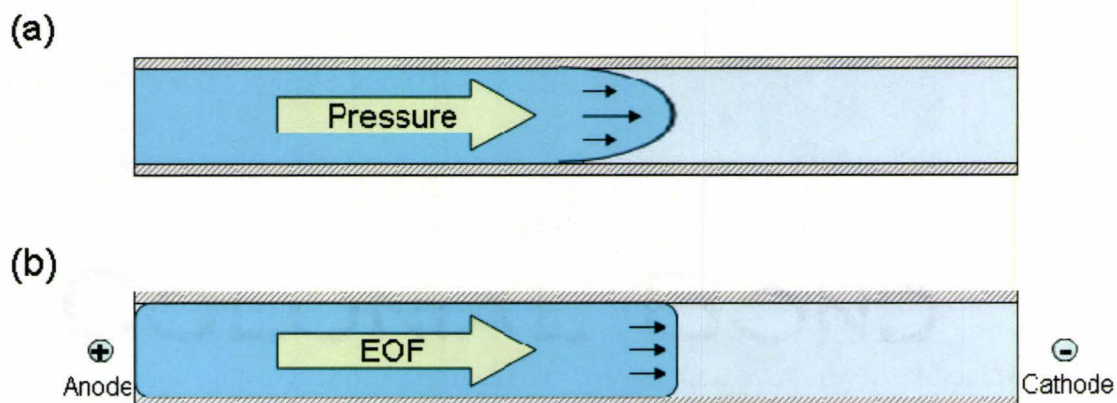
Figure 1.3. Comparison of fluid transport systems (a) parabolic flow profile generated by a use of an external pressure pump and (b) flat flow profile of EOF generated electrokinetically in CE.

$$\mu_{eo} = \frac{v}{E} = \frac{\varepsilon\zeta}{4\pi\eta} \qquad (1\text{-}1)$$

where, v is the velocity, E is the strength of the electric field, η is the viscosity of the medium, ε is the dielectric constant of the medium and ζ is the zeta potential. The magnitude of ζ is primarily dependant on the buffer pH and ionic strength of the solution since they influence the effective charge density of the capillary wall. In general, low ionic strength/alkaline buffer conditions induce a high ζ and thus a strong cathodic EOF, whereas high ionic strength/acidic buffer conditions suppress the EOF due to protonation/ionic shielding of the surface charge. Thus, ζ is highly sensitive to modifications which affect the surface properties of the capillary wall. For instance, a capillary can be covalently modified with a neutral polymer (*e.g.* polyacrylamide) to reduce ζ thereby suppressing the EOF or dynamically modified non-covalently using a positively charged surfactant (*e.g.* CTAB) to generate an excess of anions in the diffuse layer which reverses the

direction of the EOF. Since ζ, and therefore EOF, are highly dependent on the surface properties of the capillary and buffer composition of the BGE, the magnitude of the EOF can vary significantly from run to run leading to poor migration time precision, notably when operating near neutral pH conditions. The variability in the EOF therefore results absolute migration times being less reproducible in CE as compared to LC retention times. Despite the long-term variability associated with shifts in migration times in CE, analyte electrophoretic mobility is highly reproducible (coefficient of variance, CV < 1%) when using a neutral EOF marker during separations, as discussed in the following section.

1.2.3. Electrophoretic Mobility

The theory of electrophoresis in capillaries was first published in detail by Jorgenson and Lukacs[30] who defined the electrophoretic mobility of a charged analyte ($\mu_{ep,A}$) in an electric field:

$$\mu_{ep,A} = \frac{v}{E} = \frac{Q_{eff}}{6\pi\eta R_H} \tag{1-2}$$

where Q_{eff} is the effective charge and R_H is the hydrodynamic radius on an ion. The original equation assumes that the analyte is a spherical and uniformly charged ion. **Eq. 1-2** also accounts for hydration effects on the ion which results in a lower effective charge, but does not include the impact of electrolytes in solution that results in dielectric friction. **Eq. 1-2** highlights that ion mobility represents a steady-state velocity that depends on the balance of opposing
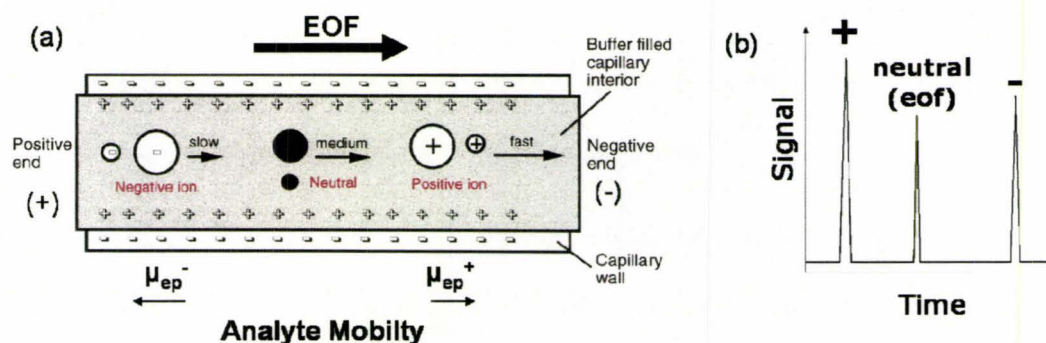
Figure 1.4. Separation of positive, neutral and negative analytes in an unmodified fused-silica capillary by CE. (a) Relative migration order in CE is based on the direction and magnitude of the analyte electrophoretic mobility relative to the EOF. (b) Representative electropherogram for a sample mixture based on the measured response of a solute as a function of time. Reprinted in part with permission from Cooper, C.L. *J. Chem. Ed.* **1998**, *75*, 343. Copyright 1998 American Chemical Society.

electrical and frictional forces during ion migration. One is the velocity imparted by the applied electric field, also expressed as the electric force, while the opposing force is the frictional hydrodynamic drag:

$$v = \mu E \tag{1-3}$$

$$F_{el} = qE \tag{1-4}$$

$$F_f = 6\pi\eta r v \tag{1-5}$$

From these equations it is clear that small, highly charged analytes will have high electrophoretic mobility, whereas bulky weakly ionic species will have low mobility.

The typical migration order of ions in CE is shown in **Figure 1.4.** Note that neutral analytes lacking a formal charge are not resolved and co-migrate with the EOF. Although intrinsic charge is a property inherent to the analyte under study, adjustments can be made to the composition of the BGE (*e.g.* ionic

strength, pH, buffer type) to improve selectivity. Thus $\mu_{ep.A}$ represents a characteristic physicochemical property of the analyte which is dependant on the electrolyte conditions, including the viscosity and temperature of the solution. Mobility can therefore be utilized as a parameter to monitor dynamic changes in analyte properties, such as hydrodynamic volume in protein unfolding, where $\mu_{ep,A}$ changes in response to urea-induced denaturation. In this example it is also important to correct for non-specific changes to mobility. In particular, a viscosity correction factor is required in protein unfolding experiments in CE to correct for the increased solution viscosity at high concentrations of urea which will be discussed in detail in Section 1.5.

1.2.4. Apparent Electrophoretic Mobility

The observed migration behaviour of an analyte in CE is the vector sum of the EOF and the μ_{ep} of the analyte which is referred to as the apparent electrophoretic mobility ($\mu_{ep}{}^{A}$):

$$\mu_{ep}^{A} = \mu_{ep,A} + \mu_{eo} \tag{1-6}$$

This can be derived experimentally from an electropherogram by measuring the analyte apparent migration time (t^A) relative to the migration time of a neutral EOF marker (t_{eo}):

$$\mu_{ep,A} = \mu_{ep}^{A} - \mu_{eo} = \frac{L_t L_d}{V}\left(\frac{1}{t^A} - \frac{1}{t_{eo}}\right) \tag{1-7}$$

Table 1.1. Separation modes in CE and typical conditions used for different classes of analytes.[47]

Mode	Conditions	Suitable Analyte Classes
CZE	Continuous electrolyte	Ions, small molecules, peptides
ITP	Discontinuous electrolyte	Ions, small molecules, peptides, proteins
MEKC	Micelle forming additives; detergents, bile salts	Small molecules, peptides, proteins, oligonucleotides
CIEF	pH gradient of ampholytes	Peptides, proteins
CGE	Seiving matrix; e.g. polyacrylaminde, agarose	Peptides, proteins, oligonucleotides, DNA
CEC	C18 packed or monolithic column	Ions, small molecules, peptides, proteins

where L_t is the total length of the capillary, L_d is the capillary length to the detector, V is the applied voltage and $\mu_{ep,\ A}$ is typically expressed in units of $cm^2V^{-1}s^{-1}$. It should be emphasized that unlike traditional electrophoresis, CE is often performed in free solution. It should also be emphasized that although t^A usually possesses relatively high variation under most conditions (CV > 10%) due to the variability of the EOF, $\mu_{ep,A}$ can be precisely measured with a CV under 1%.

1.3. Modes of Separation

Since it was first conceived to perform electrophoresis in capillaries, various separation modes have been introduced to exploit the versatility of CE to encompass a broad range of solutes ranging from ions, small molecules, peptides, proteins, oligonucleotides, to bacteria. **Table 1.1** summarizes the major sepration modes in CE including capillary zone electrophoresis (CZE)[47], micellar electrokinetic chromatography (MEKC),[48, 49] capillary isoelectric focusing (CIEF),[50] isotachophoresis (ITP),[51] capillary gel electrophoresis (CGE)[52, 53] and

capillary electrochromatography (CEC).[33, 54] Briefly, CIEF utilizes a pH gradient to focus weakly ionic polymers at their isoelectric point (*pI*) which is predominantly applied to high resolution separation of proteins. In contrast, ITP is primarily used for analysis of small ions that have intermediate mobilities relative to two or more electrolytes that function as a leading and terminating electrolyte within a discontinuous electrolyte system. Unlike the latter two free solution based electrophoretic methods, CGE employs the use of gel matrix within the capillary as a sieving agent to resolve larger biomolecules based on their size/shape during electromigration, such as proteins and DNA. CEC represents a hybrid separation technique between CE and LC where the capillary used to perform separations contains a packed-particle stationary phase (*e.g.,* reverse-phase C18) or an integral monolithic column, with separations based on differences in analyte mobility and/or partitioning. Alternatively, various types of additives can be introduced in the BGE in order to modulate analyte electromigration behaviour based on non-covalent interactions. MEKC represents one of the most widely used modes in CE based on differential partitioning of neutral analytes with ionic surfactants that function as pseudo-stationary phases. Other classes of additives can also be included in the BGE to enhance the resolution of enantiomers in CE, such as chiral selectors based on oligosaccharide macrocyles, namely cyclodextrins (CDs). In this thesis, CZE, MEKC and CD-modified CE will be the major separation modes used for characterizing the

thermodynamics and kinetics of protein-small molecule interactions, which will be discussed in further detail in subsequent chapters of the thesis.

1.3.1. Capillary Zone Electrophoresis

Capillary zone electrophoresis is the simplest mode of CE, which is often used interchangeably with the term CZE. In CE, a single continuous electrolyte system is used throughout the separation. This is the most commonly applied format of CE due to its versatility and ease of use. Selectivity in this separation mode is solely controlled by differences in μ_{ep}. Major drawbacks of CE include the requirement of as ionic analyte and low concentration sensitivity for poorly responsive and/or low abundance analytes. The latter problem stems from the use of narrow-bore capillaries which require small injection volumes (often < 10 nL) while having narrow optical path lengths for *on-line* photometric detection. In order to improve concentration sensitivity, a number of *on-line* sample pre-concentration strategies using discontinuous buffer systems have been developed to allow the injection of longer samples plugs without band broadening, including stacking,[51, 55] dynamic pH junction[56] and sweeping.[57] Analytes can also be derivatized with specific chemical labels to improve detection and selectivity, which will be described in more detail in later section of the thesis.

1.3.2. Micellar Electrokinetic Chromatography

MEKC was first introduced in 1984 by Terabe et al.[58] to enable the separation of neutral analytes by CE. In this work, Terabe and colleagues introduced the anionic detergent sodium dodecyl sulphate (SDS) into the separation buffer above its critical micelle concentration (cmc). The formation of SDS micelles created a pseudostationary phase which enabled separation of a mixture of phenols based on differences in partition coefficients (K). Since publication of this seminal paper, nearly 4000 scholarly articles have been published which utilize MEKC to date. Indeed, MEKC continues to attract novel applications and developments. New surfactants have been developed which expand the resolving power of MEKC, permitting the separation of neutral, poorly soluble, weakly ionic and chiral analytes such as amino acids, steroids and chiral drugs.[18, 59, 60] Various classes of surfactants used for MEKC and their typical applications are summarized in **Table 1.2**.

Separation by MEKC is based on two discrete mechanisms, namely electrokinetic and thermodynamic processes which are determined by differences in free analyte mobilities and/or partitioning with micelles. For neutral analytes, which possess no intrinsic mobility, separation depends solely on the magnitude of K The process is schematically illustrated in **Figure 1.4.** Here, neutral analytes migrate at mobility intermediate to the mobility of the EOF and the anionic micelle. The apparent electrophoretic mobility ($\mu_{ep}{}^{A}$) of an analyte in MEKC can thus be described by the following equations:[47, 58, 61]

Table 1.2. Common classes of surfactants used in MEKC.[47, 49, 62]

Class	Function	Surfactant
Anionic Surfactant	Increase solubility, reduce adsorption, resolve neutral analytes	Sodium dodecyl suphate (SDS)
Non-ionic	Dyanmic modification of capillary wall, resolve long chain peptides/fatty acids	Tween; Brij
Cationic Surfactant	Charge reversal on capillary wall; hydrophobic interaction, resolve highly anionic analytes	Dodecyltrimethylammonium bromide (DTAB); Cetyltrimethylammonium bromide (CTAB);
Bile Salts	Increase solubility for very hydrophobic analytes; chiral resolution	Sodium cholate (SC), Sodium taurocholate (STC); Sodium deoxycholate (SDC); Sodium taurodeoxycholate (TDC)

$$\mu_{ep}^{A} = \frac{1}{1+K[C]}\mu_{ep,A} + \frac{K[C]}{1+K[C]}\mu_{ep,mc} \qquad (1\text{-}8)$$

$$k' = K[C] \qquad (1\text{-}9)$$

$$k' = \frac{t^{A} - t_{eo}}{t_{eo}\left(1 - \dfrac{t^{A}}{t_{mc}}\right)} \qquad (1\text{-}10)$$

where, K is the partition coefficient, C is the concentration of detergent, k' is the retention factor and $\mu_{ep,A}$ and $\mu_{ep,mc}$ represent the mobilities of the free analyte and micelle, respectively. The latter parameters are determined by the apparent migration time of the solute and the micelle using a suitable micellar marker added to the sample. Typical EOF markers for MEKC are organic solvents, such as methanol or acetonitrile (ACN), which are assumed not to interact with the micelle, whereas micelle markers are neutral lipophilic dyes (*e.g.,* Sudan III), that

a
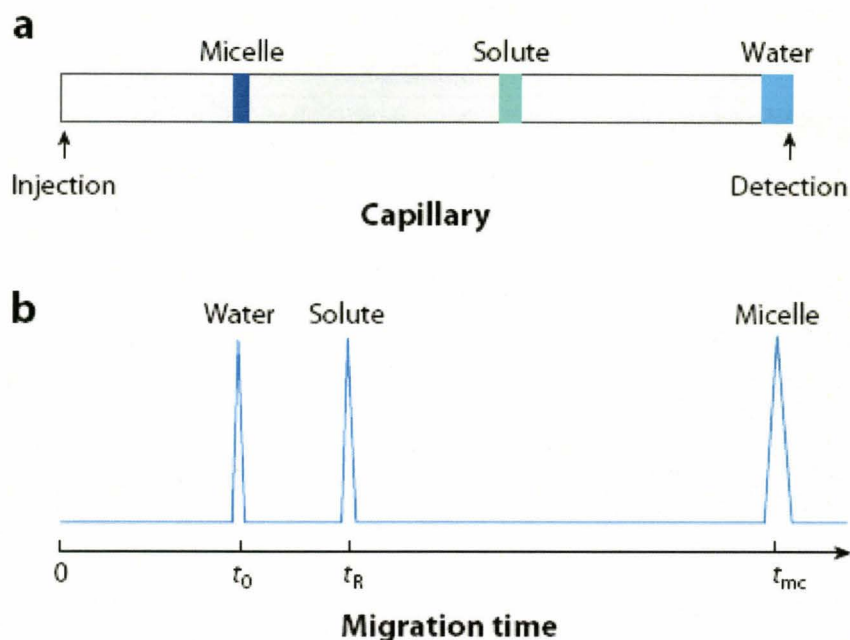
Figure 1.5. Schematic representation of separation in MEKC. Neutral analytes which partition into a negatively charged micelle in normal polarity CE, migrate at rates intermediate to the micelle and the EOF. Adapted with permission from Terabe, S.; Otsuka, K.; Ando, T., *Anal. Chem.* **1985,** *57* (4), 834. Copyright 1985 American Chemical Society.

irreversibly partition completely into the micelle. The resolution in MEKC is typically optimized through appropriate selection of micellar system and buffer conditions, such as surfactant type(s), micelle concentration, buffer pH and temperature.[49] In addition, organic solvents may be added in small amounts to the BGE (0-30 %) to tune selectivity by altering K and solubility of analytes without disrupting hydrophobic effects required for the stability of micellar structure. Unlike LC methods that rely on fixed covalently-bound stationary phases, MEKC boasts the advantage of versatility for the separation of complex sample mixtures

since several independent parameters can be used to tune selectivity, such as the

concentration of single or multiple additive(s) in free solution.

1.3.3. Cyclodextrin Macrocycles

Cyclodextrins (CDs) are the most widely used chiral selector for

separation of stereoisomers in CE and HPLC.[32, 63, 64] These compounds are cyclic

oligosaccharides which possess 6, 7, or 8 glucopyranoside units, referred to as α-,

β- and γ-CD respectively. In chromatography, CDs are typically covalently

bonded to a support matrix to serve as a stationary phase, whereas in CE they are

used in free solution to aid in resolution of complex mixtures of chiral and achiral

compounds. As depicted in **Figure 1.6**, CDs are cylindrical macrocycles with a

hydrophobic cavity that are capable of forming host-guest inclusion complexes

with small molecules. Native cyclodextrins are electrically neutral, thus they

comigrate with the EOF in CE. Accordingly, ions that form inclusion complexes

with CD exhibit slower mobilities due to the increased hydrodynamic size of the

inclusion complex. Similar to **Eq. 1-8** for MEKC, the apparent mobility of an

analyte ($\mu_{ep}{}^{A}$) can be described by the following equation based on a 1:1 dynamic

inclusion complexation model:

$$\mu_{ep}{}^{A} = \frac{1}{1 + K[C]}\mu_{ep,A} + \frac{K[C]}{1 + K[C]}\mu_{ep,AC} \qquad (1\text{-}11)$$
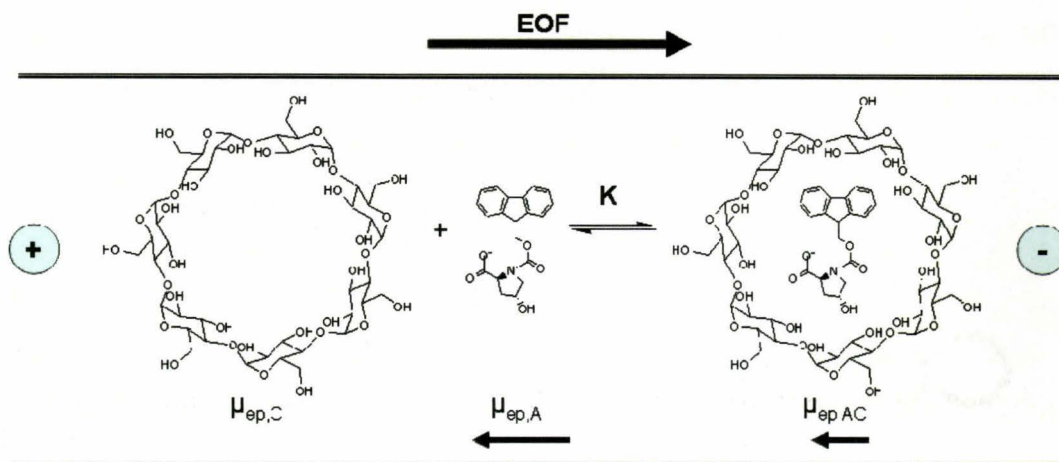
Figure 1.6. Schematic representation of Fmoc-derivatized 4-hydroxy-*L*-proline forming an inclusion complex with β-CD during electromigration in CE.

where, K is the equilibrium constant, C is the concentration of CD, and $\mu_{ep,A}$ and $\mu_{ep,AC}$ represent the mobilities of the free analyte and analyte-CD complex, respectively. CDs can be covalently modified via their hydroxyl groups in positions 2, 3 and 6, to improve aqueous solubility,[64] such as hydroxypropyl-β-CD and β-CD sulphate.[65, 66] In particular, the use anionic CDs is advantageous for resolution of electrically neutral or weakly ionic analytes since host-guest inclusion complexation increases the analyte migration time providing a larger window for separation.[67] Similarly, anionic micelles can be used in MEKC with neutral CDs to enhance selectivity based on complementary thermodynamic and electrokinetic separation mechanisms.[48] A majority of the applications for CD-modified CE have been towards characterization of chiral pharmaceuticals.[17, 59]

1.4. Separation Theory

1.4.1. Capillary Electrophoresis Performance

There are several factors which contribute to optimal performance separation. For instance, band broadening in CE may result from analyte diffusion (D), Joule heating (J), variation in sample injection plug length (I), electrophoretic dispersion (E), adsorption of the analyte to the capillary wall (A) or variation in temperature. Thus, the total apparent variance (σ^2_T) which contributes to the apparent dispersion of analyte zones in CE can be summarized as follows:

$$\sigma^2_T = \sigma^2_D + \sigma^2_I + \sigma^2_J + \sigma^2_E + \sigma^2_A + \sigma^2_{other} \qquad (1\text{-}12)$$

Most of these sources of variance can be greatly reduced by careful optimization of the several operating parameters, such as injection volume, voltage and buffer ionic strength. Under optimal conditions the major contribution to analyte dispersion is longitudinal diffusion:

$$\sigma^2_T = \sigma^2_D = 2 \cdot D \cdot t \qquad (1\text{-}13)$$

where t is the migration time of the analyte and D is its diffusion coefficient, expressed in units of $cm^2 s^{-1}$, which is associated with the size of the analyte and viscosity of the medium.[68] Assuming that analyte bands in CE exhibit a normal peak distribution and that the major source of band broadening is diffusion, then the efficiency of the separation (N) can be related to plate theory in chromatography through the following equation:[30]

$$N = \frac{L_d^2}{\sigma_T^2} = \frac{L_d^2}{2 \cdot D \cdot t} = \frac{L_d^2}{2 \cdot D \cdot \left(\dfrac{L_d^2}{\left(\mu_{ep,A} - \mu_{eo} \right) \cdot V} \right)} = \frac{\left(\mu_{ep,A} - \mu_{eo} \right) \cdot V}{2 \cdot D} \qquad (1\text{-}14)$$

where L_d is the capillary length to the detector.   From this relationship, it is evident that separations involving analytes with low diffusion coefficients (D), high voltages (V) and high positive mobilities ($\mu_{ep,A}$) under a low EOF (μ_{eo}) will maximize separation efficiency (N) by minimizing diffusion.

Since $\mu_{ep,A}$ and D reflect instrisic physicochemical properties of the analyte, the most direct way to improve N is to increase the applied voltage. Normal operating voltages range from 10-30 kV, however the practical upper limit is defined by the linear portion of an Ohm plot for the system that is dependent on the capillary dimensions and conductivity of the electrolyte solution. The non-linear region of an Ohm plot indicates Joule heating generating temperature gradients within the capillary that can result in increased band broadening and lower N.[69] The use of low ionic strength electrolytes with low conductivity, as well as using instrumentation with forced air or liquid-based temperature control can extend the maximum operating voltage without deleterious Joule heating.

In CE, the separation efficiency can be experimentally determined from an electropherogram based on the following expression:

$$N = 5.54 \cdot \left(\frac{t}{w_{1/2}} \right)^2 \qquad\qquad (1\text{-}15)$$

where $w_{1/2}$ represents the peak width at half the maximum peak height of the analyte. In general, N values for CE are in the 10^5 -10^6 range, which is comparable to the performance of GC and an order of magnitude greater than LC.

1.4.2. Selectivity

Separation selectivity (α) is another measure of separation efficiency that can be used in CE as well as chromatography to describe the ratio of the migration velocity between two analytes, A and B (where $v_A > v_B$) by the equation:[70]

$$\alpha = \frac{v_A}{v_B} \qquad (1\text{-}16)$$

In CE, where the separation is under constant electric field and the BGE is devoid of additives, the relative analyte migration velocities can be replaced by μ_{ep}:

$$\alpha = \frac{\mu_{ep,A}^A}{\mu_{ep,B}^A} = \frac{\mu_{ep,A} + \mu_{eo}}{\mu_{ep,B} + \mu_{eo}} \qquad (1\text{-}17)$$

Selectivity for weakly ionic analytes is highly dependent on buffer type, pH and ionic strength of the electrolyte. Thus, the optimization of buffer conditions is one of the most important steps in method development of assays in CE. For example, change in pH can alter the ionization state of a weakly ionic analyte, whereas changes in electrolyte ionic strength may alter its effective charge. In addition, electrolytes used for pH control can also be directly involved with selectivity in CE based on differential covalent or non-covalent interactions with specific classes of analytes. For instance, 3-nitrophenylboronic acid can function as an electrokinetic probe for the separation and detection of neutral polyol

stereoisomers via ternary boronate ester complexation formation.[71] MEKC represents one classic example where a surfactant additive can be used to enhance selectivity in CE separations.[48]

1.4.3. Resolution

Resolution (R_S) is another critical parameter to assess separation performance in CE since it takes into account both separative and dispersive transport processes. R_S can be defined in CE by adopting the equation used in chromatography based on a normal peak distribution:[30, 68]

$$R_S = \frac{1}{4}\left[\frac{\left(\mu_{ep,avg} + \mu_{eo}\right)\cdot V}{2\cdot D}\right]^{1/2}\cdot\left[\frac{\Delta\mu_{ep}}{\left(\mu_{ep,avg} + \mu_{eo}\right)}\right] = \frac{\sqrt{N}}{4}\cdot\frac{\Delta\mu_{ep}^{A}}{\mu_{ep,avg}^{A}} \qquad (1\text{-}18)$$

where $\mu_{ep,avg}$ is the average mobility, μ_{eo} is the EOF mobility, V is the applied voltage, D is the diffusion coefficient, $\Delta\mu_{ep}$ is the difference in mobility between two analytes, $\Delta\mu_{ep}^{A}$ is the difference in apparent mobility (μ_{ep}^{A}) between the two analytes. From **Eq. 1-18** it is evident that maximum resolution is obtained when $\mu_{eo} = -\mu_{ep,avg}^{A}$ based on counter-flow electrophoresis, where the magnitude of the EOF is opposite and equally balances the average mobility of analyte allowing for greater discrimination of small difference in μ_{ep}. However, under these conditions, the analysis times tends towards infinity. Therefore, a more practical strategy to enhance resolution is to optimize separation conditions to maximize N (*i.e.,* high voltages) while reducing the EOF in order to moderately extend the residence time of analytes in the capillary without contributing to significant

longitudinal diffusion (< 20 min). In CE, resolution can be experimentally determined by measuring the ratio of the average peak width (*w*) to the differences in migration time (*t*) based on the following expression:

$$R_S = \frac{2 \cdot (t_B - t_A)}{(w_A + w_B)}$$
(1-19)

1.4.4. Separation Optimization

It is possible to adapt CE separations to a wide variety of analytes, ranging in size from discrete metal ions to whole living cells. However, in order to achieve a minimum baseline resolution (*Rs* > 1.2) for two or more analyte zones, several parameters must be considered in order to determine the conditions best suited for CE separation. These include electrode polarity, applied voltage, temperature, capillary diameter, length of the capillary, type and concentration of electrolyte, as well as buffer pH. In addition to CD and detergents, other modifiers can also be added to tune separations in CE. For instance, organic solvents can be added to decrease the magnitude of the EOF, decrease thermal diffusion as well as improve solubility of hydrophobic analytes. The EOF can be further modified by use of covalently modified capillaries, dynamically coated capillaries or addition of inorganic ions (*e.g.*, Mg^{2+}) to the BGE. The mode of detection needs to be considered when developing new CE methods. Typical detection by UV or fluorescence requires use of optically transparent buffers while volatile buffers are required when using ESI-MS interfaces. The sheer number of operation parameters and separation mechanisms available for

separations in CE is a major technical advantage to traditional chromatography. CE therefore allows for far greater tuning of selectivity and resolution, whereas LC formats are limited by the types of fixed stationary phases and composition of mobile phases available.

For the work completed within this thesis, separation optimization was primarily aimed at the resolution of various protein states (*e.g.,* unfolded, *apo*-protein etc.), as well as for *D/L*-amino acid stereoisomers (*e.g.,* diastereomers, enantiomers). For protein separation (Chapters II, III, V), it was important to choose conditions that limited dispersion while maximised separative transport. Low conductivity, biocompatible and optically transparent electrolytes were used at high ionic strength to reduce the extent of protein adsorption on the capillary wall, maintain native protein conformation during separation and allow for higher voltage to be applied to enhance N. Furthermore, frequent regeneration of the capillary wall was necessary to alleviate variation in the EOF resulting from accumulation of protein and urea on the capillary wall. For resolution of amino acid stereoisomers (Chapter IV, V), selectivity was the most important parameter to optimize, which was performed in MEKC mode using various chiral/achiral additives, such as CDs and bile salt surfactants. The details of method optimization will be discussed in subsequent chapters of this thesis.

1.5. Protein Unfolding

The study of protein unfolding is an important area in chemical biology

research for understanding the intrinsic conformational stability of biological molecules. In fact, protein unfolding is a naturally occurring process that is necessary in cellular translocation.[72, 73] Protein unfolding *in vivo* is not an isolated process and many other natural biological factors are involved. For example, recognition processes based on molecular chaperones are used to identify, correct or destroy partially unfolded, fully unfolded or misfolded proteins.[74-76] Indeed, there is great interest in characterizing protein misfolding since it has been associated with the development of several neurodegenerative disorders, such as Alzheimer's disease.[77, 78] Alterations in the native protein conformation caused by oxidative stress and other mechanisms can result in impaired enzyme function, as well as induce irreversible protein aggregation.

Unfolding studies are traditionally carried out by equilibration in free solution using temperature, buffer pH, detergents or chaotropic denaturants in order to disrupt protein non-covalent interactions. Changes in protein conformation during unfolding can be probed by several different spectroscopic formats that include circular dichroism, fluorescence and NMR. In general, each technique offers complementary qualitative information regarding protein unfolding dynamics ranging from long-range changes in peptide backbone structure to atomic resolution of specific amino acid residues. A non-spectroscopic technique that has also been widely used for assessing protein unfolding is differential scanning calorimetry.[79, 80] However, it is evident that no single method has found exclusive use for protein unfolding studies due to

limitations in required sensitivity, selectivity and applicability to different types of protein systems. Thus, techniques that can be applied to a wider variety of samples are desired for future research, such as low amounts of recombinant protein, unfractionated protein mixtures and multimeric holoprotein complexes.

CE was first introduced as a new method for examining protein conformational stability in 1991 by Rush et al.[81] that offered several unique advantages over traditional platforms, such as classical slab gel electrophoresis. Since then, over 70 different CE studies have been reported for protein unfolding to date with major contributions made by the groups of Righetti[82-86] and Rochu.[87-95] However, it still remains a rather unrecognized technique for characterizing protein conformational stability in the wider biochemical community. CE provides an automated electrophoretic format using small amounts of sample and reagents. Moreover, since it is a microseparation technique, unfolding studies can be applied to unpurified samples since it can resolve protein mixtures based on differences in μ_{ep}. Biomolecular interactions involving receptor-ligand systems can also be examined, which can provide both thermodynamic and kinetic information.[96] In most cases, unfolding results in a net decrease in apparent μ_{ep} due to increases in the frictional resistance of a denatured protein during electromigration. Thus, CE can be used as a probe to detect global changes in protein conformation. In addition, the specific type of detector in CE can also provide additional spectroscopic information, such as laser-induced native fluorescence (LINF) and ESI-MS.

To date, most CE studies have examined protein unfolding via changes in temperature, pH and urea as a denaturant in the BGE. One major constraint in CE is that operation conditions are needed to avoid Joule heating when using conductive additives (*e.g.,* guanidium chloride), which can result in non-specific changes in protein mobility. Partial unfolding studies have also been performed with detergents (*e.g.,* SDS)[97, 98] and helical inducing agents (*e.g.,* methanol),[86] to study intermediate conformations of protein unfolding. To date, few reports have applied CE to characterize protein unfolding involving receptors to small ligands, such as cAMP-dependant protein kinases. In this case, receptor-ligand binding results in a significant enhancement in protein conformational stability relative to the ligand-free receptor. This section will focus on the general theory and application of protein unfolding and conformational studies in CE with emphasis on recent developments relevant to holoprotein and protein aggregation systems. Basic models and assumptions used to interpret mobility changes in CE are also presented, including relevant thermodynamic and kinetic aspects of protein unfolding. In addition, the unique benefits of CE as a complementary technique for studying protein conformational changes will be highlighted.

1.5.1. Instrumentation and Experimental Considerations

Commercial CE instruments are often thermostatted with liquid or air-cooled cartridges to dissipate heat generated by Joule heating. This also provides a more reproducible and automated format for quantifying thermodynamic

parameters associated with protein unfolding. CE instruments are also available with temperature-controlled sample trays that maintain the temperature of the buffer, sample vials and ends of the capillary by forced air convection. However, most commercially available instruments can only be used at temperatures up to about 50°C. When studying thermal unfolding of high molecular weight proteins, CE instruments can be modified with external devices to provide a wider temperature range, as reported by Rochu *et al.*[90] and Fan *et al.*[99] As mentioned in a previous section, protein adsorption can be a significant issue in CE when working with bare (uncoated) capillaries which contain partially ionized silanol groups at pH > 3. Depending on the specific properties of the protein (*e.g., pI,* solubility), several different strategies have been adopted to minimize the extent of electrostatic adsorption. CE unfolding studies can be performed under alkaline buffer conditions notably for basic proteins, however this can lead to base-catalyzed unfolding and conformational changes not indicative of physiological pH conditions. Covalent and dynamic coatings[100, 101] can be used to modify the capillary surface to be neutral and hydrophilic while masking the silanol charge density. For instance, Lucy *et al.* recently reported the use of long-chain surfactants as semi-permanent self-assembled coatings for protein separations in CE.[102] High ionic strength buffers are also commonly used to electrostatically shield both protein and capillary surface to minimize adsorption. Righetti *et al.* have demonstrated several successful protein unfolding studies using isoelectric buffers at low pH for the study of acidic proteins.[103] Verzola *et. al* included

tetraethylene pentamine as a polyamine buffer additive during protein unfolding studies to reduce protein adsorption.[84] In general, the use of high ionic strength zwitter-ionic buffers is recommended, since it does not contribute to Joule heating. In addition, the buffer pH or the use of buffer additives can be adjusted to reduce capillary adsorption, provided that the conformation of the protein is not significantly compromised.

In addition to protein adsorption effects, other factors to consider during buffer selection include compatibility with the detector, such as use of volatile buffers for ESI-MS and UV transparent buffers when using CE with absorbance detection. It is also important to perform unfolding studies at a buffer pH where the target protein is stable, as well as in a pH region where it can tolerate small changes in pH with minimal impact on μ_{ep}. This feature is beneficial since the apparent pH can change by as much as 0.8 units with the addition of urea for protein denaturation.[104] Buffer pH also influences the magnitude of the EOF and total analysis times in CE. It is also vital to correct for non-specific changes in bulk solution properties that are not a direct result of protein unfolding processes. In particular, viscosity must be corrected for with addition of a denaturant or increase in temperature to induce protein unfolding. A relative viscosity correction factor (ν) can be readily determined using CE as a viscometer,[96] where relative differences in the migration time of a plug of sample flushed through the capillary is measured under a defined pressure:

$$v = \frac{\eta}{\eta_0} = \frac{t_0}{t} \qquad\qquad (1\text{-}20)$$

where, η and t are the apparent viscosity and migration time at the specific denaturing condition, normalized to η_0 and t_0, which are the same parameters under non-denaturing conditions. Note that v is required for each denaturing condition (*i.e.,* temperature or denaturant concentration), which can be measured with good precision (CV < 1%) by CE. Thus, viscosity-corrected protein mobilities ($v\mu_{ep}$) can be used as a normalized parameter for characterizing specific changes in protein conformation as a function of denaturant. Previous unfolding studies using urea denaturation have often extrapolated protein mobilities to zero urea concentration as opposed to using an independent correction factor. However, this approach results in protein unfolding curves that are not readily comparable with other methods.

Protein unfolding studies in CE have typically been performed using on-capillary UV absorbance detection at 200 or 214 nm due to significant absorbance by aromatic amino acid residues and peptide bonds. Righetti reported differences in apparent thermodynamic parameters by measuring protein unfolding processes by CE at 214 and 280 nm, presumably due to the differential response of aromatic amino acid residues.[105] Detection by laser-induced native fluorescence has also been reported[106, 107] for protein with intrinsic tryptophan residues, which offers lower detection limits than UV absorbance without the need for fluorescent labelling. However, the high cost of UV gas lasers required for selective

tryptophan excitation (280-290 nm) has limited its widespread application. CE-ESI-MS represents a powerful hyphenated technique that has not been examined as a detector format to study protein unfolding to date. One major constraint for CE-ESI-MS is the need to use volatile buffers with low concentrations of salts or denaturants to minimize the extent of ion suppression, which can result in poor ionization efficiency. However, it has been demonstrated to be a promising technique for confirming partially denatured intermediates with modifications,[108] protein mixtures[109] and disulfide bond cleavages.[110]

1.5.2. General Principles of Unfolding in CE

Classic models for describing protein denaturation generally consider three major processes to be essential for understanding unfolding dynamics; namely the rate of unfolding, its reversibility (*i.e.,* refolding) and the number of conformational states or intermediates that exist. Most protein unfolding studies in CE assume an ideal two-state system, where a protein denatures from an ordered, compact structure to an unfolded polypeptide, often considered as a random coil. In this case, protein unfolding occurs reversibly with negligible intermediate states being populated. Thus, the two major populations are the folded native (*F*) and unfolded (*U*) states:

$$F \underset{k_2}{\overset{k_1}{\rightleftharpoons}} U$$

(1-21)

where k_1 is the unfolding rate constant and k_2 is the folding rate constant. The populations of these states relate to the unfolding constant (K_U):

$$K_U = \frac{[U]}{[F]} = \frac{k_1}{k_2} = \frac{f_U}{f_F} \tag{1-22}$$

As shown in **Eq. 1-22**, K_U is often expressed in terms of the ratio of fraction (f) of the unfolded to folded protein as described below:

$$f_F = \frac{f_F}{f_F + f_U} = \frac{1}{1 + K_U} \tag{1-23}$$

$$f_U = \frac{f_U}{f_F + f_U} = \frac{K_U}{1 + K_U} \tag{1-24}$$

An increase in hydrodynamic radius is often associated with protein unfolding, which results in an apparent decrease in μ_{ep}, assuming negligible changes in the net charge state of the protein. Protein unfolding plots in CE typically consist of measured viscosity-corrected protein mobility as a function of denaturant concentration or temperature. This generates a sigmoidal curve with a linear transition region from high to low mobility for the folded and unfolded protein states, respectively. Assuming a two-state system undergoing rapid unfolding with interconverion, the apparent viscosity-corrected mobility of the protein ($\nu\mu^A_{ep}$) within the transition region is a weighted average of the mobilities of each fraction based on the following expression:

$$\nu\mu^A_{ep} = f_F \mu_{ep,F} + f_U \mu_{ep,U} = \frac{1}{1 + K_U} \mu_{ep,F} + \frac{K_U}{1 + K_U} \mu_{ep,U} \tag{1-25}$$

where $\mu_{ep,F}$ is the mobility of the folded native protein and $\mu_{ep,U}$ is the mobility of the unfolded protein. Note that proteins unfolding under the slow-time regime, direct measurement of the peak area ratios of the resolved folded and unfolded protein states are used to determine K_U in **Eq. 1-22** instead of **Eq. 1-25**.

Hilser and Freie[111] have defined unfolding time regimes as slow, intermediate and fast, relative to the time-scale of CE separations for reversible reactions. In the slow-time regime, the time required for electrophoretic separation is less than the time required for unfolding transitions ($t << k_1^{-1} + k_2^{-1}$). In this case, the protein does not interconvert during separation, and more than one peak is observed for each population state since they can be separated in time by CE based on differences in μ_{ep}. Consequently, samples must be equilibrated or incubated off-line prior to CE analyses. Also, unlike with fast time regime unfolding, a two-state assumption is not required, since unfolding intermediates can be resolved by CE. This is a unique advantage of CE based protein unfolding studies, since unlike conventional spectroscopic techniques, it allows for the direct measurement and resolution of multiple protein unfolding intermediate conformers.

In the fast time regime, the rate for protein folding or unfolding is much faster than the time required for separation ($t >> k_1^{-1} + k_2^{-1}$), which allows the different protein fractions to reach equilibrium. This situation results in the appearance of a single protein peak in the electropherogram, which represents a weighted average of all populated states of the protein (*e.g.,* two-state system).

Since equilibrium is reached well before the sample zone migrates past the detector, unfolding studies by CE can be performed dynamically in-capillary without off-line pre-equilibration. This allows for rapid analysis times and reduced consumption of protein since the same sample (< 50 μL) can be re-injected throughout the entire study. The proteins studied in this thesis were shown to unfold with apparent two-state kinetics under the fast-time regime.

In the intermediate time regime, the length of time required for electrophoretic separation is long enough to allow only a fraction of the protein conformations to interconvert between the folded and unfolded states, while others remain unchanged $(t \sim k_1^{-1} + k_2^{-1})$. This results in the appearance of a raised band between the peaks representing partial folded/unfolded conformations and is a common indicator of a multi-step process, where intermediate conformations cannot be assumed to be negligible. In fact, some previously described two-state proteins such as ribonuclease S6 have been demonstrated to have unfolding intermediates.[112] CE conditions can be optimized (*e.g.,* capillary length, applied voltage, pre-incubation time) to improve protein peak resolution in cases where intermediate time regime unfolding processes are initially observed.

Proteins can be thermally or chemically unfolded.[113] As discussed previously, thermal unfolding often requires modification to commercially available CE instrumentation. Unfolding thermodynamics can be derived by direct adaptation of equations from differential scanning calorimetry.[80] However, many proteins are irreversibly thermally unfolded due irreversible aggregation.

Chemical unfolding is accomplished by the addition of chaotropic agents to the separation buffer such as urea,[114] which is compatible with CE studies since it is a neutral and UV transparent additive that does not contribute to Joule heating. However, the addition of high concentrations of urea (*e.g.*, 7 M urea) required for complete protein unfolding can result in significant increases in solution viscosity, which requires correction to measured protein mobilities. Within the transition region, K_U can be determined via the linear extrapolation method,[115] which was originally introduced for equilibrium analysis by optical rotation methods. The equations have since been modified to be applied to other free solution studies, including CE, by rearrangement of **Eq. 1-25**:

$$K_U = \frac{\nu\mu_{ep}^A - \mu_{ep,F}}{\mu_{ep,U} - \nu\mu_{ep}^A} \tag{1-26}$$

where, K_U is the apparent protein unfolding equilibrium constant, which can be used to calculate the apparent free energy change for protein unfolding (ΔG_U):

$$\Delta G_U = -RT \ln K_U \tag{1-27}$$

$$\Delta G_U = \Delta G_U^0 - mc \tag{1-28}$$

where ΔG_U^0 is the standard free energy change for protein unfolding extrapolated to non-denaturing conditions (*i.e.,* 0 M urea), m is the cooperativity of unfolding which is related to the rate of change of ΔG and c is the concentration of urea. The transition region is characterized by a mid-point concentration where there is an equal fraction of unfolded and folded protein states referred to as C_M. In general, a high ΔG_U^0 parameter infers a conformational stable protein more

resistant to urea denaturation. Non-linear regression methods[85] can also be used to determine these parameters from the CE unfolding curve based on re-arrangement of **Eq. 1-26** to **1-28**:

$$\nu \mu_{ep}^{A} = \frac{\mu_{ep,F} + \mu_{ep,U} \cdot \left(e^{-(\Delta G^{0} - m[urea])} \middle/ RT \right)}{1 + \left(e^{-(\Delta G^{0} - m[urea])} \middle/ RT \right)} \tag{1-29}$$

1.5.3. Applications

To date, a variety of wild-type and recombinant proteins that exhibit slow and fast kinetics have been examined by CE. Those which exhibit slow unfolding kinetics take advantage of the resolving power of CE to separate the different protein conformational states and their intermediates. For instance, the unfolding of β-lactoglobulin was first reported by Skelsey and Bushey[116] who monitored urea-induced unfolding and subsequent refolding with and without the presence of the reducing agent, dithiothreitol (DTT). In this work, since the protein unfolds slowly relative to the electrophoretic separation time after offline equilibration, urea was omitted from the separation buffer with the assumption that refolding was negligible. Skelsey and Bushey confirmed that reversible protein refolding was not observed for β-lactoglobulin in the presence of DTT after urea denaturation. The thermal unfolding of β-lactoglobulin was later reported using CE by Rochu *et al.*[89, 90] in the first report in which CE was used to determine the change in heat capacity (ΔC_p) for the unfolding process. These studies offered insight into the unfolding pathways of β-lactoglobulin demonstrating that the

extent of both oligomerization and aggregation depended on both buffer pH and temperature. For example, β-lactoglobulin at pH 6 was found to exist in its native dimeric conformation converting to the native monomer, molten globular and finally the unfolded monomer (with aggregates) in that order upon successive increase in temperature. The experiments demonstrated the utility of CE for probing the pH- and temperature-dependence of protein quaternary structure.

The kinetics of unfolding for slow unfolding reactions can also be determined by CE and was first demonstrated for muscle acylphosphatase (AcP) with urea denaturation by Verzola et al.[84] In these experiments, the rate of unfolding was determined for AcP within a urea concentration range of 4.5-8 M. The kinetics for unfolding was confirmed to be pseudo-first order since the process was unimolecular, with faster rates measured at higher urea concentrations. At 7 M urea, the apparent rate constant for unfolding was determined to be (0.00030 ± 0.00006) s^{-1}.

Several studies have also been performed on proteins that unfold irreversibly under the slow-time regime based on the Lumry-Eyring model. Protein unfolding studies by CE of phosphotriesterase (PTE) with various metal cations substituted into the active site[87, 95] as well as different cholinesterases [91, 94, 117] have been reviewed by Rochu and Masson. [92] The results obtained by CE thermal unfolding studies were validated using differential scanning calorimetry. A noteworthy study of Bungarus fasciatus acetylcholinesterase showed that this enzyme possessed a unique asymmetrical distribution of charged residues, which

leads to a denaturation-like transition as a function of increasing electric field. This effect subsequently interfered with the ability to determine specific unfolding parameters. This study demonstrated the potential bias of CE relative to other techniques when examining receptor-ligand complexes that can induce separation of a protein from its non-covalently bound ligand due to mobility differences. This effect can be avoided by initial characterization of the protein system and optimization of CE separation conditions.

Although many proteins can unfold in the fast-time regime, cytochrome c (cyt. c) has been the model protein of choice examined by CE. Ishihama et $al.$ performed thermal-induced unfolding on cyt. c and a series of other proteins with subsequent validation by circular dichroism.[118] This was the first report of dynamic unfolding by CE, referred to as direct in-capillary incubation during electromigration, which highlighted the unique benefit of studying protein unfolding in the fast-time regime. Since the time required for equilibrium is often much longer than the time required for analysis, dynamic protein unfolding by CE significantly shortens total analysis time. Additionally, since samples did not require off-line pre-incubation, the same small volume sample (< 20 μL) could be injected multiple times to complete protein unfolding studies at different temperatures. The unfolding/refolding behaviour of cyt. c was also examined by Righetti et $al.$ [119] with isoelectric buffers using both thermal and urea denaturation. The ΔG_U^0 of folding/unfolding transitions for cyt. c was later studied by the same group as a function of buffer pH. [85] A variation of 7-10

kcal/mol was found between ΔG_U^0 over the range of pH 2.5-6.0, which highlighted the electrostatic contribution to protein conformational stability. The authors suggest that at low pH cyt. *c* undergoes additional stretching of the polypeptide chain due to Columbic repulsion of positive charges thus resulting in a decrease in ΔG_U^0 with decreasing pH.[83]

The majority of unfolding studies in CE have examined monomeric ligand-free *apo*-protein systems. However, CE offers a unique format for studying the unfolding dynamics of receptor-ligand or *holo*-protein complexes, where the mobilities of the free receptor and its ligand (or cofactor) are different. In fact, many proteins act as receptors to ligands or are dependent on the presence of bound cofactors for their biological activity. Ligand binding to a receptor can induce a conformational change in the ligand-free apoprotein, which plays a vital role in the allosteric regulation of many cellular proteins.[120, 121] Few unfolding studies have been performed by CE which takes into consideration the impact of ligand-binding on proteins. A related study was reported by McIntosh *et al.* to assess the impact of additives on the stability of protein using CE.[122] In this study, the effect of various excipients on the thermal denaturation of ribonuclease A (RNase A) at low pH was examined. The authors determined that the addition of sorbitol or sucralose to the separation buffer shifted T_m to higher temperatures, whereas addition of polyethylene glycol 400 or 2-methyl-2,4-pentanediol resulted in no significant change. The resulting increase in apparent T_m was consistent with previous reports, which indicates that high concentrations of sugar additives

such as sorbitol stabilize the folded conformation of the protein. In the absence of water, sugar hydrogen bonding can replace water hydrogen bonds to polar or charged sites in the protein.

The impact of a protein-dependent co-factor was considered by Gudiksen *et al.* using bovine carbonic anhydrase.[123] Unfolding was performed in GdnHCl with refolding by dilution in a separation buffer containing the metal cofactor Zn^{2+}. Although the cofactor was not required for refolding to occur, its presence allowed for a greater recovery of refolded protein, providing evidence that ligand addition enhanced stability of the native state of protein. Similarly, Rochu and co-workers demonstrated that decamethonium bound to the gorge of cholinesterases stabilizes the protein native state, which resulted in an increase in apparent T_m by 9.5°C. [94] The increase in protein stability was believed to be due to the additional non-covalent bonds formed with the bound-ligand. The discovery of the residual decamethonium bound cholinesterase in their preparations highlighted an important advantage of performing unfolding studies by CE for assessing the purity of protein samples. It also provides a means for comparative study of the impact of bound ligand on the conformational stability of the protein directly by CE without sample pre-treatment. Chapters II and III of the thesis will discuss the advantages in using CE for comparative assessment of protein-ligand stability with allosteric regulatory proteins.

1.6. Enzyme Kinetics

The sensitivity and small sample volumes used in CE make it an ideal tool for studying enzyme reactions. Compared to traditional methods (*eg.* photometric, colorimetric or coupled assays), in CE enzyme products and substrates can be measured simultaneously in a rapid, label-free manner with high sensitivity and low sample/reagent consumption[124] which makes evaluation of single enzymes possible.[125] These assays can be performed in heterogeneous and homogeneous manners with pre-, post- and in-capillary reactions. Post-capillary reactions are traditionally performed with substrate, cofactor or enzymes that have been separated by CE. Post-capillary reactions are predominantly performed with home-made instruments and are typically incompatible with commercially available instruments.[126] They are therefore most suitable for microchip based systems and will not be discussed further. Fundamental principles and major assay types will be described in this section. Detailed assay development will be provided in Chapter IV which highlights the versatile selectivity offered by CE-based assays as general strategy for assessment of enzyme kinetics.

1.6.1. Michaelis-Menten Enzyme Kinetics

Many enzymes can be described by the kinetic equations developed by Leonor Michaelis and Maud Menten.[127] This kinetic model is based on steady-state behaviour in a large excess of substrate. It is assumed that the enzyme-substrate complex (ES) is formed quickly and that the rate of ES formation and

breakdown is essentially constant over the time course the reaction is measured. It is thereby assumed that the enzyme remains essentially saturated. The typical Michealis-Menten curve is shown in **Figure 1.7** and the rate of the reaction is described by the following equations:

$$E + S \underset{k_{-1}}{\overset{k_1}{\rightleftharpoons}} ES \overset{k_2}{\rightleftharpoons} E + P$$

$$(1\text{-}30)$$

$$V_0 = \frac{V_{max} \cdot [S]}{K_M + [S]}$$

$$(1\text{-}31)$$

where V_0 is the initial velocity of the reaction, V_{max} is the maximum velocity, $[S]$ is the substrate concentration, and K_M is the Michaelis-Menten constant defined as the substrate concentration at half the maximum velocity. K_M is related to the kinetic rate constants in **Eq. 1-30** and provides a measure of substrate affinity when k_2 is rate limiting ($k_2 \ll k_{-1}$). The rate limiting step of a saturated Michaelis-Menten reaction (**Eq. 1-30**) can be described by the turnover number (k_{cat}):

$$k_{cat} = \frac{V_{max}}{E_T}$$

$$(1\text{-}32)$$

where E_T is the total enzyme concentration. This parameter as well as K_M and V_{max} vary for different enzymes and the specificity constant (k_{cat}/K_M) is often used to compare different enzymes or different substrates. Most enzymes possess specificity constants towards $10^8 - 10^9$ $M^{-1}s^{-1}$ which is the diffusion controlled upper limit. K_M and V_{max} can be determined from non-linear regression of
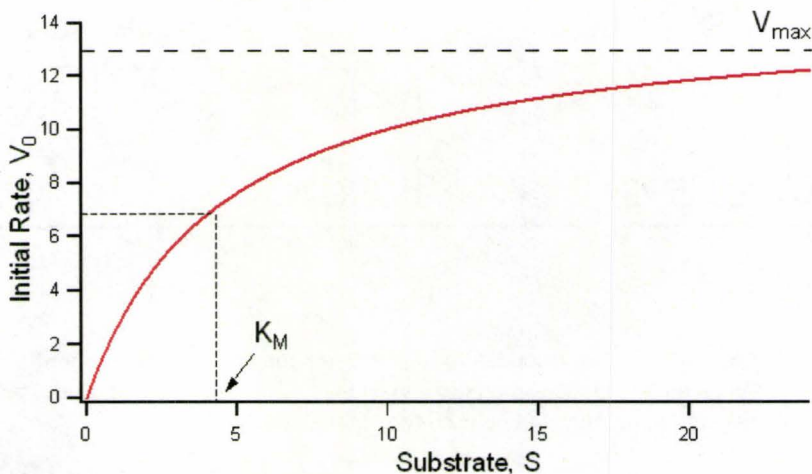
Figure 1.7. Effect of substrate concentration on the initial velocity of a typical enzyme-catalyzed reaction.

experimental data using **Eq. 1-31** or by linearizing the data via the double-reciprocal plot as described by the Lineweaver-Burke equation:

$$\frac{1}{V_0} = \frac{K_M}{V_{max} \cdot [S]} + \frac{1}{V_{max}}$$

(1-33)

Inhibitors (competitive, non-competitive, mixed) are typically classified based on their effect on K_M and V_{max}, and subsequent effect on the appearance of the Lineweaver-Burke plot (**Figure 1.8**). The extent to which K_M and V_{max} are modified, by factors α and α' for respective competitive and non-competitive inhibition, can be used to determine the inhibition constant (K_I):

$$\alpha = 1 + \frac{[I]}{K_I}$$

(1-34)

The potency of inhibition is typically expressed in terms of the half maximal inhibitory concentration (IC_{50}), which is the concentration of inhibitor which
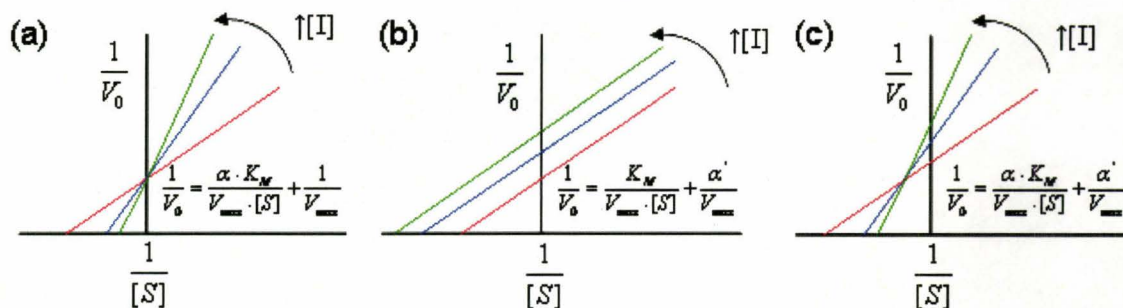
Figure 1.8. The effect of increasing concentration of competitive (a), non-competitive (b), and mixed (c) inhibitors in an enzyme reaction on the appearance of the Lineweaver-Burke plot, where α and α' are the modifying factors that can be used to calculate K_I.

reduces enzyme activity by 50%. IC_{50} can be calculated from dose-dependant curves or from known K_I values based the following expression:[128]

$$K_I = \frac{IC_{50}}{1 + \frac{[S]}{K_M}} \tag{1-35}$$

1.6.2. Pre-Capillary Assays

Pre-capillary assays involve breaking up the complete analysis into the kinetic reaction followed by separation.[124, 129, 130] There are two main types of pre-capillary assays. The first typically involves performing a bulk enzyme reaction where aliquots are withdrawn at different time points and quenched by addition of a denaturant (*e.g.* acetonitrile, acid or base) or by thermal denaturation of the enzyme (*e.g.* boiling). The advantage to performing this type of assay is that once quenched, stability permitting, samples can be stored for later analysis or loaded into a sequence on an automated instrument. Having an individual sample for each time point also allows replicate measurements, which permits

determination of instrumental precision and accuracy, and permits for longer analysis times in order to resolve complex sample mixtures such as amino acid stereoisomers. Sample pre-treatment (*e.g.* extraction, filtration, labelling, etc) is also possible if the reaction conditions are less than optimal for CE. Although off-line quenching is arguably the simplest approach to evaluation of kinetics by CE, it is also the most time consuming. Therefore methods which further utilize instrument automation and minimize sample handling are desirable.

The second type of pre-capillary assay involves performing repeated, sequential injections onto the CE column from the bulk enzyme reaction in order to sample the reaction mixture at discrete time intervals.[129] In this case, the injected sample can be completely electrophoresed out of the column before injection of the next time point, or if resolution permits, electrophoresis may be started for the first sample, then paused while the next sample is injected, resulting in a series of product peaks representing different time points in the same electropherogram. This approach is advantageous, due to the reduced sample handling and low reaction volume required, however it also suffers from several drawbacks. Replicate measurements cannot be performed for the same sample at each time point and the reaction kinetics and reaction matrix must be suitable for analysis. For example, in order to evaluate an enzyme with fast reaction kinetics, the matrix must be simple to permit resolution of the substrate and/or product. If the matrix is complex, the substrate/product may not be resolved from interferences or too few points captured in the enzyme's linear

range. Assays can be repeated in order to obtain replicate data, however, the pooled data would represent inter- vs. intra-assay error. Lastly, one practical aspect that must be accounted for is the time required by the robotics of commercial instruments during sampling as the total lag from robotics movements can contribute to several minutes for a single CE run.

1.6.3. In-Capillary Assay

To simplify the sample handling while providing more control over timing and separation optimization, Bao and Regnier introduced electrophoretically mediated microanalysis (EMMA).[131] EMMA can be further subdivided into continuous or plug-plug mode (**Figure 1.9**). In continuous mode, the entire capillary is filled with either substrate (or enzyme). A plug of enzyme (or substrate) is then introduced into the capillary and is mixed during electrophoresis. The product accumulates as the enzyme plug migrates through the capillary and appears as a broad, flat-topped peak in the electropherograms. The concentration of the product can then be correlated to the height of area of this peak.

In plug-plug mode, the enzyme and substrate are introduced into the capillary as separate plugs which are them mixed by the application of voltage. In normal mode CE, the reactant with the lower electrophoretic mobility is typically loaded onto the capillary first, followed by a spacer, then by the reactant of higher electrophoretic mobility. The spacer serves to prevent the enzyme and substrate
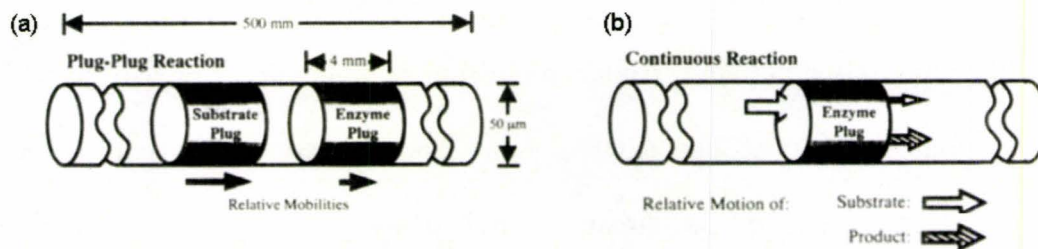
Figure 1.8. Schematic representation of plug-plug (a) and continuous (b) mode of EMMA. Adapted with permission from Avila, L. Z.; Whitesides, G. M., *J. Org. Chem.* **1993,** *58* (20), 5508. Copyright 1993 American Chemical Society.

from interacting prior to mixing, avoiding premature accumulation of product before the programmed mixing and reaction (wait) time. Plug-plug embodies a highly advantageous approach to performing enzyme assays since it takes true advantage of the microscale nature of CE platforms utilizing only nL of enzyme and substrate per assay. Stock solutions (µL) can be injected multiple times for CE assays with different programmed reaction times allowing data for an entire Michaelis-Menten curve to be collected with a single set of solutions.

Since the publication of Bao and Regnier's seminal paper, where they measured the activity of NADP-dependant glucose-6-phosphate dehydrogenase in 1992, more than 100 papers have been published utilising EMMA to perform CE-based enzyme kinetics. Adaptations have been made to allow for analysis of enzymes which require a different reaction buffer than what is optimal for CE separation. Notably, Van Dyck *et al.* introduced a partial filling method, in which part of the capillary is filled with reaction buffer while the rest is filled with the appropriate BGE.[132] In this assay, bovine plasma amine oxidase (PAO) activity was measured by combining EMMA and MEKC with partial filling where the

reaction buffer was devoid of micelle forming agents since they interfered with the optimal enzyme activity. This combination of techniques enabled them to detect minute levels of product (LOD = 3 μM) using microscale levels of enzyme (0.021 U/mL). Further developments in EMMA technology have lowered detection to picomolar levels[133] and allowed application to online protein digestion[134] as well as inhibitor screening.[135, 136]

1.7. Drug discovery

Recent advances in science and economic pressure have prioritized the need for the development of rapid, cost effective drug screening technology. Plate based assays embody the backbone of HTS in the pharmaceutical industry. These assays rely heavily on robotics and high-density well microplates (96, 384, 1536 wells) and are based on traditional biochemical assays such as ELISA (enzyme-linked immunosorbant assay), proliferation/cytotoxicity, reporter or binding assays. ELISA represents the majority of the heterogeneous HTS assay while homogeneous assays predominantly utilize fluorescent or radiolabels as reporters. Major advances to HTS involve strategies which minimize costs by reduction or elimination of labour, including new automation and computation for *in silico* screening,[137] or more information-rich approaches, such as NMR for evaluating protein-ligand interaction[138] or cell-based assays.[139]

The adoption of combinatorial chemistry approaches have dramatically increased the size of compound libraries to be screened for drug activity, while

new developments in biology continue to uncover growing numbers of new potential therapeutic targets.[140] A typical library can range from 100 000 to 2 000 000 compounds. In order to cope with the volume and costs associated with such large screens, HTS has moved towards miniaturization, with preference towards systems which utilize microscale quantities of reagents and can incorporate multiple sample pre-treatment steps. There has also been movement towards the development of cell-based assays for high-content screening (HCS) to address problems with late-stage attrition associated with traditional HTS screens.[10, 141, 142] By obtaining more information and evaluating pharmacokinetic properties (ADME – adsorption, distribution, metabolism, excretion) earlier in the screening process, newer screening formats aim to circumvent late-stage attrition by eliminating hits with inappropriate ADME properties[143] and by accurately evaluating potential interactions.[144]

CE offers high resolving power for evaluating intact drugs from their metabolic and degradation products in biological matrices while having distinct advantages relative to LC techniques. A diverse array of applications have been reported using CE for drug screening based on enzyme activity,[145] pK_a evaluation,[146, 147] and $logP$[148] to list a few. CE has also played important roles in fundamental characterization of potential drugs, with much work focusing on stability and ADME,[149-152] interactions and adduct formation[153] as well as chiral purity analysis.[154] Many of these applications have been adopted to a multi-capillary array system, typically 96-capillaries suitable for HTS[155] and new

developments in microchip technology that benefit from miniaturization for improving sample throughput of electrophoretic assays.[156] However, adoption of CE by the greater scientific community has been slow, with major pharmaceutical industries preferring more traditional assays, such as fluorescence, scintillation proximity assays or immunoassays, adapted to plate formats for identification and evaluation of drug hits and leads.[157]

Although these assays are well-established, they are not without flaws. The use of labels in fluorescent and scintillation assays are advantageous, by providing a highly sensitive detection format. However, they are also cumbersome since the assays require covalent attachment of the reporter which can adversely affect the binding event being examined resulting in less than desirable *in vivo* activity. Assay flexibility, for adaptations to new targets, is also limited, particularly with immuno-based assays which require raising of antibodies for the protein or enzyme being targeted which is a labour intensive process. Moreover, traditional assays are often unable to appropriately target and characterize non-ideal systems such as allosteric enzymes which undergo large conformational changes removed from the orthosteric substrate binding site. In some cases these problems stem from lack of appropriate physical information, for example, *in silico* screening for allosteric modulators requires identification of the allosteric binding site and adoption of the appropriate scaffold into the modelling program,[158] which is limited by crystal structure availability and further conformational evaluation to appropriately establish sites. In other cases, the

assay itself is too simple to provide apt assessment for non-competitive phenomena, since allosteric modulator strength of binding does not necessarily translate to a conformational change.[159]   Thus, in order to screen for these types of inhibitors, a combination of equilibrium binding, non-equilibrium kinetic and functional assays are necessary.[160]   Consequently, although allosteric targets such as G-protein coupled receptors (GPCRs) represent ~30% of clinically prescribed drugs, the majority of these drugs are competitive inhibitors which target the orthosteric ligand-binding site due to the higher developmental costs associated with performing multiple analyses.[13, 161]   Allosteric sites of both protein receptors and enzymes therefore represent a largely untapped resource for drug development due to the need for new integrative screening approaches and validation methodology.

1.8. Research Objectives

The development of robust, high-quality screening methods for successful identification of biologically active ligands is critical in drug discovery. In this context, CE offers a unique platform in which integration of sample pre-treatment and control of dynamic interactions (*e.g.* protein-small molecule) can be achieved for analysis of complex systems (*e.g.* regulatory proteins and isomerase enzymes). There is a particular need for new analytical strategies for improved characterization and evaluation of allosteric targets and discovery of modulators. In order to enhance candidate selection in drug screening, the research in this

thesis is focused on development of novel CE strategies for evaluating biomolecular interactions. The ultimate objective is the design of a superior separation platform based on CE for high-quality screening. The work performed to achieve this goal can be grouped into two major research sections; evaluation of (a) receptor-ligand binding and (b) enzyme-substrate interactions. Within this thesis, several practical and fundamental challenges are addressed such as multivariate analysis of the thermodynamics of conformational change, integration of sample pre-treatment during chemical analysis, accurate prediction of binding affinity and activity in non-ideal systems and unbiased evaluation of isomerase kinetics for inhibitor screening. The latter includes development of stereoselective protocol that is suitable for screening of enantiomers, diastereomers, and structural isomers, which highlights the versatility of CE. Finally, the thesis will conclude with a summary of the unique contributions the work presented has made to the greater scientific community, as well as highlight future directions for research, most notably in discovery of allosteric modulators that can serve as pharmaceutical chaperones.[162-164]

1.9. References

1.   Schou, C.; Heegaard, N. H. H., *Electrophoresis* **2006**, *27*, 44.

2.   Colton, I. J.; Carbeck, J. D.; Rao, J.; Whitesides, G. M., *Electrophoresis* **1998**, *19*, 367.

3.   Rundlett, K. L.; Armstrong, D. W., *Electrophoresis* **2001**, *22*, 1419.

4.   Krylov, S. N., *Electrophoresis* **2007**, *28*, 69.

5.   Desai, M. J.; Armstrong, D. W., *Microbiol. Mol. Biol. Rev.* **2003**, *67*, 38.

6.   Lantz, A. W.; Bao, Y.; Armstrong, D. W., *Anal. Chem.* **2007**, *79*, 1720.

7.   Turner, E. H.; Lauterbach, K.; Pugsley, H. R.; Palmer, V. R.; Dovichi, N. J., *Anal. Chem.* **2007**, *79*, 778.

8.   Olson, K. J.; Ahmadzadeh, H.; Arriaga, E. A., *Anal. Bioanal. Chem.* **2005**, *382*, 906.

9.   Dovichi, N. J.; Zhang, J. Z., *Angew. Chemie Int. Ed.* **2000**, *39*, 4463.

10.   Bleicher, K. H.; Bohm, H. J.; Muller, K.; Alanine, A. I., *Nat. Rev. Drug Discovery* **2003**, *2*, 369.

11.   Dove, A., *Nat. Biotechnol.* **2003**, *21*, 859.

12.   Fenton, A. W., *Trends Biochem. Sci.* **2008**, *33*, 420.

13.   Milligan, G.; Smith, N. J., *Trends Pharmacol. Sci.* **2007**, *28*, 615.

14.   Giddings, J. C., *Unified Separation Science*. John Wiley & Sons: New York, 1991.

15.   Yeung, E. S., *J. Chromatogr. A* **1999**, *830*, 243.

16.   Armstrong, D. W.; Schulte, G.; Schneiderheinze, J. M.; Westenberg, D. J., *Anal. Chem.* **1999,** *71*, 5465.

17.   Fanali, S., *J. Chromatogr. A* **2000,** *875*, 89.

18.   Poinsot, V.; Rodat, A.; Gavard, P.; Feurer, B.; Couderc, F., *Electrophoresis* **2008,** *29*, 207.

19.   Vesterberg, O., *Electrophoresis* **1993,** *14*, 1243.

20.   Kohlrausch, F., *Wiedemans Ann.* **1897,** *62*, 209.

21.   Tiselius, A., *Trans. Faraday Soc.* **1937,** *33*, 524.

22.   Svedberg, T., *J. Biol. Chem.* **1933,** *103*, 311.

23.   Svensson, H., *Arkiv. Kemi Mineral. Geol.* **1946,** *22A*.

24.   Longsworth, L. G., Moving Boundary Electrophoresis - Theory. In *Electrophoresis, Theory, Methods and Applications*, Bier, M., Ed. Academic Press: New York, 1959; pp 91.

25.   Dole, V. P.; Braun, E., *J. Clin. Invest.* **1944,** *23*, 708.

26.   Cramer, R.; Svensson, H., *Cell. Mol. Life Sci.* **1961,** *17*, 49.

27.   Hjerten, S., *Biochim Biophys Acta* **1961,** *53*, 514.

28.   Hjerten, S., *Chromatogr Rev* **1967,** *9*, 122.

29.   Mikkers, F. E. P., *J. Chromatogr.* **1979,** *169*, 11.

30.   Jorgenson, J. W.; Lukacs, K. D., *Anal. Chem.* **1981,** *53*, 1298.

31.   Jorgenson, J. W.; Lukacs, K. D., *Science* **1983,** *222*, 266.

32.   Gubitz, G.; Schmid, M. G., *J. Chromatogr. A* **1997,** *792*, 179.

33.   Kasicka, V., *Electrophoresis* **2009,** *30*, 2257.

34.   Pritchett, T.; Robey, F. A., Capillary Electrophoresis of Proteins. In *Handbook of Capillary Electrophores*, 2nd ed.; Landers, J. P., Ed. CRC Press: Boca Raton, 1997; pp 259.

35.   Dolnik, V., *Electrophoresis* **2008,** *29*, 143.

36.   Righetti, P. G.; Gelfi, C.; D'Acunto, M. R., *Electrophoresis* **2002,** *23*, 1361.

37.   Chen, F. T. A.; Liu, C. M.; Hsieh, Y. Z.; Sternberg, J. C., *Clin. Chem.* **1991,** *37*, 14.

38.   Benavente, F.; Hernandez, E.; Guzman, N. A.; Sanz-Nebot, V.; Barbosa, J., *Anal. Bioanal. Chem.* **2007,** *387*, 2633.

39.   Tagliaro, F.; Bortolotti, F., *Electrophoresis* **2008,** *29*, 260.

40.   Martinez, D.; Cugat, M. J.; Borrull, F.; Calull, M., *J. Chromatogr. A* **2000,** *902*, 65.

41.   Menzinger, F.; Schmitt-Kopplin, P.; Freitag, D.; Kettrup, A., *J. Chromatogr. A* **2000,** *891*, 45.

42.   Mischak, H.; Coon, J. J.; Novak, J.; Weissinger, E. M.; Schanstra, J. P.; Dominiczak, A. F., *Mass Spec. Rev.* **2009,** *28*, 703.

43.   Shanmuganathan, M.; Britz-McKibbin, P., Screening for allosteric modulators of γλυχοχεραμιδασε βψ χapillary electrophoresis. McMaster University: Hamilton, 2009.

44.   Margulies, M.; Egholm, M.; Altman, W. E.; Attiya, S.; Bader, J. S.; Bemben, L. A.; Berka, J.; Braverman, M. S.; Chen, Y. J.; Chen, Z. T.;

Dewell, S. B.; Du, L.; Fierro, J. M.; Gomes, X. V.; Godwin, B. C.; He, W.; Helgesen, S.; Ho, C. H.; Irzyk, G. P.; Jando, S. C.; Alenquer, M. L. I.; Jarvie, T. P.; Jirage, K. B.; Kim, J. B.; Knight, J. R.; Lanza, J. R.; Leamon, J. H.; Lefkowitz, S. M.; Lei, M.; Li, J.; Lohman, K. L.; Lu, H.; Makhijani, V. B.; McDade, K. E.; McKenna, M. P.; Myers, E. W.; Nickerson, E.; Nobile, J. R.; Plant, R.; Puc, B. P.; Ronan, M. T.; Roth, G. T.; Sarkis, G. J.; Simons, J. F.; Simpson, J. W.; Srinivasan, M.; Tartaro, K. R.; Tomasz, A.; Vogt, K. A.; Volkmer, G. A.; Wang, S. H.; Wang, Y.; Weiner, M. P.; Yu, P. G.; Begley, R. F.; Rothberg, J. M., *Nature* **2005,** *437*, 376.

45.   Reyes, D. R.; Iossifidis, D.; Auroux, P. A.; Manz, A., *Anal. Chem.* **2002,** *74*, 2623.

46.   Camilleri, P., *Chem. Comm.* **1996,** *16*, 1851.

47.   Landers, J. P., *Handbook of Capillary Electrophoresis.* CRC Press: Boca Raton, FL, USA, 1997.

48.   Terabe, S., *Annu. Rev. Anal. Chem.* **2009,** *2*, 99.

49.   Mazzeo, J. R., Micellar Electrokinetic Chromatography. In *Handbook of Capillary Electrophoresis*, Second ed.; Landers, J. P., Ed. CRC Press: New York, 1997; pp 49.

50.   Silvertand, L. H. H.; Torano, J. S.; van Bennekom, W. P.; de Jong, G. J., *J. Chromatogr. A* **2008,** *1204*, 157.

51.   Beckers, J. L.; Bocek, P., *Electrophoresis* **2000,** *21*, 2747.

52.   Swerdlow, H.; Gesteland, R., *Nucleic Acids Res.* **1990,** *18*, 1415.

53.   Swerdlow, H.; Wu, S.; Harke, H.; Dovichi, N. J., *J. Chromatogr.* **1990,** *516*, 61.

54.   Steiner, F.; Scherer, B., *J. Chromatogr. A* **2000,** *887*, 55.

55.   Quirino, J. P.; Terabe, S., *J. Chromatogr. A* **2000,** *902*, 119.

56.   Britz-McKibbin, P.; Chen, D. D. Y., *Anal. Chem.* **2000,** *72*, 1242.

57.   Britz-McKibbin, P.; Terabe, S., *J. Chromatogr. A* **2003,** *1000*, 917.

58.   Terabe, S.; Otsuka, K.; Ichikawa, K.; Tsuchiya, A.; Ando, T., *Anal. Chem.* **1984,** *56*, 111.

59.   Fanali, S., *J. Chromatogr. A* **1996,** *735*, 77.

60.   Otsuka, K.; Terabe, S., *J. Chromatogr. A* **2000,** *875*, 163.

61.   Terabe, S.; Otsuka, K.; Ando, T., *Anal. Chem.* **1985,** *57*, 834.

62.   Matsubara, N.; Terabe, S., *Chromatographia* **1992,** *34*, 493.

63.   Li, S.; Purdy, W. C., *Chem. Rev.* **1992,** *92*, 1457.

64.   Gutterman, A., Capillary Electrophoresis Separatin of Enantiomers by Cyclodextrin Array Chiral Analysis. In *Handbook of Capillary Electrophoresis*, Second ed.; Landers, J. P., Ed. CRC Press: New York, 1997; pp 75.

65.   Luong, J. H. T.; Nguyen, A. L., *J. Chromatogr. A* **1997,** *792*, 431.

66.   Stalcup, A. M.; Gahm, K. H., *Anal. Chem.* **1996,** *68*, 1360.

67.   de Boer, T.; de Zeeuw, R. A.; de Jong, G. J.; Ensing, K., *Electrophoresis* **2000,** *21*, 3220.

68.   Oda, R. P., Introduction to Capillary Electrophoresis. In *Handbook of Electrophoresis*, 2nd ed.; Landers, J. P., Ed. CRC Press: Boca Raton, Landers, J. P.; pp 1.

69.   Ptolemy, A. S. Single-Step Analysis of Metabolites by Capillary Electrophoresis using On-Line Sample Pre-Concentration with Chemical Derivatization. Ph.D., McMaster University, Hamilton, 2007.

70.   Bowser, M. T.; Bebault, G. M.; Peng, X. J.; Chen, D. D. Y., *Electrophoresis* **1997**, *18*, 2928.

71.   Kaiser, C.; Segui-Lines, G.; D'Amaral, J. C.; Ptolemy, A. S.; Britz-McKibbin, P., *Chem. Comm.* **2008**, 338.

72.   Matouschek, A., *Curr. Opin. Struct. Biol.* **2003**, *13*, 98.

73.   Matouschek, A.; Bustamante, C., *Nat. Struct. Biol.* **2003**, *10*, 674.

74.   Burton, B. M.; Baker, T. A., *Protein Sci.* **2005**, *14*, 1945.

75.   Markossian, K. A.; Kurganov, B. I., *Biochemistry-Moscow* **2004**, *69*, 971.

76.   Saibil, H., *Curr. Opin. Struct. Biol.* **2000**, *10*, 251.

77.   Lee, C.; Yu, M. H., *Protein folding and diseases*. 2005; Vol. 38, p 275.

78.   Soto, C., *Nat. Rev. Neurosci.* **2003**, *4*, 49.

79.   Bruylants, G.; Wouters, J.; Michaux, C., *Curr. Med. Chem.* **2005**, *12*, 2011.

80.   Makhatadze, G. I., Thermal unfolding of proteins studied by calorimetry. In *Protein Folding Handbook*, Buchner, J.; Kiefhaber, T., Eds. Wiley-VCH: Weinheim, 2005; Vol. 1, pp 70.

81.   Rush, R. S.; Cohen, A. S.; Karger, B. L., *Anal. Chem.* **1991,** *63*, 1346.

82.   Righetti, P. G., *Biopharm. Drug. Disp.* **2001,** *22*, 337.

83.   Stellwagen, E.; Gelfi, C.; Righetti, P. G., *J. Chromatogr. A* **1999,** *838*, 131.

84.   Verzola, B.; Chiti, F.; Manao, G.; Righetti, P. G., *Anal. Chem.* **2000,** *282*, 239.

85.   Verzola, B.; Fogolari, F.; Righetti, P. G., *Electrophoresis* **2001,** *22*, 3728.

86.   Verzola, B.; Perduca, M.; Mezo, G.; Hudecz, F.; Righetti, P. G., *Electrophoresis* **2003,** *24*, 794.

87.   Rochu, D.; Beaufet, N.; Renault, F.; Viguie, N.; Masson, P., *Biochim. Biophys. Acta* **2002,** *1594*, 207.

88.   Rochu, D.; Clery-Barraud, C.; Renault, F.; Chevalier, A.; Bon, C.; Masson, P., *Electrophoresis* **2006,** *27*, 442.

89.   Rochu, D.; Ducret, G.; Masson, P., *J. Chromatogr. A* **1999,** *838*, 157.

90.   Rochu, D.; Ducret, G.; Ribes, F.; Vanin, S.; Masson, P., *Electrophoresis* **1999,** *20*, 1586.

91.   Rochu, D.; Georges, C.; Repiton, J.; Viguie, N.; Saliou, B.; Bon, C.; Masson, P., *Biochem. Biophys. Acta* **2001,** *1545*, 216.

92.   Rochu, D.; Masson, P., *Electrophoresis* **2002,** *23*, 189.

93.   Rochu, D.; Pernet, T.; Renault, F.; Bon, C.; Masson, P., *J. Chromatogr. A* **2001,** *910*, 347.

94.   Rochu, D.; Renault, F.; Masson, P., *Electrophoresis* **2002,** *23*, 930.

95.   Rochu, D.; Viguie, N.; Renault, F.; Crouzier, D.; Froment, M. T.; Masson, P., *Biochem. J.* **2004**, *380*, 627.

96.   Gavina, J. M. A.; Das, R.; Britz-McKibbin, P., *Electrophoresis* **2006**.

97.   De Lorenzi, E.; Grossi, S.; Massolini, G.; Giorgetti, S.; Mangione, P.; Andreola, A.; Chiti, F.; Bellotti, V.; Caccialanza, G., *Electrophoresis* **2002**, *23*, 918.

98.   Heegaard, N. H. H.; Sen, J. W.; Kaarsholm, N. C.; Nissen, M. H., *J. Biol. Chem.* **2001**, *276*, 32657.

99.   Fan, Z. H.; Jensen, P. K.; Lee, C. S.; King, J., *J. Chromatogr. A* **1997**, *769*, 315.

100.   Horvath, J.; Dolnik, V., *Electrophoresis* **2001**, *22*, 644.

101.   Righetti, P. G.; Gelfi, C.; Verzola, B.; Castelletti, L., *Electrophoresis* **2001**, *22*, 603.

102.   Yassine, M. M.; Lucy, C. A., *Anal. Chem.* **2005**, *77*, 620.

103.   Righetti, P. G.; Gelfi, C.; Bossi, A.; Olivieri, E.; Castelletti, L.; Verzola, B.; Stoyanov, A. V., *Electrophoresis* **2000**, *21*, 4046.

104.   Kawahara, K.; Tanford, C., *J. Biol. Chem.* **1966**, *241*, 3228.

105.   Righetti, P. G.; Verzola, B., *Electrophoresis* **2001**, *22*, 2359.

106.   Jensen, P. K.; Lee, C. S.; King, J. A., *Anal. Chem.* **1998**, *70*, 730.

107.   Segui-Lines, G.; Gavina, J. M. A.; D'Amaral, J.; Britz-McKibbin, P., *Analyst* **2007**, *132*, 741.

108.   Heegaard, N. H. H.; Rovatti, L.; Nissen, M. H.; Hamdan, M., *J. Chromatogr. A* **2003**, *1004*, 51.

109.   Stutz, H.; Bordin, G.; Rodriguez, A. R., *Electrophoresis* **2004**, *25*, 1071.

110.   Thannhauser, T. W.; Rothwarf, D. M.; Scheraga, H. A., *Biochemistry* **1997**, *36*, 2154.

111.   Hilser, V. J.; Freire, E., *Anal. Biochem.* **1995**, *224*, 465.

112.   Otzen, D., *PEDS* **2005**, *18*, 547.

113.   Buchner, J.; Kiefhaber, T., *Protein folding handbook*. Wiley-VCH: Weinheim, 2005; Vol. 1-5.

114.   Kilar, F.; Hjerten, S., *J. Chromatogr.* **1993**, *638*, 269.

115.   Greene, R. F.; Pace, C. N., *J. Biol. Chem.* **1974**, *249*, 5388.

116.   Skelsey, K. R.; Bushey, M. M., *J. Chromatogr. Sci.* **1996**, *34*, 85.

117.   Rochu, D.; Pernet, T.; Renault, F.; Bon, C.; Masson, P., *Journal of Chromatography A* **2001**, *910*, 347.

118.   Ishihama, Y.; Oda, Y.; Asakawa, N.; Iwakura, M., *Anal. Sci.* **1997**, *13*, 931.

119.   Stellwagen, E.; Gelfi, C.; Righetti, P. G., *Journal of Chromatography A* **1999**, *838*, 131.

120.   Swain, J. F.; Gierasch, L. M., *Curr. Opin. Struct. Biol.* **2006**, *16*, 102.

121.   Lindsley, J. E.; Rutter, J., *PNAS* **2006**, *103*, 10533.

122.   McIntosh, K. A.; Charman, W. N.; Charman, S. A., *J. Pharm. Biomed. Anal.* **1998**, *16*, 1097.

123.   Gudiksen, K. L.; Urbach, A. R.; Gitlin, I.; Yang, J.; Vazquez, J. A.; Costello, C. E.; Whitesides, G. M., *Anal. Chem.* **2004,** *76,* 7151.

124.   Bao, J. J.; Fujima, J. M.; Danielson, N. D., *J. Chromatogr. B* **1997,** *699,* 481.

125.   Craig, D. B.; Arriaga, E. A.; Wong, J. C. Y.; Lu, H.; Dovichi, N. J., *JACS* **1996,** *118,* 5245.

126.   Emmer, A.; Roeraade, J., *J Chromatogr* **1994,** *662,* 375.

127.   Nelson, D. L.; Cox, M. M., *Lehninger Priniples of Biochemistry.* Third ed.; Worth Publishers: New York, 2000.

128.   Howland, R. D.; Mycek, M. J., *Pharmacology.* 3rd ed.; Lippincott Williams & Wilkins: Baltimore, 2006.

129.   Glatz, Z., *J. Chromatogr. B.* **2006,** *841,* 23.

130.   Schultz, N. M.; Tao, L.; Rose, D. J. J.; Kennedy, R. T., Immunoassays and Enzyme Assays using Capillary Electrophoresis. In *Handbook of Capillary Electrophoresis*, Landers, J. P., Ed. CRC Press: New York, 1997; pp 611.

131.   Bao, J.; Regnier, F. E., *J. Chromatogr. A* **1992,** *608,* 217.

132.   Van Dyck, S.; Van Schepdael, A.; Hoogmartens, J., *Electrophoresis* **2001,** *22,* 1436.

133.   Lee, I. H.; Pinto, D.; Arriaga, E. A.; Zhang, Z. R.; Dovichi, N. J., *Anal. Chem.* **1998,** *70,* 4546.

134.   Zeisbergerova, M.; Adamkova, A.; Glatz, Z., *Electrophoresis* **2009**, *30*, 2378.

135.   Tang, Z. M.; Wang, Z. Y.; Kang, J. W., *Electrophoresis* **2007**, *28*, 360.

136.   Wang, T. D.; Kang, J. W., *Electrophoresis* **2009**, *30*, 1349.

137.   Abagyan, R.; Totrov, M., *Curr. Opin. Chem. Biol.* **2001**, *5*, 375.

138.   Meyer, B.; Peters, T., *Angew. Chemie Int. Ed.* **2003**, *42*, 864.

139.   Durr, O.; Duval, F.; Nichols, A.; Lang, P.; Brodte, A.; Heyse, S.; Besson, D., *J. Biomol. Screen.* **2007**, *12*, 1042.

140.   Golebiowski, A.; Klopfenstein, S. R.; Portlock, D. E., *Curr. Opin. Struct. Biol.* **2001**, *5*, 273.

141.   Haney, S. A.; LaPan, P.; Pan, J.; Zhang, A., *Drug Discovery Today* **2006**, *11*, 889.

142.   Keseru, G. M.; Makara, G. M., *Drug Discovery Today* **2006**, *11*, 741.

143.   White, R. E., *Annu. Rev. Pharmacol. Toxicol.* **2000**, *40*, 133.

144.   vonMoltke, L. L.; Greenblatt, D. J.; Schmider, J.; Wright, C. E.; Harmatz, J. S.; Shader, R. I., *Biochem. Pharmacol.* **1998**, *55*, 113.

145.   Ma, L. J.; Gong, X. Y.; Yeung, E. S., *Anal. Chem.* **2000**, *72*, 3383.

146.   Wan, H.; Ulander, J., *Expert Opin. Drug Metab. Toxicol.* **2006**, *2*, 139.

147.   Gong, X. Y.; Figus, M.; Plewa, J.; Levorse, D. A.; Zhou, L. L.; Welch, C. J., *Chromatographia* **2008**, *68*, 219.

148.   Wong, K. S.; Kenseth, J.; Strasburg, R., *J. Pharm. Sci.* **2004**, *93*, 916.

149.   Pascoe, R. J.; Masucci, J. A.; Foley, J. P., *Electrophoresis* **2006**, *27*, 793.

150.   Rudnev, A. V.; Foteeva, L. S.; Kowol, C.; Berger, R.; Jakupec, M. A.; Arion, V. B.; Timerbaev, A. R.; Keppler, B. K., *J. Inorg. Biochem.* **2006,** *100*, 1819.

151.   Wang, Y. J.; Sun, J.; Liu, H. Z.; He, Z. G., *Chromatographia* **2007,** *65*, 173.

152.   Bhoopathy, S.; Sarkar, M.; Karnes, H. T., *J. Pharm. Biomed. Anal.* **2001,** *25*, 721.

153.   Martinez-Pla, J. J.; Martinez-Gomez, M. A.; Martin-Biosca, Y.; Sagrado, S.; Villanueva-Camanas, R. M.; Medina-Hernandez, M. J., *Electrophoresis* **2004,** *25*, 3176.

154.   Rocheleau, M. J., *Electrophoresis* **2005,** *26*, 2320.

155.   Pang, H.-m.; Kenseth, J.; Coldiron, S., *Drug Discovery Today* **2004,** *9*, 1072.

156.   Sundberg, S. A.; Chow, A.; Nikiforov, T.; Wada, H. G., *Drug Discovery Today* **2000,** *5*, S92.

157.   *Assay Guidance Manual Version 5.0*, **2008**, Eli Lilly and Company and NIH   Chemical   Genomics   Center. http://www.ncgc.nih.gov/guidance/manual_toc.html (accessed Sept. 3, 2008).

158.   Simard, J. R.; Kluter, S.; Grutter, C.; Getlik, M.; Rabiller, M.; Rode, H. B.; Rauh, D., *Nat. Chem. Biol.* **2009,** *5*, 394.

159.   Kostenis, E.; Mohr, K., *Trends Pharmacol. Sci.* **1996,** *17*, 280.

160. Christopoulos, A.; Kenakin, T., *Pharmacol. Rev.* **2002,** *54*, 323.

161. Hopkins, A. L.; Groom, C. R., *Nat. Rev. Drug Discovery* **2002,** *1*, 727.

162. Tropak, M. B.; Blanchard, J. E.; Withers, S. G.; Brown, E. D.; Mahuran, D., *Chem Biol.* **2007,** *14*, 153.

163. Tropak, M. B.; Mahuran, D., *FEBS J.* **2007,** *274*, 4951.

164. Hayouka, Z.; Rosenbluh, J.; Levin, A.; Loya, S.; Lebendiker, M.; Veprintsev, D.; Kotler, M.; Hizi, A.; Loyter, A.; Friedler, A., *PNAS* **2007,** *104*, 8316.

(Intentionally Blank)

Chapter II

Dynamic Unfolding of a Regulatory Subunit of cAMP-dependent Protein

Kinase by Capillary Electrophoresis: Impact of cAMP Dissociation on

Protein Stability

II. Dynamic Unfolding of a Regulatory Subunit of cAMP-dependent Protein Kinase by Capillary Electrophoresis: Impact of cAMP Dissociation on Protein Stability

2.1. Abstract

Characterization of the unfolding dynamics of a recombinant type IA regulatory subunit (RIα) of cyclic adenosine monophosphate (cAMP)-dependent protein kinase (cAPK) was examined by CE with UV detection. Electrophoretic separation of RIα by CE in a buffer devoid of cAMP resulted in rapid dissociation of the complex from the original sample due to the high negative mobility of the ligand relative to receptor. This process enabled in-capillary generation of cAMP-stripped RIα, which was used to estimate the apparent dissociation constant (K_d) of (0.6 ± 0.2) μM. A comparison of RIα dynamic unfolding processes with urea denaturation was performed by CE with (*i.e.*, RIα–cAMP) and without (*i.e.*, cAMP-stripped RIα) excess cAMP in the buffer during electromigration. The presence of cAMP in the buffer confirmed greater stabilization of the protein, as reflected by a higher standard free energy change (ΔG_U^0) of (10.1 ± 0.5) kcal·mol^{-1} and greater cooperativity in unfolding (*m*) of (22.30 ± 0.11) kcal·mol^{-1}M^{-1}. CE offers a rapid, yet versatile platform for probing the thermodynamics of cAPK and other types of receptor–ligand complexes in free solution.

2.2. Introduction

CE is increasingly being recognized as a versatile biophysical tool for characterizing biomolecular interactions in free solution, ranging from high affinity protein–DNA interactions[1,2] to weaker host–guest inclusion complexation[3, 4] There is considerable interest in understanding the dynamics of folding in wild-type and recombinant protein due to its importance in determining its conformational state, thermodynamic stability, and overall biological activity. Protein unfolding plays an important role in normal cellular translocation and degradation *in vivo*.[5] In addition, protein misfolding has been implicated as a significant factor leading to the formation of amyloid fibril deposits associated with neurodegenerative disorders, such as Alzheimer's disease.[6] Traditionally, electrophoretic protein unfolding studies have been performed using transverse gradient slab gel electrophoresis which uses urea as a denaturant.[7] Fully denatured proteins have typically been modeled as fully solvated random coils in solution.[8] In such cases, unfolding often results in an increase in the effective hydrodynamic radius of a protein that is offset by any changes in charge, thereby resulting in a lower apparent mobility relative to its native folded conformation. CE offers a convenient microseparation platform for characterizing protein unfolding[9-11] due to its rapid analysis time, small sample volume requirement, and automation using in-capillary detection based on UV absorbance. To date, there have been only a limited number of quantitative protein unfolding studies reported in CE exploring the thermodynamics of protein stability.[12-18] Thermal protein

denaturation experiments require precise temperature control of the entire capillary and sample tray over a wide range for reliable analyses.[19-20] Urea is a compatible chemical denaturant in CE studies[21] since it is a neutral chaotropic agent that does not contribute to Joule heating. In all cases, nonspecific changes in protein mobility,[22] not associated with unfolding (*e.g.*, viscosity, pH), need to be corrected for accurate determination of thermodynamic parameters reflective of protein stability, such as the standard free energy change for unfolding (ΔG_U^0).

Cyclic adenosine monophosphate (cAMP)-dependent protein kinase (cAPK) represents a major class of protein kinase relevant in eukaryotic cell signaling whose holoenzyme consists of two distinct subunit types, namely dimeric regulatory and catalytic subunits.[23] Downstream chemical signaling *via* phosphorylation of specific substrates by the activated catalytic subunit is first initiated by cAMP binding to the two domains (A and B) of the regulatory subunit.[24] In addition to its inhibitory influence on the catalytic subunit, the regulatory subunit also provides a docking site for anchoring with A Kinase anchoring proteins.[25] In this study, CE was explored as an alternative technique for characterizing the unfolding dynamics of a recombinant construct of the type IA regulatory subunit (RIα) of cAPK, which is typically studied by intrinsic fluorescence spectroscopy and circular dichroism.[26] To the best of our knowledge, this is the first CE study reported to quantitatively assess cAPK unfolding based on normalized apparent mobility changes as a function of urea concentration, which confirmed the importance of cAMP binding on receptor

stability. It is noteworthy that dynamic RIα-cAPK unfolding studies by CE with UV detection enabled direct analyses of low amounts of recombinant protein without time-consuming offline sample preincubation. Moreover, electrophoretic stripping of cAMP from the receptor complex was achieved in-capillary due to irreversible dissociation of the high mobility ligand from slower migrating protein in a buffer devoid of cAMP. This permitted *in situ* formation of the labile-stripped RIα-cAPK protein, whose unfolding properties were readily compared with the ligand-saturated receptor, which was performed with excess cAMP added to the buffer during electromigration.

2.3. Experimental

2.3.1. Chemicals and Reagents

Deionized water for buffer and sample preparations was obtained using a Barnstead EASYpure→II LF ultrapure water system (Dubuque, IA, USA). MES, adenosine 3',5'-cyclic monophosphate (cAMP), adenosine 5'-monophosphate (AMP), adenosine (A), sodium hydroxide, urea, DTT, EGTA, guanidine hydrochloride (grade I), benzyamide hydrochloride, leupeptin, AEBSF, pepstatin, 1-chloro-3-(tosylamino)-7-amino-L-2-heptanone (TLCK), L-1-(tosylamino)-2-phenylethyl chloromethyl ketone (TPCK), EDTA, 3-isobutyl-1-methylxanthine (IBMX), sodium azide, potassium dihydrophosphate, and ammonium sulfate were all purchased from Sigma (St. Louis, MO, USA). Luria Bertani (LB) broth and sodium chloride were obtained from BioShop Canada (Burlington, ON, Canada).

2.3.2. RIα Protein Expression and Purification

The recombinant RIα was expressed according to the procedure described by Hamuro *et al.*[27] Briefly, *Escherichia coli* BL21 (DE3) containing a plasmid, pRSET, encoding for the RIα was grown in LB broth (1 L) with ampicillin (100 mg/mL). All subsequent procedures were carried out at 47°C. Cells were isolated by centrifugation at 5 krpm for 10 min and resuspended in lysis buffer (20 mM MES, 2 mM Na_2EDTA, 2 mM EGTA, 100 mM NaCl, and 5 mM DTT, pH 6.5). Cells were lysed by French press at 1000 psi. The cell lysate was then centrifuged at 14 krpm for 40 min, the supernatant collected and precipitated with 45% ammonium sulfate over 1 h. The resulting precipitate was centrifuged at 10 krpm for 10 min and resuspended in lysis buffer containing protease inhibitors (10 mM benzamidine, 0.4 mM AEBSF, 1 mM pepatatin, 1 mM leupeptin, 28 mM TPCK, 28 mM TLCK, and 10 mM IBMX). This solution was equilibrated with cAMP-conjugated Sepharose resin overnight and the protein was eluted with lysis buffer containing 25, 35, and 40 mM cAMP. The protein was further purified using an FPLC gel filtration column (HiLoad 16/26 Superdex column from GE Healthcare) and exchanged with 20 mM KH_2PO_4 (pH 6.5), 100 mM NaCl, and 1 mM cAMP. The protein was then dialyzed against 20 mM KH_2PO_4 (pH 6.5), 100 mM NaCl for 36 h and finally dialyzed against 50 mM MES (pH 6.5), 100 mM NaCl, and 0.02% NaN_3. RIα-cAPK was further characterized by ESI-MS in the positive ion mode (MH^+) using an Agilent XCT IT mass analyzer (Agilent Technologies, DE,

USA), which resulted in apparent masses of 14.3 and 14.6 kDa for the stripped and cAMP-bound receptor, respectively.

2.3.3. Capillary Electrophoresis

All separations were performed on an automated P/ACE 2100 CE system (Beckman-Coulter, Fullerton, CA, USA). Uncoated fused-silica capillaries with 50 μm i.d., 360 mm o.d., and 47 cm total length (Polymicro Technologies, Phoenix, AZ, USA) were used for protein denaturation studies. Separations began by rinsing the capillary for 1 min with 0.1 M NaOH, followed by a 5 min rinse with buffer. All separations were performed thermostated at 20°C using 30 kV and UV absorbance was monitored at 214 nm. Hydrodynamic injection of sample was performed onto the capillary inlet using low pressure (0.5 psi or 3.5 kPa) for 10 s. The capillary was rinsed at the end of each day for 5 min with 0.1 M NaOH and stored overnight in separation buffer. Protein unfolding studies by CE were performed in 100 mM MES (pH 6.5; adjusted by 0.1 M NaOH) buffer with or without 0.5 mM cAMP and/or urea. Separation buffers containing cAMP and urea were prepared prior to use from stock solutions of 7 M urea in 100 mM MES (pH 6.5) and 20 mM cAMP dissolved in water. Stock solutions of 10 mM adenosine and 10 mM AMP were also prepared in water and added to the sample prior to analysis, which were used as neutral EOF marker and internal standard, respectively. CE experiments required less than 2 nmol of RIα (*e.g.*, 57 μM in 30 μL) sample which was prepared with excess cAMP. Unfolding studies of RIα were carried out in separation buffer containing increasing concentrations of urea

with and without 0.5 mM cAMP. The relative viscosity correction factor (v), required to normalize the apparent protein mobilities, was measured using CE by comparing the average time ($n = 5$) of a sample plug to travel to the detector window using a low pressure rinse (0.5 psi) at a specific concentration of urea relative to 0 mM urea. It was determined that significant changes in solution viscosity occurred at concentrations >0.5 M urea (2.1%) with a maximum viscosity increase of about 95.2% at 7 M urea. Relative viscosity correction factors were generally measured with excellent precision under 1% CV. The average relative viscosity correction factor data ($n = 27$) ranging from 0–7 M urea concentration (C_U) was fitted to a polynomial expression[28] with good correlation:

$$v = (1.0 + 4.79 \times 10^{-2}) \, C_U + (7.89 \times 10^{-3}) \, C_U^2 + (7.07 \times 10^{-4}) \, C_U^3.$$

2.3.4. Theory

In the case of fast protein unfolding transitions ($\tau > 0.01 \text{ s}^{-1}$) studied by CE, a single time-averaged signal is observed whose mobility represents a weighted average of all relevant protein population states.[9] Assuming a two-state system, where the native folded (F) protein isomerizes to a single unfolded (U) state, the apparent protein mobility (μ^A_{ep}) can be expressed by the following expression:

$$v\mu_{ep}^A = f_F \mu_{ep,F} + f_U \mu_{ep,U} = \frac{1}{1 + K_U} \mu_{ep,F} + \frac{K_U}{1 + K_U} \mu_{ep,U} \qquad (2\text{-}1)$$

where, ν is the relative viscosity correction factor that normalizes all measured protein mobilities to 0 M urea concentration, f_F is the fraction of folded protein, f_U is the fraction of unfolded protein, $\mu_{ep,\,F}$ is the mobility of folded protein, $\mu_{ep,\,U}$ is the mobility of unfolded protein and K_U is the apparent unfolding equilibrium constant. It should be noted that previous protein unfolding studies in CE using urea denaturation typically extrapolate mobilities to zero urea concentration after the protein unfolding transition in order to derive $\mu_{ep,\,U}$.[10] However, viscosity-corrected mobility plots allow for direct comparison with other techniques used for protein unfolding, as well as providing a more accurate estimation of $\mu_{ep,\,U}$.

In this study, a recombinant 125 amino acid RIα-cAPK construct, containing two tryptophan residues at positions 188 and 222 located in a single cAMP binding domain A,[29] was used as a model receptor-ligand system for protein unfolding by CE. RIα-cAPK is an acidic protein, thus it has a negative mobility under weakly acidic conditions (pH 6.5). As such, a two-state unfolding process for RIα-cAPK can be described in CE by the **Scheme 2.1**. Note that when probing cAPK unfolding in the presence of excess cAMP by conventional spectroscopy techniques, urea denaturation results in unfolding of the binding domain of RIα-cAPK with subsequent dissociation of bound cAMP. However, this may not be the case for reversible complexes with fast dissociation rate constants ($k_{off} \gg 1s^{-1}$) under an external electric field, where the mobility of receptor and ligand are distinct. **Scheme 2.1** illustrates a two-stage process involving rapid electrophoretic dissociation of the receptor-ligand complex and

$$RI\alpha\text{-cAMP} \xrightarrow{\ k_{off}\ } RI\alpha \ + \ cAMP \rightleftharpoons^{K_{U1}} RI\alpha$$

$$+ \qquad \qquad \mu_{ep,\,F} \qquad \qquad \mu_{ep,\,S} \qquad \mu_{ep,\,L} \qquad \qquad \mu_{ep,\,U} \qquad -$$
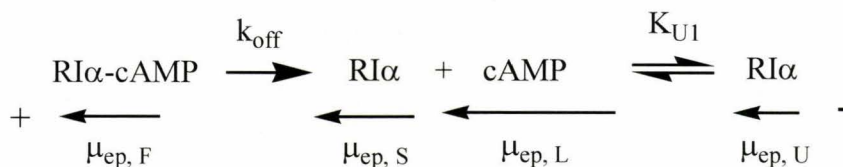
Scheme 2.1. Two-step process depicting *in-situ* electrophoretic stripping of cAMP from *holo*-RIα complex followed by dynamic unfolding of *apo*-RIα with urea denaturation.

formation of the cAMP-stripped receptor ($\mu_{ep,\,S}$) and free ligand cAMP ($\mu_{ep,\,L}$). The ligand-free receptor then undergoes dynamic unfolding with urea denaturation due to irreversible separation of cAMP. This process occurs when performing protein unfolding studies in a buffer devoid of ligand. In CE, the intrinsic thermodynamic stability of a protein is characterized by the magnitude of K_U, which can be transformed into the apparent free energy change (ΔG_U) by measuring changes in the apparent protein mobility:

$$K_U = \frac{\nu \mu_{ep}^A - \mu_{ep,F}}{\mu_{ep,U} - \nu \mu_{ep}^A} \qquad (2\text{-}2)$$

$$\Delta G_U = -RT \ln K_U \qquad (2\text{-}3)$$

$$\Delta G_U = \Delta G_U^o - mc \qquad (2\text{-}4)$$

The standard free energy change of a protein with urea denaturation (ΔG°_U) and the cooperativity in unfolding (m) are two major parameters used to assess the thermodynamic stability of a protein, which can be derived by linear regression of ΔG within the transition region of unfolding or via non-linear

$$\text{RI}\alpha\text{-cAMP} \;\; \underset{}{\overset{K_{U2}}{\rightleftharpoons}} \;\; \text{RI}\alpha \;\; + \;\; \text{cAMP}$$

+ ← — — ← — — ← — — -

$\mu_{ep, F}$ $\mu_{ep, U}$ $\mu_{ep, L}$
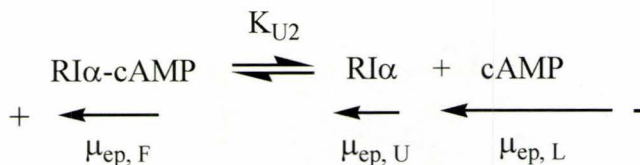
Scheme 2.2. Single-step process depicting dynamic unfolding of *holo*-RIα–cAMP complex with urea denaturation when using excess cAMP in the buffer during separation.

regression.[9] Linear regression of the protein unfolding curve can be used to ascertain adherence to a two state model, as well as derive ΔG°_{U} and m parameters based on y-intercept and slope, respectively. In order to assess the impact of cAMP on the conformational stability of the protein during unfolding, the receptor-ligand complex must remain intact during electromigration based on **Scheme 2.2**. One way to ensure receptor saturation during separation in CE is to include an excess of ligand continuously in run buffer. Thus, $K_{U1} \neq K_{U2}$ or $\Delta G^{\circ}_{U1} \neq \Delta G^{\circ}_{U2}$ if cAMP binding confers enhanced protein conformational stability and greater resistance to urea denaturation. In this study, dynamic unfolding of RIα was compared by CE using two different separation formats, namely discontinuous conditions where initial sample plug contains excess cAMP whereas buffer is devoid of cAMP (**Scheme 2.1**), and continuous conditions where both sample and buffer contain excess cAMP (**Scheme 2.2**). This feature of CE is advantageous since it can also be used to directly assess the apparent dissociation constant (K_d) of the protein-ligand complex without having to independently prepare the labile cAMP-stripped protein based on **Scheme 2.3**. Assuming rapid dissociation of cAMP upon voltage application, the apparent K_d

$$RI\alpha\text{-cAMP} \quad \underset{}{\overset{K_d}{\rightleftharpoons}} \quad RI\alpha \quad + \quad cAMP$$

$$+ \quad \xleftarrow{} \qquad \xleftarrow{} \quad \xleftarrow{} \qquad -$$

$$\mu_{ep, F} \qquad\qquad \mu_{ep, S} \qquad \mu_{ep, L}$$
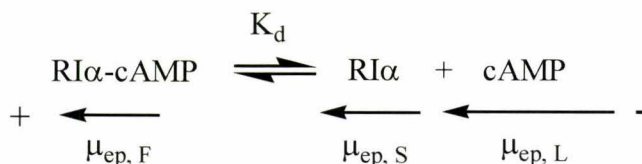
Scheme 2.3. Direct assessment of ligand binding affinity (K_d) by titration of *apo*-RIα with increasing levels cAMP in the buffer by CE that results in larger absorbance responses

can then be estimated by CE via a direct titration of cAMP added to buffer based on increases in measured relative absorbance (peak area, PA) of the receptor-ligand complex (RL) signal using non-linear regression:

$$[RL] = \frac{PA_{max}[L]}{K_d + [L]} \tag{2-5}$$

Hence, CE can be used as a single platform under different conditions for assessing the thermodynamics of folded, unfolded and cAMP-stripped protein states, as well as the affinity of RIα-cAMP interactions in free solution.

2.4. Results and Discussion

2.4.1. pH Dependence on RIα-cAMP and Nucleotide Mobility

Preliminary experiments were first performed to determine the pH mobility dependence of RIα as compared to its specific target nucleotide, cAMP and its non-cyclic analogue AMP. MES was used as a high ionic strength zwitterionic buffer in this study due to its low conductivity to reduce Joule heating, as well as minimize protein adsorption to the capillary wall. **Figure 2.1** shows that RIα is anionic at pH > 5.5 with an apparent *pI* of about 5.3, which is in close agreement with a predicted *pI* of 5.1 based on its primary amino acid

sequence.[30] Previously, it has been reported that addition of 7 M urea to a low ionic strength isoelectric buffer can increase the apparent buffer pH by over 0.8 pH units.[14] As depicted in **Figure 2.1(a)**, there are only minor relative changes in protein mobility (< 2.0 %) within a pH range of 6.0-7.0, which minimizes the impact of any changes in apparent buffer pH with urea addition when performing protein unfolding studies. Further experiments in the study were performed using 100 mM MES, pH 6.5 as shown in **Figure 2.1(b)**. It is evident that RIα has a significantly lower negative mobility compared to both cAMP and AMP. Note that AMP is a diprotic acid that undergoes increasing deprotonation at pH > 6.0 with a measured pK_{a2} of (6.4 ± 0.2), unlike the monoprotic cAMP due to its 3',5'-cyclic phosphonate ester structure. This fact highlights the major charge density difference among the nucleotides, thus the high specificity for cAMP binding to RIα. Hence, minimal differences in protein mobility with urea addition caused by apparent pH changes serve to permit accurate determination of thermodynamic parameters for protein unfolding by CE. However, the relative viscosity correction factor is vital for correcting for non-specific changes in apparent protein mobility not associated with protein unfolding due to increases in bulk viscosity with urea addition.

2.4.2. Rapid Dissociation of RIα-cAMP Complex During Electromigration

Preliminary CE experiments of RIα demonstrated that the measured peak
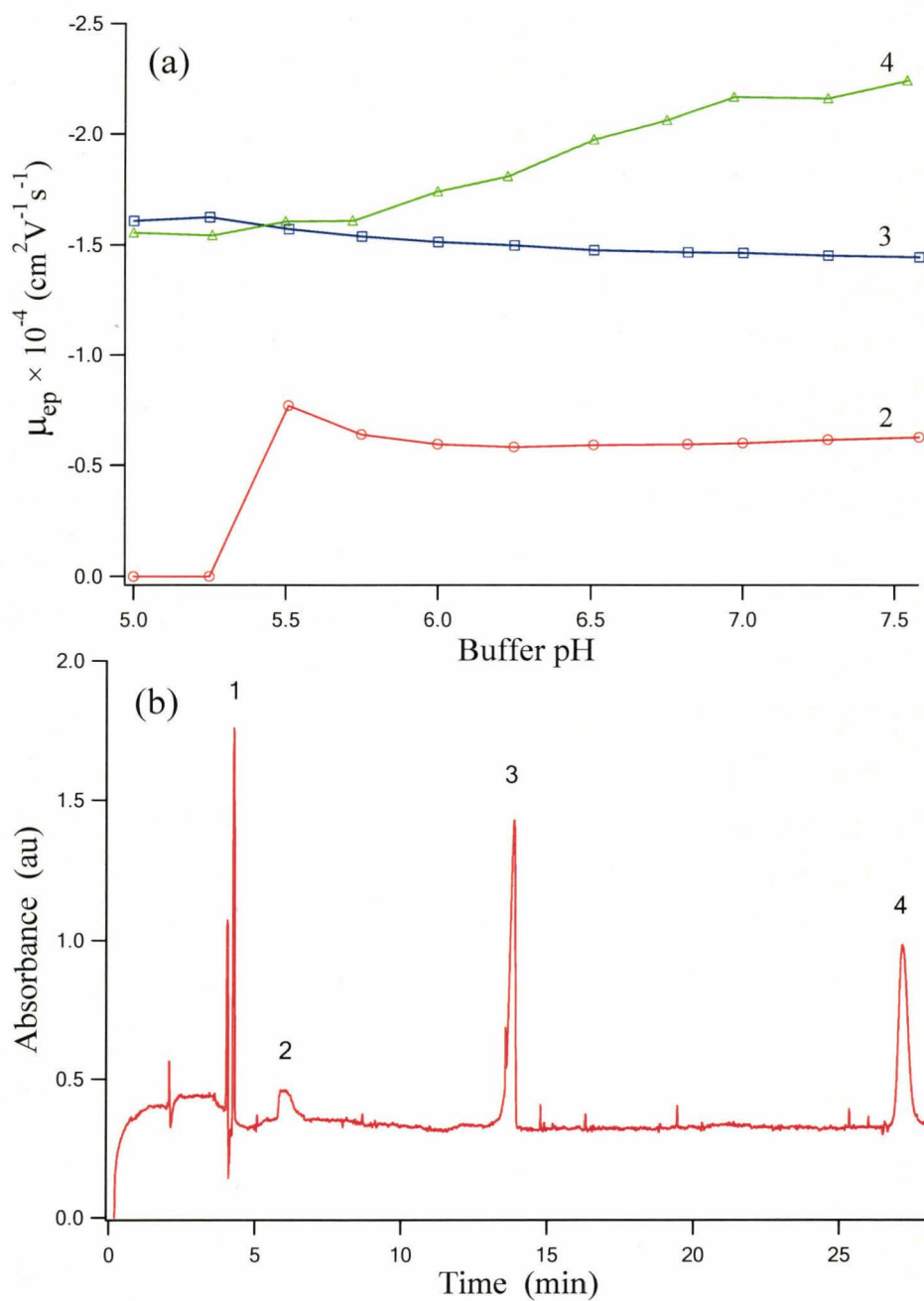
Figure 2.1 (a) A plot showing the pH-dependent mobility changes of (2) RIα, (3) cAMP and (4) AMP using 100 mM MES by CE. The apparent pI of RIα is about 5.3, whereas cAMP does not undergo significant mobility changes within the pH range examined unlike its diprotic non-cyclic analogue AMP.   (b)   Electropherogram   of   protein   sample   at   pH   6.5   containing   57   μM RIα, 0.4 mM cAMP and 0.2 mM AMP. Conditions: buffer, 100 mM MES, pH 6.5; voltage, 30 kV; capillary length, 47 cm; temperature, 20°C; UV @ 214 nm.   Note that (1) represents adenosine, which was used as the neutral EOF marker.

area of the protein was significantly lower than expected based on its molar absorptivity of $\varepsilon_{214} \sim 4.09 \times 10^5$ M^{-1}cm^{-1} as determined by UV absorbance spectroscopy. Since the protein sample was prepared with excess cAMP in order to ensure improved stability and CE separations were performed in buffer devoid of cAMP, it was hypothesized that the equilibrium RIα-cAMP mixture present in original sample was electrophoretically separated upon voltage application due to the different mobilities of receptor and ligand. Krylov[31] has recently introduced non-equilibrium capillary electrophoresis of equilibrium mixtures (NECEEM) as a promising technique for characterizing the kinetics and thermodynamics of aptamer-protein interactions, which typically have intermediate dissociation rate constants $(k_{off} \sim 10^{-4}$ to 1 s$^{-1})$ relative to the time-scale of CE separations.[31] This suitable range is typically indicated by an exponentially decaying receptor-ligand complex peak. However, in our case, RIα-cAMP was surmised to undergo rapid dissociation (*i.e.*, $k_{off} \gg 1$ s^{-1}) as there were no significant peak tailing observed in either protein or cAMP peaks, as shown in **Figure 2.1(b)**. This observation is supported by previous studies characterizing the wild-type APK protein with an apparent k_{off} of 60 s^{-1} for the RIα site.[32] In addition, further experiments (data not shown) were performed using shorter effective capillary lengths (*e.g.*, 1-30 cm) by placing the protein sample plug at closer distances to the detector window using a defined applied hydrodynamic pressure time interval prior to voltage application. However, there were no significant changes observed for protein or cAMP peak shapes under shorter time intervals (effective capillary length of 7

cm; total migration time of 4 min) necessary to resolve the receptor and ligand. Thus, it was concluded that RIα-cAMP complex rapidly dissociated (< 20 ms) upon voltage application due to the large mobility differences of protein and ligand when using MES buffer devoid of cAMP, where the rate of complex dissociation was much faster than time scale of separation. Interestingly, a similar effect has been recently reported in CE by Rochu *et al.*[33] involving reversibly-bound charged inhibitors of acetylcholinesterase for assessing the purity of ligand-free receptors.

Figure 2.2 clearly demonstrates the reversibility of RIα-cAMP binding that can be controlled by titrating increasing concentrations of cAMP in MES buffer during protein electromigration directly in the capillary. **Figure 2.2(a)** shows that there was a dramatic increase in measured absorbance signal of the protein with cAMP addition in the run buffer, which did not change significantly above 50 μM cAMP. The increase in absorbance is related to the greater molar absorptivity of the receptor-ligand complex upon cAMP association. Noteworthy, there was no noticeable change in protein peak width or shape with cAMP addition. However, there was a minor increase in protein mobility upon cAMP association due to increase in charge density and/or conformational compactness of the folded RIα-cAMP complex relative to cAMP-stripped RIα (*i.e.,* $\mu_{ep, F} >$ $\mu_{ep,S}$). This data further supports the premise of rapid electrophoretic dissociation of RIα-cAMP complex during electromigration. Moreover, this process also provides estimation of dissociation constant (K_d) of RIα-cAMP based on a
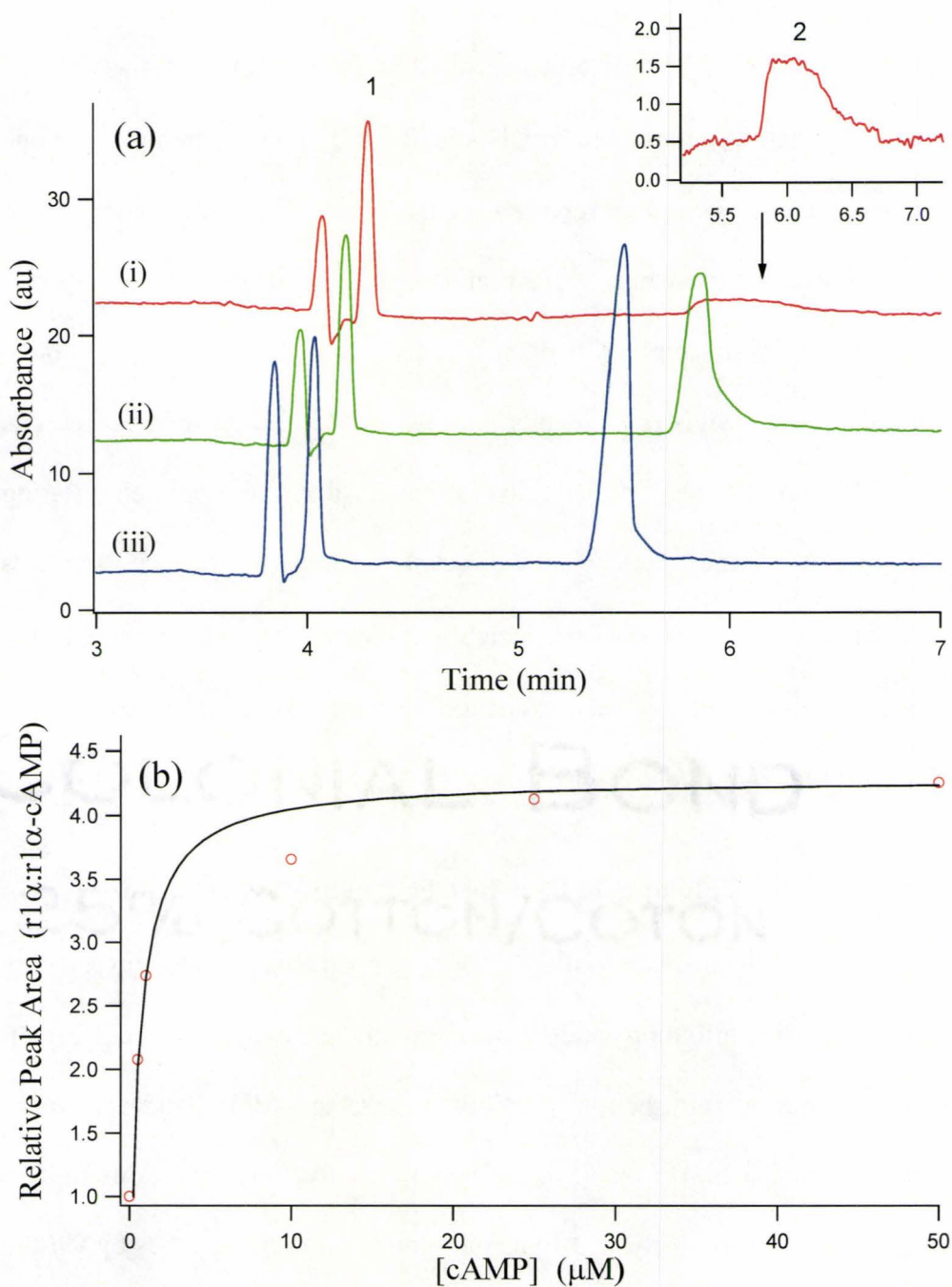
Figure 2.2 (a) Series of electropherograms that demonstrate in-capillary cAMP-stripping of RIα that is reversible with addition of increasing concentrations cAMP (i) 0 μM, (ii) 10 μM and (iii) 50 μM to buffer. (b) Binding isotherm used to estimate the apparent K_d of RIα-cAMP binding based on increases in the relative peak area of protein signal by CE upon cAMP addition to buffer. Note that saturation occurs above 50 μM cAMP for the single cAMP-binding domain recombinant protein. Conditions and analyte peak numbering are the same as Fig. 2.1(b).

rectangular hyperbola binding isotherm as described by **Eq. 2-5** and **Figure 2.2(b)** using the relative increase in peak area measured for the protein.

The apparent K_d determined by CE was (0.6 ± 0.2) µM, which is about one order of magnitude weaker than reported for the wild-type APK by competitive (^3H)cAMP radioactive exchange with ammonium sulphate precipitation.[29,32] It is not clear whether this discrepancy is due to differences in the recombinant protein construct relative to wild-type receptor or bias in the CE method since it is assumed that cAMP has been fully stripped from the protein during electromigration. Further work will be directed at comparing K_d measurements using a purified cAMP-stripped RIα, which is typically prepared by partial urea denaturation with buffer dialysis exchange or size exclusion separation of dissociated cAMP from refolded RIα.[29]

2.4.3. Dynamic RIα Unfolding in Urea by CE: Ligand-Free Receptor

Further evidence of the formation of the cAMP-stripped RIα was also revealed by comparative protein unfolding studies by CE with and without excess cAMP added to the buffer. Although previous cAPK unfolding studies require preincubation (*e.g.,* 3 hrs) to achieve sufficient equilibration of various protein population states prior to analysis,[28] dynamic protein unfolding studies by CE are often amenable to low molecular weight proteins that tend to have rapid unfolding kinetics. This property was supported by performing time-dependent CE experiments of protein unfolding in 0 M, 3 M and 5 M urea over a three hour time

frame without significant differences in measured protein mobilities. Thus, the same small volume protein sample (*i.e.*, 30 μL) can be analyzed repeatedly by CE without preincubation, thereby providing a rapid yet convenient format for characterizing recombinant protein. In addition, in-capillary generation of the cAMP-stripped RIα provides a unique way to prepare the labile ligand-free receptor *in-situ* by CE that avoids time-consuming off-line preparative work-up, which typically is viable for less than 2 days due to its propensity for proteolysis.[25]

Figure 2.3 depicts the RIα unfolding titration curve with urea denaturation based on viscosity-corrected protein mobility measurements. Interestingly, the protein peak shape is observed to gradually sharpen at higher urea concentrations along with a significant decrease in apparent mobility due to protein unfolding as shown in **Figure 2.3(a)**. A two-state cooperative unfolding process is indicative in the RIα unfolding titration curve illustrated in **Figure 2.3(b)**, where the major transition occurs within a concentration range of 1-3 M urea with a C_M of 2.03 M corresponding to the concentration of urea where the fraction of protein unfolding is 50%. Linear regression ($R^2 = 0.9994$) of the apparent ΔG_U as a function of urea concentration within the RIα unfolding transition resulted in ΔG^o_U of (3.13 ± 0.07) kcal mol^{-1} and a *m* of (-1.54 ± 0.03) kcal mol^{-1} M^{-1} as summarized in **Table 2.1**. The latter property is related to a cooperative unfolding transition without apparent stable partially unfolded intermediates, whereas the former property is
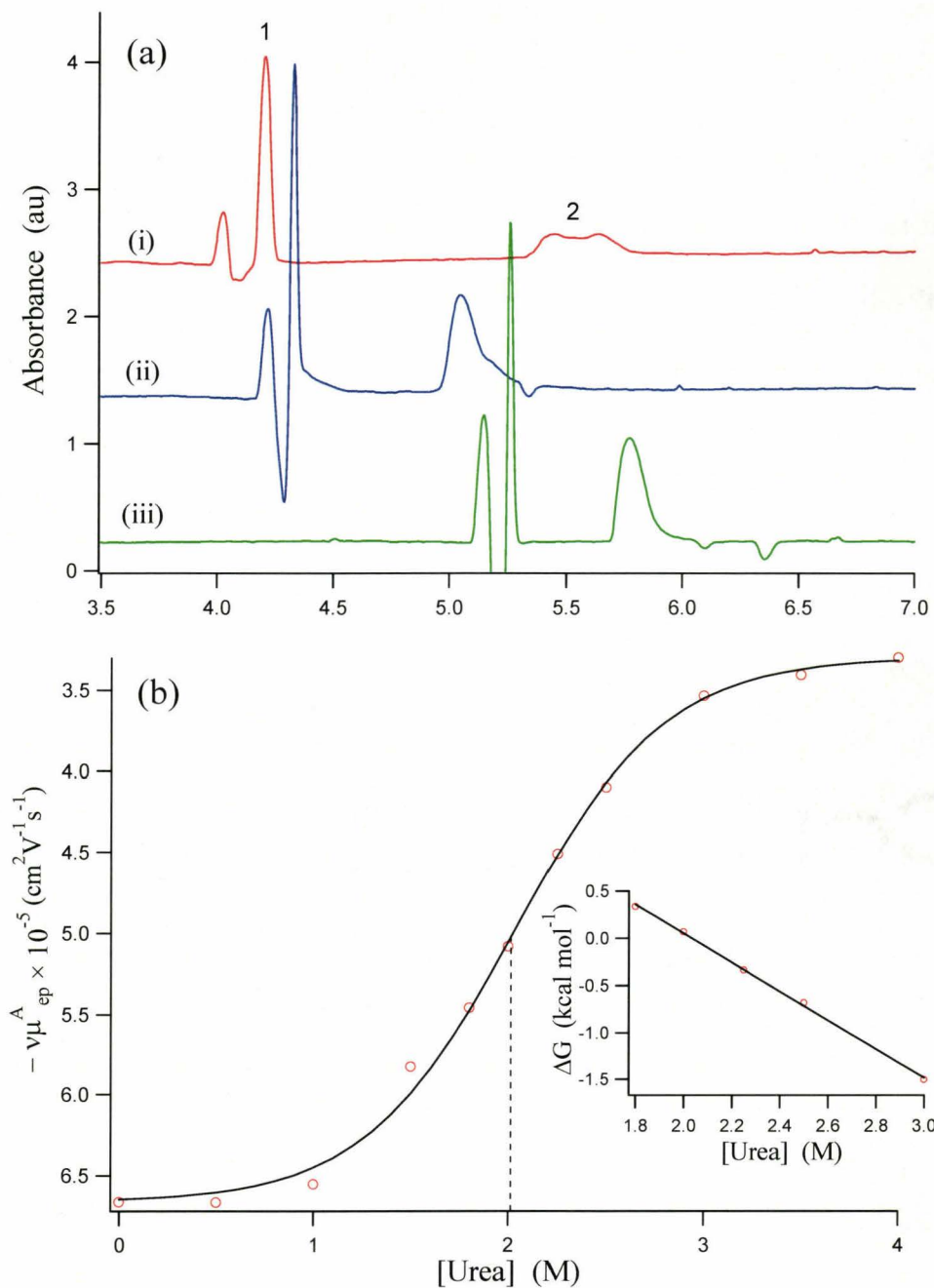
Figure 2.3 (a) Series of electropherograms that highlight RIα dynamic unfolding studies performed without excess cAMP (*i.e.*, cAMP-stripped RIα) in buffer by CE with (i) 0 M, (ii) 2 M and (iii) 4 M urea. (b) Protein unfolding mobility curve based on viscosity-corrected apparent mobilities as a function of urea concentration. The inset represents linear regression of apparent ΔG_U within the unfolding transition to determine thermodynamic parameters $\Delta G°_U$ and m. Conditions and analyte peak numbering are the same as Fig. 1(b) except for addition of 0-4 M urea in buffer.

Table 2.1 Thermodynamic parameters of R1α urea denaturation studies by CE in (a)100 mM MES, pH 6.5 and (b) 100 mM MES, pH 6.5 with 0.5 mM cAMP.

Buffer Condition	$\Delta G°$ (kcal mol^{-1})	m (kcal mol^{-1}M^{-1})	C_m (M)	$\mu_{ep\,F} \times 10^{-5}$ (cm^{2}V^{-1}s^{-1})	$\mu_{ep\,U} \times 10^{-5}$ (cm^{2}V^{-1}s^{-1})
(a)	(3.13 ± 0.07)	(-1.54 ± 0.03)	2.03	(-6.65 ± 0.08)	(-3.30 ± 0.06)
(b)	(10.1 ± 0.5)	(-2.30 ± 0.11)	4.40	(-7.17 ± 0.04)	(-3.40 ± 0.02)

All parameters were calculated using linear regression analysis of apparent ΔG derived from viscosity-corrected apparent RIα mobilities during unfolding transition based on duplicate measurements, where the error represents the standard deviation.

indicative of the reduced thermodynamic stability of the ligand-free RIα. This thermodynamic data is correlated well with a previous report by Canaves *et al.*[26] using fluorescence spectroscopy on a purified cAMP-stripped wild-type RIα dimer with an apparent $\Delta G°_U$ of about 3.7 kcal mol^{-1}. The major advantage of the CE technique is that cAMP-stripping and dynamic protein unfolding processes are performed simultaneously during electromigration using small amounts of recombinant protein. Thus, sample purification and protein thermodynamic studies are integrated within a single automated platform.

2.4.4. Dynamic RIα Unfolding in Urea by CE: Ligand-Saturated Receptor

Figure 2.4 compares the protein unfolding titration study that was performed by CE using excess cAMP in the buffer to ensure complete saturation of the RIα-cAMP complex during electromigration. As shown in **Figure 2.4(a)**, the protein signal at 0 M urea is significantly increased due to association with cAMP. Also, note that the dynamics of protein unfolding is qualitatively different from **Figure 2.3** reflected by peak broadening until the transition range, followed
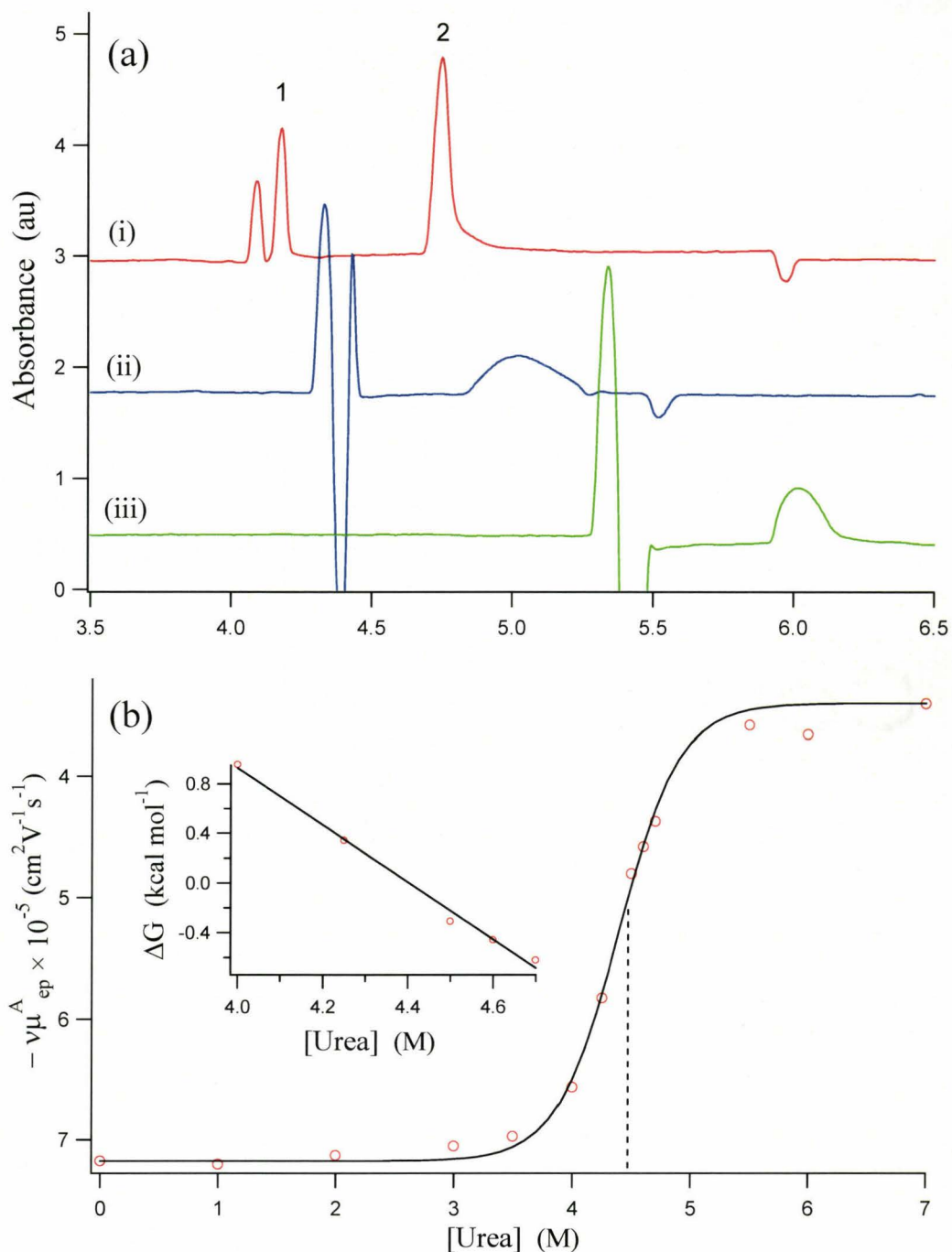
Figure 2.4 (a) Series of electropherograms that highlight RIα dynamic unfolding studies performed with 0.5 mM cAMP (*i.e.,* RIα-cAMP complex) in buffer by CE with (i) 0 M, (ii) 4.5 M and (iii) 7 M urea. (b) Protein unfolding mobility curve based on viscosity-corrected apparent mobilities as a function of urea concentration. The inset represents linear regression of apparent ΔG_U within the unfolding transition to determine thermodynamic parameters $\Delta G°_U$ and *m*. Conditions and analyte peak numbering are the same as Fig. 2.3 except for excess cAMP was added in buffer to ensure RIα-cAMP saturation during electromigration.

by peak sharpening upon full denaturation. **Figure 2.4(b)** clearly demonstrates the impact of cAMP on the inherent stability of the protein that is indicated by significantly greater C_M, ΔG°_U and m parameters as highlighted in **Table 2.1**.

Noteworthy, protein unfolding occurs at a higher urea concentration range with greater cooperativity along with a higher ΔG°_U of (10.1 ± 0.5) kcal mol^{-1}. Similarly, this value is consistent with previous unfolding studies for the wild-type RIα in excess cAMP with a ΔG°_U of about 9.5 kcal mol^{-1}.[25] Thus, there is about a 7 kcal mol^{-1} increase in the intrinsic thermodynamic stability of the protein with cAMP saturation, which highlights the major impact of cAMP on protein non-covalent conformational properties. As shown in **Table 2.1**, CE is able to distinguish differences in cAMP-stripped (folded), cAMP-saturated (folded in excess cAMP) and unfolded RIα based on normalized mobility measurements. Further work will be directed at using CE as a complementary biophysical tool to characterize different mutant strains of RIα, as well as probe intermolecular interactions involving the binding of regulatory and catalytic subunits.[34]

2.5. Conclusions

Characterization of the thermodynamic properties of a recombinant construct of RIα-APK was performed by CE using UV detection. This study demonstrated that in-capillary electrophoretic dissociation of bound cAMP from the receptor-ligand complex can be used to both estimate the apparent K_d, as well

as characterize the thermodynamic unfolding processes of the cAMP-stripped RIα. This technique provided a simple, rapid and convenient way to compare the impact of cAMP association on protein stability since protein purification and unfolding processes can be integrated within a single platform without labor intensive off-line sample pretreatment. The use of a relative viscosity correction factor, as well as performing analyses at a buffer pH range where the protein exhibits minimal mobility changes ensured accurate determination of thermodynamic parameters. Comparative RIα unfolding studies performed by CE with and without excess cAMP in the buffer clearly demonstrated enhanced cooperativity and improved stability upon urea denaturation due to cAMP association which was supported by previous studies. CE represents a promising yet unrecognized technique for characterizing cAPKs compared to conventional spectroscopic methods based on fluorescence and circular dichroism.

2.6. References

1.   Krylov, S. N., *J. Biomol. Screening* 2006, *11*, 115-122.

2.   Mendosa, S. P., Bowser, M. T., *JACS* 2005, *127*, 9382-9383.

3.   Heegaard, N. H. H., Nissen, M. H., Chen, D. D. Y., *Electrophoresis* 2002, *23*, 815-822.

4.   Samson, S., Britz-McKibbin, P., *Electrophoresis* 2006, *27*, 842-851.

5.   Matouschek, A., *Curr. Opin. Struct. Biol.* 2003, *13*, 98-109.

6.   Soto, C., *Nature Rev. Neurosci.* 2003, *4*, 49-60.

7. Creighton, T. E., *J. Mol. Biol.* 1979, *129,* 235-264.

8. Modig, K., Kurian, E., Prendergast, F. G., Halle, B., *Protein Sci.* 2003, *12*, 2768-2781.

9. Hilser, V. J., Freire, E., *Anal. Biochem.* 1995, *224*, 465-485.

10. Righetti, P. G., Verzola, B., *Electrophoresis* 2001, *22*, 2359-2374.

11. Rochu, D., Masson, P., *Electrophoresis* 2002, *23*, 189-202.

12. Verzola, B., Perduca, M., Mezo, G., Hudecz, F., Righetti, P. G., *Electrophoresis* 2003, *24*, 794-800.

13. Verzola, B., Chiti, F., Manao, G., Righetti, P. G., *Anal. Biochem.* 2000, *282*, 239-244.

14. Stellwagen, E., Gelfi, C., Righetti, P. G., *J. Chromatogr. A* 1999, *838*, 131-138.

15. Fan, Z. H., Jensen, P. K., Lee, C. S., King, J., *J. Chromatogr. A* 1997, *769*, 315-323.

16. Hilser, V. J., Worosila, G. D., Freire, E., *Anal. Biochem.* 1993, *208*, 125-131.

17. Strege, M. A., Lagu, A. L., *J. Chromatogr. A* 1993, *652*, 179-188.

18. Rush, R. S., Cohen, A. S., Karger, B. L., *Anal. Chem.* 1991, *63*, 1346-1350.

19. Rochu, D., Pernet, T., Renault, F., Bon, C., Masson, P., *J. Chromatogr. A* 2001, *910*, 347-357.

20. Rochu, D., Ducret, G., Masson, P., *J. Chromatogr. A* 1999, *838*, 157-165.

21. Kilar, F., Hjerten, S., *J. Chromatogr.* 1993, *638*, 269-276.

22. Verzola, B.; Fogolari, F.; Righetti, P. G., *Electrophoresis* 2001, 22, 3728-3735.

23. Taylor, S. S., Yang, J., Wu, J., Haste, N. M., Radzio-Andzelm, E., Anand, G. S., *Biochim. Biophys. Acta* 2004, *1697*, 259-269.

24. Taylor, S. S., Kim, C., Vigil, D., Haste, N. M., Yang, J., Wu, J., Anand, G. S., *Biochim. Biophys. Acta* 2005, *1754*, 25-37.

25. Johnson, D. A., Akamine, P., Radzio-Andzelm, E., Madhusudan, Taylor, S. S., *Chem. Rev.* 2001, *101*, 2243-2270.

26. Canaves, J. M., Leon, D. A., Taylor, S. S., *Biochemistry* 2000, *39*, 15022-15031.

27. Hamuro, Y., Anand, G. S., Kim, J. S., Juliano, C., Stranz, D. D., Taylor, S. S., Woods, V. L. Jr., *J. Mol. Biol.* 2004, *340*, 1185-1196.

28. Kawahara, K., Tanford, C., *J. Biol. Chem.* 1966, *241*, 3228-3232.

29. Leon, D. A., Canaves, J. M., Taylor, S. S., *Biochemistry* 2000, *39*, 5662-5671.

30. *Protein Calculator v. 3.3*, http://www.scripps.edu/~cdputnam/protcalc.html.

31. Krylov, S. N., *J. Biomol. Screening* 2006, *11*, 115-122.

32. Zorn, M., Fladmark, K. E., Ogreid, D., Jastorff, B., Doskeland, S. O., Dostmann, W. R. G., *FEBS Letters* 1995, *362,* 291-294.

33. Rochu, D., Clery-Barraud, C., Renault, F., Chevalier, A., Bon, C., Masson, P. *Electrophoresis* 2006, *27,* 442-451.

34. Gullingsrud, J., Kim, C., Taylor, S. S., McCammon, J. A., *Structure* 2006, *14*, 141-149.

(Intentionally Blank)

Chapter III

Label-free Assay for Thermodynamic Analysis of Protein-Ligand

Interactions: A Multivariate Strategy for Allosteric Ligand Screening

III. Label-free Assay for Thermodynamic Analysis of Protein-Ligand Interactions: A Multivariate Strategy for Allosteric Ligand Screening

3.1. Abstract

The binding of allosteric ligands to protein can induce changes to *holo*-protein conformation, stability and activity that impact unfolding dynamics. Herein we report a label-free strategy for determining the dissociation constant of protein-ligand interactions over a wide dynamic range ($> 10^4$, $K_d \approx$ nM-mM) using capillary electrophoresis that overcomes the constraints of an ideal two-state protein unfolding model. Multivariate analysis of thermodynamic parameters associated with *holo*-protein unfolding and ligand binding is demonstrated for the classification of cyclic nucleotide analogs that function as allosteric modulators of regulatory protein, such as the exchange protein directly activated by cAMP (EPAC).

3.2. Introduction

Successful identification of small molecule modulators of cellular activity is a critical step in modern drug discovery.[1] To date, high-throughput screening methods have relied primarily on fluorescence and competitive radiolabel assays for ligand selection since binding affinity is related to drug potency.[2] There is growing interest in the development of label-free strategies which are compatible with small amounts of impure protein samples and/or complex ligand mixtures, such as frontal affinity chromatography-electrospray ionization-MS[3] and matrix-

assisted laser desorption ionization-MS.[4] New methods that avoid protein immobilization, chemical labeling and/or complicated *off-line* sample preparation while providing additional thermodynamic criteria for assessing high affinity interactions are also desirable features to improve lead optimization of drug candidates.[5] Herein, we describe a label-free strategy for determining the dissociation constant (K_d) of effector molecules to protein receptors over a wide dynamic range using dynamic ligand exchange-affinity capillary electrophoresis (DLE-ACE),[6] which is based on the relative conformational stability of different *apo/holo*-protein states upon unfolding (refer to Supplemental Information). A unique feature of DLE-ACE is the ability to electrokinetically generate different *apo/holo*-protein states directly in-capillary using fmol of protein sample with conventional UV detection[7] (refer to Supplemental Information). Access to multiple thermodynamic parameters associated with *holo*protein unfolding and ligand binding can provide insight into the function of allosteric ligands that activate or inhibit the activity of regulatory protein involved in signal transduction.[8]

3.3. Results and Discussion

The thermodynamics of EPAC (residues 149-318) binding to various cyclic nucleotide (cNT) analogues was examined as a model system in this work, which is a recently discovered cAMP-responsive guanine nucleotide exchange factor for the small GTP-binding proteins Rap1 and Rap2.[9] There is growing

interest in the development of ligands that selectively target EPAC due to its altered expression in several chronic disorders, such as Alzheimer's disease.[10] **Figure 3.1** depicts the chemical structures of six cNT analogs (*i.e.,* training set), as well as an overlay of protein unfolding curves derived from DLE-ACE experiments, which highlights the significant impact of ligand binding on *holo*-protein conformational stability. In general, cNTs that possess higher affinity for EPAC (*e.g.,* 8-pCPT-cAMP) generate *holo*-EPAC-cNT complexes with greater intrinsic stability (ΔG°_U) and higher unfolding cooperativity (*m*) (*i.e.,* slope of unfolding transition region) relative to *apo*-EPAC. Stronger binding was also directly associated with an increase in the mid-point for urea denaturation (C_M). Interestingly, *Rp*-cAMPS was the only ligand that resulted in a major decrease in C_M relative to *apo*-EPAC despite its apparent greater ΔG°_U. This anomaly suggests that EPAC binding to this phosphothioate cNT analogue induces destabilization of the native protein conformation that is more susceptible to urea denaturation.[11] Indeed, *Rp*-cAMPS has been reported to function as an allosteric inhibitor of EPAC activation unlike its stereoisomer *Sp*-cAMPS that is an allosteric agonist.[12] The higher ΔG°_U for *holo*-EPAC-*Rp*-cAMPS relative to *apo*-EPAC is likely an artifact from extrapolation to zero urea concentration due to their differences in *m* values.[13]

The apparent dissociation constant (K_d) for protein-ligand interactions can be derived from protein unfolding experiments based on the relative free energy change ($\Delta\Delta G^\circ_U$) measured between *holo*-EPAC-cNT and *apo*-EPAC states (refer
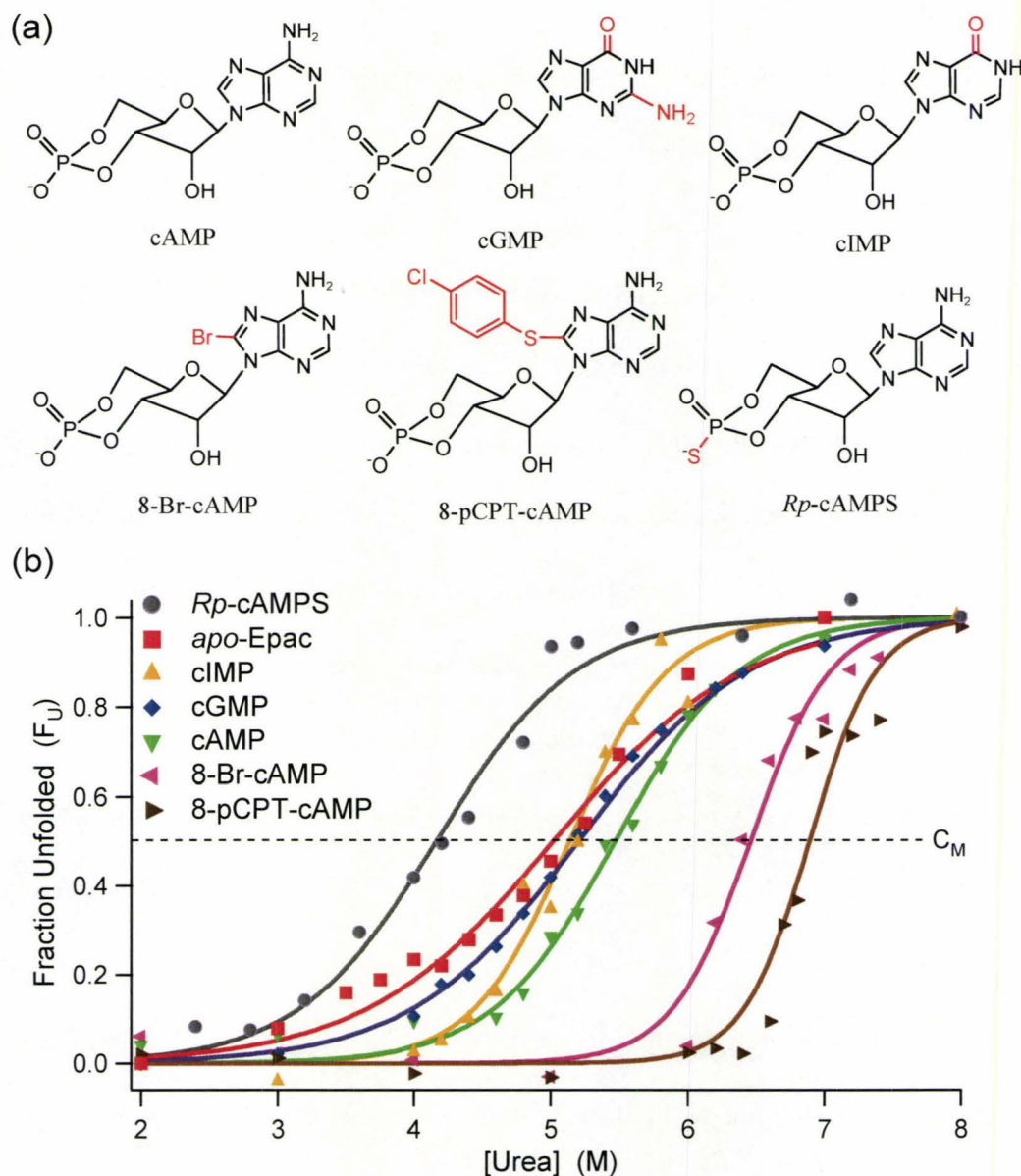
Figure 3.1. Impact of cNT binding on the conformational stability of EPAC upon urea denaturation by DLE-ACE, where (a) shows 2D chemical structures of different cNT analogs and (b) compares *apo/holo*protein unfolding curves based on average viscocity-corrected apparent mobility of protein, $\nu\mu^{A}_{ep}$ (symbols, *n*=3, CV < 5%) assuming an ideal two-state model, where C_M represents the mid-point for urea denaturation ($F_u = 0.5$).

to Supplemental Information). However, several caveats apply to ensure accurate

determination of absolute K_d, which include equivalent *m* values for both *apo*- and

holo-protein states undergoing a reversible two-state unfolding process without partially folded intermediates.[4, 14] The latter assumptions can result in a significant bias in K_d determination when characterizing allosteric protein such as EPAC, which requires multiple structural changes upon ligand binding to release self-inhibition of the catalytic region of the protein.[15] Moreover, *apo*-EPAC has recently been shown to exist in dynamic equilibrium between active and inactive states in the absence of cAMP[16] that is consistent with an allosteric activation model where ligand binding induces shifts in pre-existing conformer populations.[8] In this study, only $\Delta\Delta G°_U$ values for cGMP provided a reasonable estimate for K_d ≈ 20 μM[17] due to its similar *m* value with *apo*-EPAC, whereas highly overestimated binding affinity was determined for all other cNT analogs when using apparent $\Delta\Delta G°_U$ values (refer to **Table 3.2** of Supplemental Information). The magnitude of this bias was proportional to the difference in unfolding cooperativity between *apo*- and *holo*- EPAC-cNT states (Δm). The large increase in Δm values measured for most *holo*-EPAC-cNT complexes relative to *apo*-EPAC can be attributed to their reduction in solvent accessible surface area[18] and/or the lack of partially unfolded intermediates in the transition region[13] that is suggestive of an increasingly homogeneous conformer population. In cases when Δm values for different *holo*-protein states are similar in magnitude yet different from *apo*-EPAC, then relative K_d values can be determined directly from unfolding parameters[6] without bias caused by $\Delta G°_U$ extrapolation to native conditions.

Table 3.1. Relative thermodynamic parameters associated with *holo*-EPAC-cNT unfolding and ligand binding affinity by DCE-ACE.

cNT[a]	$\Delta\Delta G_U^{0[b]}$ (kcal/mol)	$\Delta m^{[b]}$ (kcal/molM)	$\Delta C_M^{[c]}$ (M)	$K_d^{[d]}$ (μM)	$K_d^{[e]}$ (μM)
Rp-cAMPS	0.54	0.26	-0.58	305	340
cGMP	0.97	0.12	0.41	33	37
Sp-cAMPS	2.44	0.56	-0.10	28	34
cAMP	2.70	0.33	0.94	4.6	2.9
cIMP	4.52	0.83	0.13	12	10
8-Br-cAMP	8.72	1.12	1.70	0.23	0.36
8-pCPT-2′-*O*Me-cAMP[f]	11.4	1.94	0.79	0.13	0.41
8-pCPT-cAMP	16.9	2.20	2.10	0.051	0.045

[a] $\Delta G°_U$, m and C_M values for *apo*-EPAC were (4.28 ± 0.12) kcal/mol (0.90 ± 0.02) kcal/molM and (4.75 ± 0.04) M, respectively, [b] fitting error from protein unfolding curves, CV (±1σ): 2-12%, [c] $\Delta C_M = [(\Delta G°_U/m)_{holo} - (\Delta G°_U/m)_{apo}]$, [d] Predicted K_d of model cNTs using MLR calibration, CV (±1σ): 38-80%, [e] K_d from Christensen *et al.*[17] using competitive [^{3}H]-cAMP radiolabel assay, [f] rapid unfolding assay (< 1 hr) with limited data for K_d estimation. Note that *Sp*-cAMPS and 8-pCPT-2-OMe-cAMP were used for subsequent validation of the MLR model.

Table 3.1 summarizes the three major thermodynamic parameters determined for holo-EPAC-cNT unfolding relative to apo-EPAC. It was observed that there was a significant linear correlation ($R^2 = 0.9474$) between ΔC_M parameters from unfolding studies in this work and $-\log K_d$ reported using a competitive [^{3}H]-cAMP binding assay.[17] However, multiple linear regression (MLR) using all three thermodynamic variables provided improved correlation ($R^2 = 0.9910$) and greater predictive accuracy for K_d over a 10^4-fold dynamic range ($K_d \approx$ nM-mM) as shown in **Figure 3.2(a)**. Since ΔC_M is defined as the relative ratio of $[(\Delta G°_U/m)_{holo} - (\Delta G°_U/m)_{apo}]$, it serves as a useful parameter for normalizing changes in apparent $\Delta G°_U$ when comparing different *holo*-EPAC-cNT states (refer to Supplemental Information). The inset of **Figure 3.2(a)** confirms that ΔC_M is statistically the most significant ($P = 0.05$) thermodynamic variable positively correlated with higher binding affinity. Overall, the average
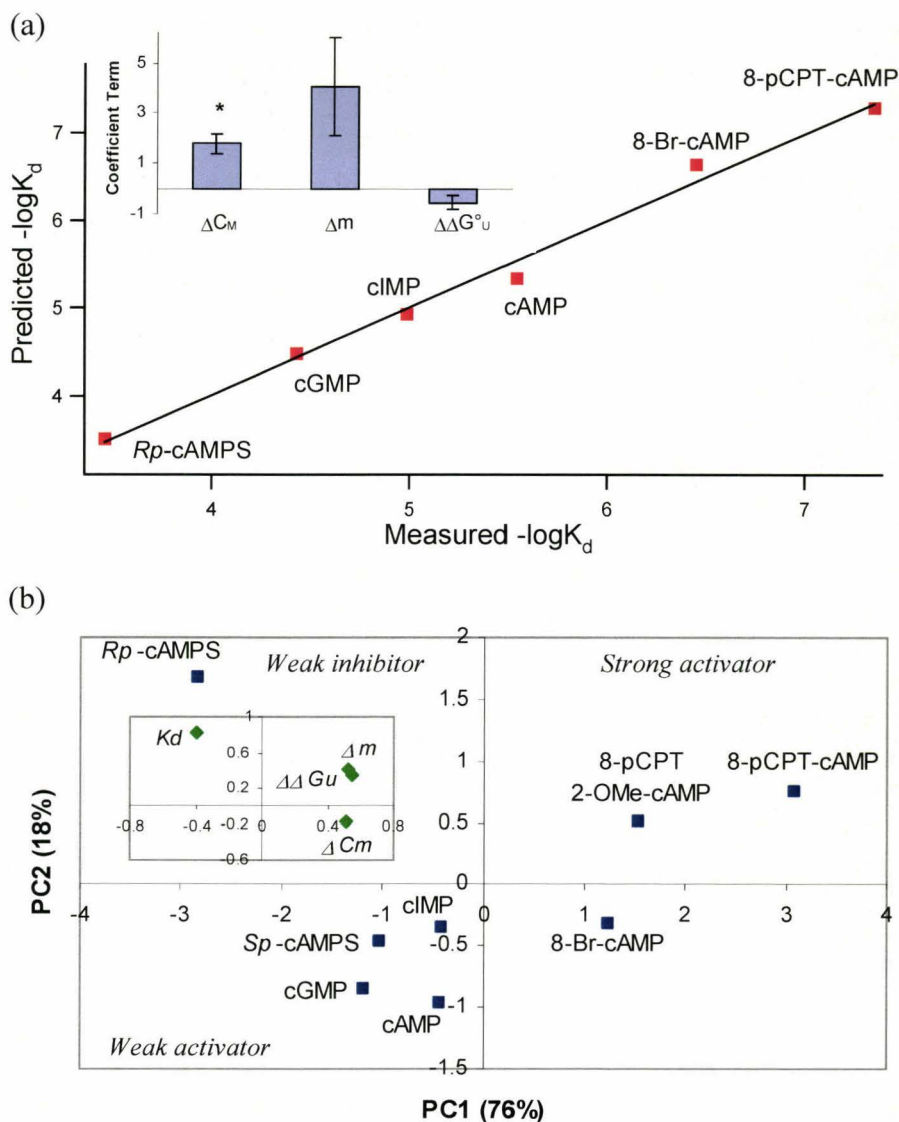
Figure 3.2. (a) Linear correlation plot (y= 0.990x + 0.049; R^2 =0.9954) between predicted $-logK_d$ derived from *holo*-EPAC-cNT unfolding studies using DLE-ACE and measured $-logK_d$ of EPAC-cNT binding by competitive radiolabel assay.[17] The inset graph shows that ΔC_M was the most significant thermodynamic variable (*, $P < 0.05$) directly correlated with higher EPAC-cNT binding affinity unlike $\Delta\Delta G°_U$ when using MLR, where error bars represent $\pm 1\sigma$, (b) 2D scores plot using principal component analysis (PCA) for classifying different cNTs based on multiple thermodynamics criteria associated with *holo*-EPAC-cNT unfolding and binding for prediction of allosteric ligand function, where the inset depicts a loadings plot that highlights the contribution of each thermodynamic variable on cNT coordinates within the scores plot.

relative error in the absolute K_d values was about 16% when comparing results with a validated radiolabel assay.[17] Two additional cNT analogs (*i.e.,* test set) were also examined to further validate the predictive capability of the model (**Figure 3.5** of Supplemental Information). **Table 3.1** shows that *Sp*-cAMPS was observed to have $\Delta\Delta G°_U$ and Δm terms similar to cAMP but with a 6-fold lower affinity ($K_d \approx 28$ µM), which is consistent with its function as a weak EPAC activator.[17] Recent studies have demonstrated that 8-pCPT-2-OMe-cAMP has about a 10^3-fold increase in target selectivity for EPAC relative to cAMP-dependent protein kinase A with super-agonist activity.[12, 17] In this case, a limited unfolding study for *holo*-EPAC-8-pCPT-2-OMe-cAMP was also performed (refer to Supplemental Information) to demonstrate the feasibility for rapid K_d estimation by DLE-ACE. **Table 3.1** confirms that improving EPAC selectivity via 2-OMe ribose modification of 8-pCPT-cAMP results in a net decrease in its binding affinity.

There is growing recognition that small globular proteins can often undergo multi-state unfolding transitions despite being adequately described by an ideal two-state model in the absence of detectable partially folded intermediates.[13] In this work, we have demonstrated that non-ideality can be revealed by the disparity in *apo/holo*-protein unfolding cooperativity as inferred by significant differences in Δm, which hampers accurate K_d determination directly from $\Delta\Delta G°_U$ values. **Figure 3.2(b)** summarizes the results from **Table 3.1** using a 2D scores plot from principal component analysis (PCA), which was applied to

compare eight different cNT analogs based on their four different thermodynamic variables associated with EPAC-cNT interactions, namely ΔC_M, Δm, $\Delta \Delta G°_U$ and K_d (refer to Supplemental Information). It is evident that three major groups of allosteric ligands can be classified on this multivariate thermodynamic map, which provides insight into their putative mechanism of allosteric activation. For instance, Rp-cAMPS and the 8-modified cNT analogs represent two distinct classes of ligands for EPAC relative to cAMP, which is consistent with their reported activity as a weak antagonist and strong agonists, respectively.[12] In contrast, Sp-cAMPS, cGMP and cIMP appear as a group to function more similar to native cAMP, although cGMP and cIMP have been shown to behave as weak partial agonists of EPAC activation.[17] Improved prediction of putative allosteric ligand function may be realized when using a full length protein that undergoes global conformational changes upon ligand binding unlike the truncated protein construct used in this study.

Ligands that target allosteric sites of protein offer promising therapeutic benefits compared to traditional orthosteric drug design.[19] However, caution is needed when comparing equilibrium unfolding studies involving regulatory protein to different allosteric ligands since differences in Δm contribute to bias in $\Delta \Delta G°_U$ and K_d values. Our studies suggest that Δm is a parameter related to an overall increase in the homogeneity/ordering of $holo$-protein conformation(s) relative to the apo-state, whereas the sign and magnitude of ΔC_M is associated with the extent of ligand-induced stabilization/destabilization that can be

quantitatively related to K_d via multivariate calibration Future work will explore multivariate thermodynamic maps for improved selection of novel allosteric drugs by DLE-ACE, such as chemical chaperones[20] that are relevant in enzyme enhancement therapy for in-born errors of metabolism based on ligand-induced conformational stabilization of misfolded proteins.

3.4. Supplemental Information

3.4.1 Chemicals and Reagents

De-ionized water for buffer and sample preparations was obtained using a Barnstead EASYpure® II LF ultrapure water system (Dubuque, IA, USA). Adenosine 3',5'-cyclic monophosphate (cAMP), 8-bromo adenosine 3',5'-cyclic monophosphate (8-Br-cAMP), guanosine 3',5'-cyclic monophosphate (cGMP), Rp-adenosine 3',5'-cyclic monophosphorothioate (Rp-cAMPS), Sp-adenosine 3',5'-cyclic monophosphorothioate (Sp-cAMPS), inosine 3',5'-cyclic monophosphate (cIMP), 8-($para$-chlorophenylthio)adenosine 3',5'-cyclic monophosphate (8-pCPT-cAMP), 8-($para$-chlorophenylthio)-2'-O-methyladenosine 3',5'-cyclic monophosphate (8-pCPT-2-OMe-cAMP), ammonium carbonate (NH_4CO_3), potassium phosphate monobasic (KH_2PO_4), sodium phosphate dibasic (Na_2HPO_4), ethylenediaminetetraacetic acid (EDTA), glycerol, Tris(2-carboxyethyl)phosphine hydrochloride (TCEP), ammonium chloride (NH_4Cl), TRIZMA base, sodium azide (NaN_3) and sodium hydroxide (NaOH) were all purchased from Sigma (St. Louis, MO, USA). Sodium chloride,

potassium chloride, urea (molecular biology grade) and 4-(2-hydroxyethyl)-1-piperazineethanesulfonic acid (HEPES) were obtained from BioShop Canada Inc. (Burlington, ON, Canada).

3.4.2. Protein Preparation

A truncated human EPAC1 (149-318) construct with a single cyclic nucleotide binding domain was used in this work since it has been previously shown to be a good model for cNT binding relative to its full length isoform by Rehmann et al.[12] A human EPAC1 (149-318) truncated protein construct was expressed according to the procedure described by Mazhab-Jafari et al.[21] Briefly, E. coli BL21 (DE3) containing the pGEX-4T3 expression vector EPAC1(149-318) was grown at 37°C in minimal media supplemented with trace metals, vitamins (10 mg/L thiamine and biotin), salts (NaCl, KH_2PO_4, and Na_2HPO_4), 1 g/L 15N-ammonium chloride, 100 μg/mL ampicillin, and 3 g/L glucose until they reached $OD_{600nm} = 0.6$. Cells were then induced with 1 mM IPTG and harvested after 3 hrs. Cells were isolated by centrifugation for 10 min at 8000 g and resuspended in lysis buffer (PBS: 10 mM phosphate, 137 mM NaCl, 2.7 mM KCl, pH 7.4; 10 mM EDTA; 10% v/v glycerol). Cells were lysed by EmulsiFlex-C5 homogenizer (AVESTIN) at 5000 psi. The cell lysate was then centrifuged at 14,000 g for 40 min, the supernatant collected, separated and incubated with pre-equilibrated Glutathione Sepharose T4 Fast Flowbeads (Amersham Biosciences, Inc.) with rotation for 4 h at 4°C. The beads were washed with 0.5 M NaCl in 50 mM Tris, pH 8 and the expressed protein was cleaved from the GST tag using

biotinylated thrombin (Novagen). The thrombin was removed by incubation with streptavidin beads, and further purification was achieved by ion exchange chromatography using a Q-column (GE Health Sciences). The protein was then dialyzed against 50 mM HEPES at pH 7.6, 50 mM NaCl, 1 mM TCEP, 0.02% w/v NaN_3 and concentrated to 24 µM using Pall Nanasep 3 kDa omega centrifuge tubes (VWR, AZ, USA). EPAC1(149-318) was further characterized by CE-ESI-MS in the positive mode (MH^+) using an Agilent XCT IT mass analyser (Agilent Technologies, DE, USA) which resulted in an apparent mass of 19.45 kDa for the both *apo* and *holo*-cAMP-Epac1$_h$(149-318), confirming irreversible cAMP-stripping from the receptor during electrophoresis. Conditions for capillary electrophoresis were 100 mM NH_4CO_3, pH 6.5 at a voltage of +17 kV. MS conditions were 4 kV capillary voltage with a scan range from 200-1800 m/z. The apparent *pI* of the acidic protein was 5.46 as predicted from the amino acid sequence by the ProtParam tool on the ExPASy server (http://ca.expasy.org/tools/protparam.html).

3.4.3. Capillary Electrophoresis

Samples for DLE-ACE unfolding studies consisted of 10 µM EPAC, 300 µM cAMP and 350 µM caffeine (neutral EOF marker). A single sample of 30 µL total volume was sufficient to complete an unfolding curve experiment with triplicate measurements at each urea concentration. Separations were performed on an automated P/ACE 5500 system equipped with UV detection (Beckman-Coulter Inc., Fullerton, CA, USA) in a 50 µm i.d., 360 µm o.d. uncoated fused-

silica capillary (Polymicro Technologies, Phoenix, USA) 27 cm in length (20 cm to the detector window). All separations were thermostatted to 25°C and electropherograms were collected at 214 nm. New capillaries were conditioned by rinsing with methanol for 5 min, water for 5 min, 1 M NaOH for 5 min, background electrolyte (BGE: 100 mM HEPES, pH 7.4) for 5 min and were left to equilibrate overnight. At the beginning of each day, the capillary was rinsed for 5 min with 0.1 M NaOH and BGE for 5 min. Separations began by rinsing the capillary for 3 min with BGE followed by a 0.2 min wait in water. DLE was performed by addition of a 10-fold excess of cNT (100 μM) to the BGE while protein unfolding was performed by addition of increasing concentrations of urea (0-8 M) to the BGE. Samples were injected by low pressure (0.5 psi or 3.5 kPa) for 5 s and separated by application of +10 kV. Between sets of replicate measurements, the capillary was rinsed for 2 min with 0.1 M NaOH and 5 min with BGE. At the end of the day, the capillary was rinsed for 5 min with 0.1 M NaOH and 5 min with BGE and stored overnight in BGE. For longer storage, the capillary was rinsed for 5 min with 0.1 M NaOH, 5 min water and then stored in air. Daily cleaning of electrodes was required due to rapid salt build-up from urea usage in BGE. The viscosity correction factor (v) was calculated by CE by the average time (n = 5) required for a sample plug to travel to the detector window under low pressure by Seguí-Lines et al.[6]

3.4.4. Data Processing

All data processing and linear/non-linear regression was performed using

Igor Pro 5.0 (Wavemetrics Inc., Lake Oswego, OR, USA). Multiple linear regression (MLR) for correlation of thermodynamic unfolding parameters associated with *holo*-cNT-EPAC with measured K_d using a validated radiometric assay[17] was performed by Excel (Microsoft Inc., Redmond, WA, USA). Apparent K_d for model and test cNTs based on measured unfolding parameters were predicted using the equation $-\log K_d = (1.79 \pm 0.41)\Delta C_M + (4.1 \pm 1.9)\Delta m - (0.54 \pm 0.29)\Delta G°_U + (3.80 \pm 0.22)$ with a $R^2 = 0.9910$. Principal component analysis (PCA) of four major thermodynamic parameters associated with protein unfolding and ligand binding was performed using a multivariate analysis add-in for excel developed by Dr. Richard Brereton that is freely available for download at http://www.chm.bris.ac.uk/org/chemometrics/addins/index.html. PCA was performed as an unsupervised dimensionality reduction method for correlating inter-sample variations for eight different cNT analogues in terms of their four measured thermodynamic variables associated with protein unfolding and ligand binding to EPAC (ΔC_M, Δm, $\Delta\Delta G°_U$ and K_d). This was useful for identifying sample groupings, outliers and qualitative trends among cNTs that can provide insight into their putative biological activity in terms of allosteric ligand function and potency (*e.g.*, weak or strong activators/inhibitors). Improved screening of allosteric ligands may be realized by this approach when using full length EPAC constructs that undergo global conformational changes as a result of cNT binding.

3.4.5. Theory

CE offers a convenient microseparation format for performing protein
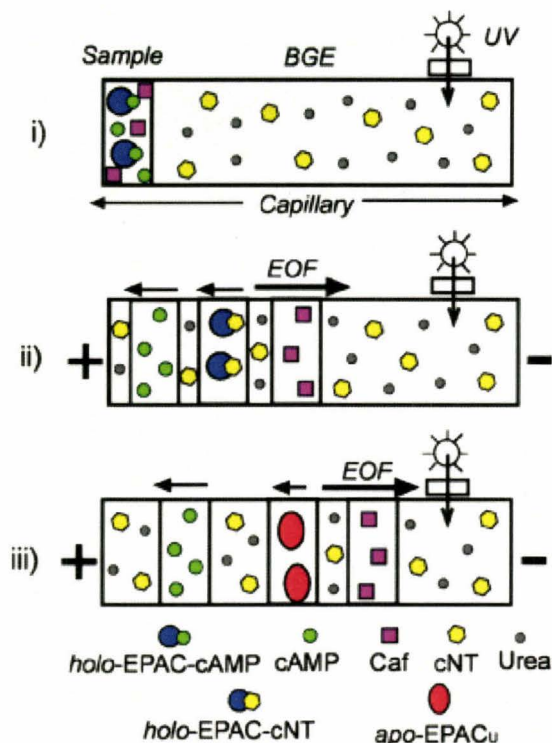
Figure 3.3. Three-step electrokinetic process in DLE-ACE depicting i) initial sample injection, ii) cAMP-stripping with *apo*-EPAC generation (no cNT in BGE) or ligand exchange with *holo*-EPAC-cNT formation and iii) EPAC unfolding with cNT dissociation upon urea denaturation (*apo*-EPAC$_U$). Note that prior to voltage application, a discontinuous electrolyte system was used consisting of a sample zone (caffeine or Caf is the neutral EOF marker) and background electrolyte (BGE), where cNT type and urea concentration in BGE was varied to generate different protein states directly in-capillary during electromigration. Note that the magnitude of the mobilities (μ_{ep}) of free ligand and protein states is reflected by vector arrows.

unfolding studies that is applicable to small amounts of impure protein samples.[22-24] In most cases, the electrophoretic mobility (μ_{ep}) of low molecular weight ligands (*e.g.*, anionic cNTs) is much greater in magnitude than bulky protein, which permits irreversible electrokinetic separation of bound and excess cAMP in the original protein sample.[6] Different protein states (*e.g.*, *apo*, *holo*, unfolded etc.) can be readily generated by DLE- ACE during electromigration based on changes in the composition of the background electrolyte (BGE), such as cNT

type/concentration and urea content as depicted in **Figure 3.3**. Provided that fast and reversible ligand exchange occurs prior to protein unfolding, then the conformational stability of different *holo*-EPAC-cNT complexes can be compared via changes in the viscosity-corrected apparent mobility ($v\mu_{ep}{}^{A}$) of the protein.[6] This method is distinct from classical mobility-shift assays in ACE[25-29] that are often dependent on the separation and quantification of a fluorescently-labeled protein, ligand and/or protein-ligand complex under non-denaturing conditions. In contrast, DLE-ACE is ideally suited for assessing high affinity protein-ligand interactions (K_d < nM) without chemical labeling when using conventional UV detection since responses are directly related to changes in *holo*-protein conformational stability, unlike conventional binding assays that are limited by detector sensitivity. Thus, DLE-ACE offers a simple yet integrated method for in-situ preparation and characterization of different protein states without off-line sample pre-treatment that is important when studying labile *apo*-protein states.[7] The fraction of unfolded protein (F_U) can be determined by changes in average $v\mu_{ep}{}^{A}$ of EPAC as a function of urea concentration (c) to generate *apo/holo*-EPAC-cNT unfolding curves assuming an ideal two-state system:

$$F_U = \frac{v\mu_{ep}^{A} - \mu_{ep,F}}{\mu_{ep,U} - \mu_{ep,F}} \tag{3-1}$$

where, $\mu_{ep,F}$ and $\mu_{ep,U}$ represent the mobility of fully folded and unfolded protein states, respectively. **Figure 3.4** qualitatively shows differences in $v\mu_{ep}^{A}$ for different *holo*-EPAC-cNT complexes at 5 M urea, where *Rp*-cAMPS and 8-
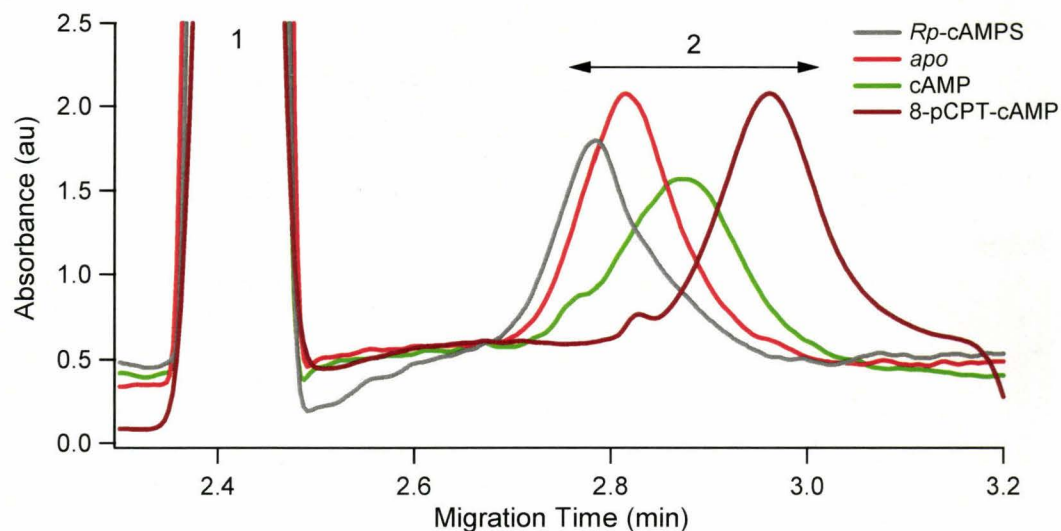
Figure 3.4. Impact of cNT on the conformational stability of EPAC using DLE-ACE that shows overlay electropherograms for different *apo/holo*-EPAC-cNT states at 5 M urea, where peaks detected include the neutral EOF marker, caffeine (1) and *apo/holo*-EPAC complex (2). Note that *Rp*-cAMPS and 8-pCPT-cAMP generated the least and most resistant *holo*-EPAC-cNT complexes to urea denaturation relative to *apo*-EPAC.

pCPT-cAMP represent the fully unfolded and folded protein states, respectively. In most cases, unfolding of the native protein structure results in a decrease in its $\nu\mu^A_{ep}$ (*i.e.,* shorter migration time) due to increased hydrodynamic frictional resistance that migrates as a single average peak.[7] Non-linear regression of protein unfolding curves was performed to derive apparent free energy change ($\Delta G°_U$) and cooperativity (*m*) parameters using **Eq. 3-2**:

$$F_U = \frac{\exp\left(-\dfrac{\Delta G_U^0 - mc}{RT}\right)}{1 + \exp\left(-\dfrac{\Delta G_U^0 - mc}{RT}\right)} \qquad (3\text{-}2)$$

In this study, non-linear regression was found to be provide more reliable thermodynamic parameters compared to the classical linear extrapolation method

notably for ligands that induced highly cooperative EPAC unfolding (*e.g.,* large positive *m* values) in the transition region over a narrow urea concentration range. This is mainly attributed to the fact that linear extrapolation methods are more subject to bias since they depend only on a subset of data in the unfolding transition region (typically $F_U \approx 0.2$-0.8), which can be experimentally difficult to acquire. Our previous report[6] validated DLE-ACE for measuring thermodynamic unfolding parameters using the regulatory sub-unit of protein kinase A as a model system that were consistent with native fluorescence spectroscopy. To the best of our knowledge, this is the first unfolding study of *apo/holo*-EPAC reported in the literature to date. **Figure 3.5** shows unfolding curves for additional cNT analogues used for model validation relative to *holo*-EPAC-cAMP, namely *Sp*-cAMPS and 8-pCPT-2-OMe-cAMP, which represent an EPAC agonist and super-agonist, respectively. Ligand binding affinity can be derived from protein unfolding experiments assuming a reversible two-state approximation based on the relative free energy change measured between *holo*-EPAC-cNT and *apo*-EPAC states ($\Delta\Delta G^\circ_U$),[4, 30] where, *[L]* represents the free ligand concentration, ΔG°_d is the free energy for ligand dissociation and $\Delta\Delta G^\circ_U$ is the relative free energy change for unfolding that is equivalent to $(\Delta G^\circ_{U,holo} - \Delta G^\circ_{U,apo})$. Despite the apparent adherence to a two-state unfolding model in this work based on goodness of fit ($X^2 < 4.0 \times 10^{-10}$) of predicted unfolding curves derived from **Eq. 3-2** to experimental data, most proteins (*e.g.,* regulatory protein)
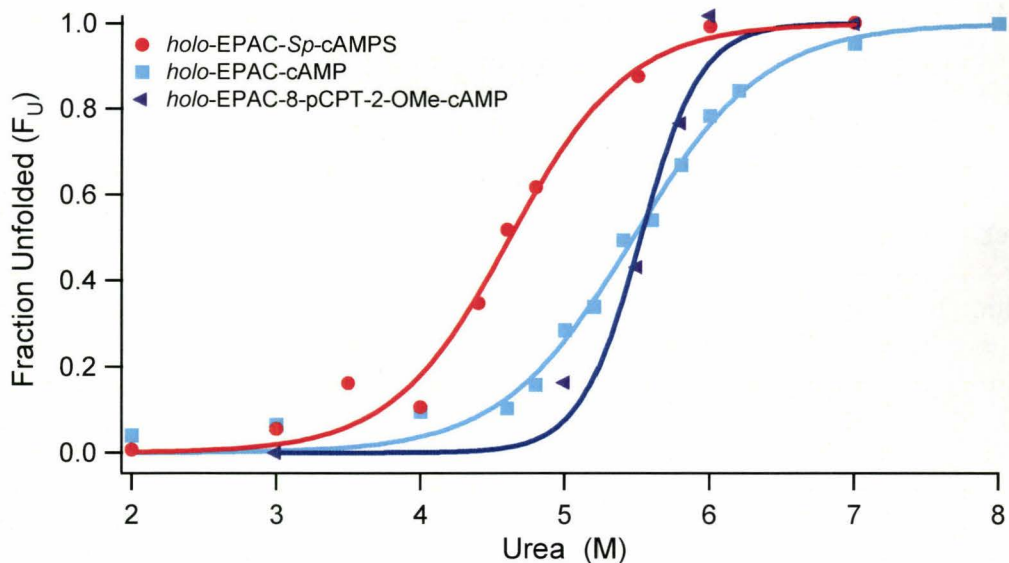
Figure 3.5. Overlay plots showing *holo*-EPAC-cNT unfolding curves by DLE-ACE, where symbols represent average F_u using eq. (1), whereas solid lines were derived from eq. (2) for determination of $\Delta G°_U$ and m using non-linear regression. Note that Rp-cAMPS and 8-pCPT-2-OMe-cAMP were used for validation of MLR model using normal (> 10 conditions in triplicate) and minimal data sets (6 conditions in duplicate, < 1 hr), respectively. The latter study was performed to demonstrate the feasibility for rapid estimation of apparent K_d.

tend to exhibit partially folded intermediates populated during unfolding transitions, which are nonetheless difficult to detect by conventional methods.[13] This phenomenon was inferred by major differences in relative *apo/holo*-protein unfolding cooperativity (Δm) that confounded $\Delta\Delta G°_U$ values while resulting in significant overestimates in binding affinity ($K_d^{[c]}$) except for cGMP as summarized in **Table 3.2**. In general, the presence of partially folded intermediates and thus a more heterogeneous conformer population tends to reduce the slope within the unfolding transition[13] (m) based on an ideal two-state model, which was most evident in the cases of *apo*-EPAC and *holo*-EPAC-cGMP. In contrast, cNT binding that resulted in enhanced *holo*-EPAC stability resulted in

Table 3.2. Apparent thermodynamic parameters measured for *holo*-EPAC-cNT unfolding and ligand binding by DCE-ACE highlighting significant bias in direct K_d determination from $\Delta\Delta G_U°$.

cNT	$\Delta G_U^{0[a]}$ (kcal/mol)	$m^{[a]}$ (kcal/mol M)	$C_M^{[a, b]}$ (M)	$K_d^{[c]}$ (μM)	$K_d^{[d]}$ (μM)	$K_d^{[e]}$ (μM)
apo-EPAC	(4.28 ± 0.12)	(0.904 ± 0.024)	(4.75 ± 0.04)	--	--	--
Rp-cAMPS	(4.82 ± 0.26)	(1.16 ± 0.06)	(4.25 ± 0.02)	40	305	340
cGMP	(5.25 ± 0.08)	(1.02 ± 0.02)	(5.16 ± 0.02)	19	33	37
Sp-cAMPS	(6.72 ± 0.82)	(1.46 ± 0.18)	(4.65 ± 0.05)	1.6	28	34
cAMP	(6.98 ± 0.27)	(1.23 ± 0.05)	(5.51 ± 0.02)	1.0	4.6	2.9
cIMP	(8.80 ± 0.55)	(1.73 ± 0.11)	(5.09 ± 0.03)	0.048	12	10
8-Br-cAMP	(13.0 ± 1.0)	(2.02 ± 0.16)	(6.37 ± 0.03)	4.0 E-5	0.23	0.36
8-pCPT-2′-OMe-cAMP[f]	(15.7 ± 3.7)	(2.84 ± 0.66)	(5.53 ± 0.05)	4.3 E-7	0.13	0.41
8-pCPT-cAMP	(21.2 ± 3.1)	(3.10 ± 0.28)	(6.82 ± 0.02)	3.9 E-11	0.051	0.045

[a] All errors in thermodynamic parameters associated with protein unfolding represent fitting error ($\pm 1\sigma$) from non-linear regression [b] C_M was determined graphically from *apo/holo*-protein unfolding curves as the urea concentration when $F_u = 0.5$, [c] Apparent K_d of model cNTs derived from *apo/hol-o*protein unfolding studies, where $K_d = EXP_{-}(\Delta\Delta G_U°-RTln[L])/RT$, [d] Predicted K_d of model cNTs using MLR calibration, CV ($\pm 1\sigma$): 38-80%, [e] K_d from reference [4] using competitive $[^3H]$-cAMP radiolabel assay, [f] rapid unfolding assay (< 1 hr) with limited data points for K_d estimation. Note that *Sp*-cAMPS and 8-pCPT-2-OMe-cAMP were used for subsequent validation of the MLR model.

sharp unfolding transitions with an increasingly homogeneous conformer population that unfolded cooperatively, such as *holo*-EPAC-pCPT-cAMP and *holo*-EPAC-8-Br-cAMP complexes. The latter protein states were less likely to have significantly populated partially unfolded intermediates; however this prevented direct comparisons with *apo*-EPAC for accurate K_d determination without adequate data normalization. Indeed, the statistically most significant parameter directly associated with higher binding affinity (low K_d or high $-logK_d$) was ΔC_M (where, $\Delta G_U = \Delta G°_U - mC_M = 0$ at equilibrium when $F_u = 0.5$), which was determined experimentally by the expression below in order to correct for

differences in *m* that biased apparent $\Delta G°_U$ values when comparing different

apo/holo-protein states:

$$\Delta C_M = \left[\left(\frac{\Delta G_U^o}{m} \right)_{holo} - \left(\frac{\Delta G_U^o}{m} \right)_{apo} \right]$$
(3-4)

It should be noted that cGMP was previously characterized to fully

activate the regulatory sub-unit of cAMP-dependent protein kinase A[6] resulting in

Δm values of similar magnitude than cAMP in contrast to EPAC. However, recent

work by Christensen *et al.*[17] demonstrated that cGMP and other 6-modified cAMP

analogs poorly activate EPAC, which suggests that EPAC is weakly activated *in-*

vivo by cGMP despite its higher intracellular concentration relative to cAMP.

Thus, our data suggests that cGMP binding does not induce a major change in

conformational population states of *apo*-EPAC as reflected by its low Δm value,

which allows for reasonably accurate K_d determination directly from $\Delta\Delta G°_U$.

3.4.6. Validation of EPAC Unfolding Dynamics

The assumptions of fast and reversible protein unfolding dynamics were

confirmed experimentally by DLE-ACE.   Fast unfolding was verified by

incubating EPAC in 7 M urea and then analyzing for significant changes in EPAC

$\nu\mu^A_{ep}$ as a function of time. The sample was injected into the capillary filled with

a buffer with 7M urea and excess cAMP at times 0-3 hrs after initial off-line

denaturation at room temperature. It was observed that there were no significant

changes $\nu\mu^A_{ep}$ with increased denaturation time supporting the conclusion that

unfolding is complete within the timescale of the separation (< 3 min). It should be noted that the kinetics of ligand exchange with EPAC necessarily occurs at a faster timescale than unfolding since alterations of cNT type and concentration in the BGE resulted in significant changes in apparent EPAC conformational stability.

The reversibility of unfolding was similarly verified by refolding experiments in which *apo*-EPAC was unfolded by incubation in 7M urea. The denatured protein was then dynamically refolded and analyzed by DLE-ACE by performing separations in a BGE devoid of cNT/urea. Non-linear regression of the refolding curve provided thermodynamic parameters $\Delta G_U^0 = 4.3 \pm 0.4$ kcal mol^{-1} and $m = 1.0 \pm 0.1$ kcalmol^{-1}K^{-1} which are within error to the values determined during unfolding, $\Delta G_U^0 = 4.3 \pm 0.1$ kcal mol^{-1} and $m = 0.90 \pm 0.02$ kcal mol^{-1}K^{-1}. Additional refolding studies with selected cNTs were also performed by addition of a 10-fold excess of ligand to the BGE without urea. In general, there were no significant differences observed in $\nu\mu^A{}_{ep}$ when comparing native and refolded *holo*-protein states with the exception of R_p-cAMPS. This anomaly is likely due to the destabilizing effect of R_p-cAMPS on the active conformer of EPAC, which prevents the protein from regaining its native state upon refolding as reported by Dostmann[31] for *Rp*-cAMPS with the regulatory sub-unit of protein kinase A. This mechanism is also consistent with its lower C_M value that destabilizes the conformational stability of *holo*-R_p-cAMPS-EPAC relative to *apo*-EPAC.

3.5. References

1. Bleicher, K. H.; Bohm, H.-J.; K.Muller; A.I.Alanine, *Nat. Rev. Drug Discovery* **2003**, *2*, 369.

2. Hertzberg, R. P.; Pope, A. J., *Current Opinion Chem. Biol.* **2000,** *4*, 445.

3. Ng, E. S.; Chen, N. W.; Lewis, D. F.; Hindsgaul, O.; Schriemer, D. C., *Nature Protocol* **2007,** *2*, 1907.

4. Tang, L.; Hopper, E. D.; Tong, Y.; Sadowsky, J. D.; Peterson, K. J.; Gellman, S. H.; Fitzgerald, M. C., *Anal. Chem.* **2007,** *79*, 5869.

5. Ruben, A. J.; Kiso, Y.; Freire, E., *Chem. Biol. Drug. Res.* **2006,** *67*, 2.

6. Segui-Lines, G.; Gavina, J. M. A.; D'Amaral, J.; Britz-McKibbin, P., *Analyst* **2007,** *132*, 741.

7. Gavina, J. M. A.; Das, R.; Britz-McKibbin, P., *Electrophoresis* **2006,** *27*, 4196.

8. Changeux, J.-P.; Edelstein, S. J., *Science* **2006,** *308*, 1424.

9. de Rooij, J.; Zwartkruis, F. J. T.; Verheijen, M. H. G.; Cool, R. H.; Nijman, S. M. B.; Wittinghofer, A.; Bos, J. L., *Nature* **1998,** *396*, 474.

10. McPhee, I.; Gibson, L. C. D.; Kewney, J.; Darroch, C.; Stevens, P. A.; Spinks, D.; Cooreman, A.; MacKenzie, S. J., *Biochem. Soc. Trans.* **2005,** *33*, 1330.

11. Cimmperman, P.; Baranauskiene, L.; S.Jachimoviciute; Jachno, J.; Torresan, J.; Michailoviene, V.; Matuliene, J.; Sereikaite, J.; Bumelis, V.; Matulis, D., *Biophys. J.* **2008,** *95*, 3222.

12.   Rehmann, H.; Schwede, F.; Doskeland, S. O.; Wittinghofer, A.; Bos, J. L., *J. Biol. Chem.* **2003**, *278*, 38548.

13.   Mayne, L.; Englander, S. W., *Protein Science* **2000,** *9*, 1873.

14.   Powell, K. D.; Fitzgerald, M. C., *Biochemistry* **2003,** *42*, 4962.

15.   Das, R.; Mazhab-Jafari, M. T.; Chowdhury, S.; SilDas, S.; Selvaratnam, R.; Melacini, G., *J. Biol. Chem.* **2008**, *283*, 19691.

16.   Harper, S. M.; Wienk, H.; Wechselberger, R. W.; Bos, J. L.; Boelens, R.; Rehmann, H., *J. Biol. Chem.* **2008,** *283*, 6501.

17.   Christensen, A. E.; Selheim, F.; de Rooij, J.; Dremier, S.; Schwede, F.; Dao, K. K.; Martinez, A.; Maenhaut, C.; Bos, J. L.; Genieser, H. G.; Doskeland, S. O., *J. Biol. Chem.* **2003,** *278*, 35394.

18.   Myers, J. K.; Pace, C. N.; Scholtz, J. M., *Protein Science* **1995,** *4*, 2138.

19.   Christopoulos, A., *Nature Rev. Drug Discovery* **2002,** *1*, 198.

20.   Tropak, M. B.; Mahuran, D., *FEBS J.* **2007,** *274*, 4951.

21.   Mazhab-Jafari, M. T.; Das, R.; Fotheringham, S. A.; SilDas, S.; Chowdhury, S.; Melacini, G., *JACS* **2007,** *129*, 14482.

22.   Rochu, D.; Clery-Barraud, C.; Renault, F.; Chevalier, A.; Bon, C.; Masson, P., *Electrophoresis* **2006,** *27*, 442.

23.   Rush, R. S.; Cohen, A. S.; Karger, B. L., *Anal. Chem.* **1991,** *63*, 1346.

24.   Verzola, B.; Perduca, M.; Mezo, G.; Hudecz, F.; Righetti, P. G., *Electrophoresis* **2003,** *24*, 794.

25.   Chu, Y. H.; Avila, L. Z.; Biebuyck, H. A.; Whitesides, G. M., *J. Med. Chem.* **1992,** *35*, 2915.

26.   Chu, Y. H.; Dunayevskiy, Y. M.; Kirby, D. P.; Vouros, P.; Karger, B. L., *JACS* **1996,** *118*, 7827.

27.   Drabovich, A. P.; Okhonin, V.; Berezovski, M.; Krylov, S. N., *JACS* **2007,** *129*, 7260.

28.   Lewis, L. M.; Engle, L. J.; Pierceall, W. E.; Hughes, D. E.; Shaw, K. J., *J. Mol. Screen.* **2004,** *9*, 303.

29.   Zhang, H. Q.; Li, X. F.; Le, X. C., *JACS* **2008,** *130*, 34.

30.   Powell, K. D.; Ghaemmaghami, S.; Wang, M. Z.; Ma, L. Y.; Oas, T. G.; Fitzgerald, M. C., *JACS* **2002,** *124*, 10256.

31.   Dostmann, W. R. G., *FEBS Lett.* **1995,** *375*, 231.

Chapter IV

A Stereoselective Platform for Kinetic Studies of Isomerase Enzymes:

Evaluation of 4-Hydroxyproline-2-Epimerase Activity by Capillary

Electrophoresis

IV. A Stereoselective Platform for Kinetic Studies of Isomerase Enzymes: Evaluation of 4-Hydroxyproline-2-Epimerase Activity by Capillary Electrophoresis

4.1. Abstract

Isomerases involved in the metabolism of D/L-amino acids represent promising therapeutic targets for treatment of disease. Herein we report a simple yet tunable platform for the unbiased assessment of enzymatic kinetics involving amino acid isomerization based on capillary electrophoresis that offers improved selectivity and sensitivity over traditional methods. Enzyme activity and competition assays were evaluated for a variety of hydroxyproline diastereoisomers, proline enantiomers and their structural analogues using 4-hydroxyproline-2-epimerase as a model system, which is required for the discovery of novel inhibitors with epimerase and/or racemase activity.

4.2. Introduction

Hydroxyproline-2-epimerase (HyPRE) is an important enzyme that is expressed in various pathogenic bacteria, including *Pseudomonas sp.*[1-4] These organisms are capable of using 4-hydroxy-L-proline (4-L-Hyp) derived from collagen as their sole source of carbon, nitrogen and energy.[5-7] Since infections from *P. aeruginosa* are typically nosocomial, their appearance in throat flora has been linked to the terminal downfall of patients with cystic fibrosis.[8] In

Pseudomonas sp., HyPRE is required in the first step of 4-*L*-Hyp catabolism[9] involving epimerization of the α-carbon to generate 4-*D*-Hyp.[10] Indeed, the unique metabolism of organisms that utilize *D*-amino acids for energy metabolism, cell wall biosynthesis and/or neurochemical signaling, makes enzymes involved in these processes promising therapeutic targets for drug development. For instance, recent efforts have been aimed at developing specific inhibitors targeting proline racemase (PRAC) of *Trypanosoma cruzi*, the parasitic protozoan responsible for Chagas' disease in humans.[11, 12]

In this report, we introduce a stereoselective platform based on capillary electrophoresis (CE) for the quantitative analysis of isomerase kinetics using *P. aeruginosa* HyPRE as a model system. CE provides a versatile microseparation format for the resolution of complex mixtures of enantiomers, diastereomers and structural isomers[13, 14] that offers improved selectivity, greater sensitivity and lower sample consumption compared to traditional methods based on polarimetry[15] and coupled enzyme colorimetric assays. [16] Indeed, the latter technique is prone to bias when assessing HyPRE activity since it requires formation of the colorimetric product pyrrole 2-carboxylic acid (PYC), which inhibits activity of both HyPRE and the *D*-amino acid oxidase used in the assay. [17] In contrast, our approach utilizes 9-fluorenylmethyl chloroformate (Fmoc-Cl) as a convenient pre-column derivatization agent prior to CE separations, which is suitable for rapid labeling of both primary (*e.g.,* Ala, Glu, *etc.*) and secondary amines (*i.e.* Hyp) with low micromolar detection limits.

4.3. Results and Discussion

In this study, we performed a quantitative comparison of the selectivity of HyPRE to several different Hyp/Pro stereoisomers and their structural analogues as depicted in **Figure 4.1(a)**. All of the compounds examined were resolved by CE, which allowed for unbiased assessment of HyPRE and/or PRAC activity in the presence of various competitive inhibitors as shown in **Figure 4.1(b)**. Unlike previous LC and CE methods that depend on chiral thiol co-reagents with *ortho*-phthalaldehyde labeling of primary amino acids for diastereomer resolution, [18-20] this method takes advantage of stereospecific non-covalent interactions of Fmoc-labeled amino acids with chiral selectors migrating in free solution (refer to **Figure 4.2**). Noteworthy, this strategy is also applicable for assessing isomerase activity for other *D/L*-amino acids of biological significance, including Ala, Ser, Pro, Asp, Glu and diaminopimelic acid (DAP) as highlighted in **Figure 4.3**.

P. aeruginosa HyPRE is a 36 kDa pyridoxal phosphate-independent epimerase, where stereoinversion of the chiral α-carbon centre of the bound substrate is mediated by a dual-acid/base paired mechanism involving catalytic thiol sulfhydryls that are critical to its overall activity[9] similar to other isomerases, including Pro/Glu/Asp racemases and DAP epimerase.[21] **Figure 4.4(a)** depicts a series of electropherograms under optimum buffer conditions showing increased formation of 4-*D*-Hyp from excess 4-*L*-Hyp (1 mM substrate) as a function of HyPRE incubation time, which was used to examine the reversibility of enzyme-catalyzed *D/L*-Hyp interconversion. Although the reaction catalyzed by HyPRE is
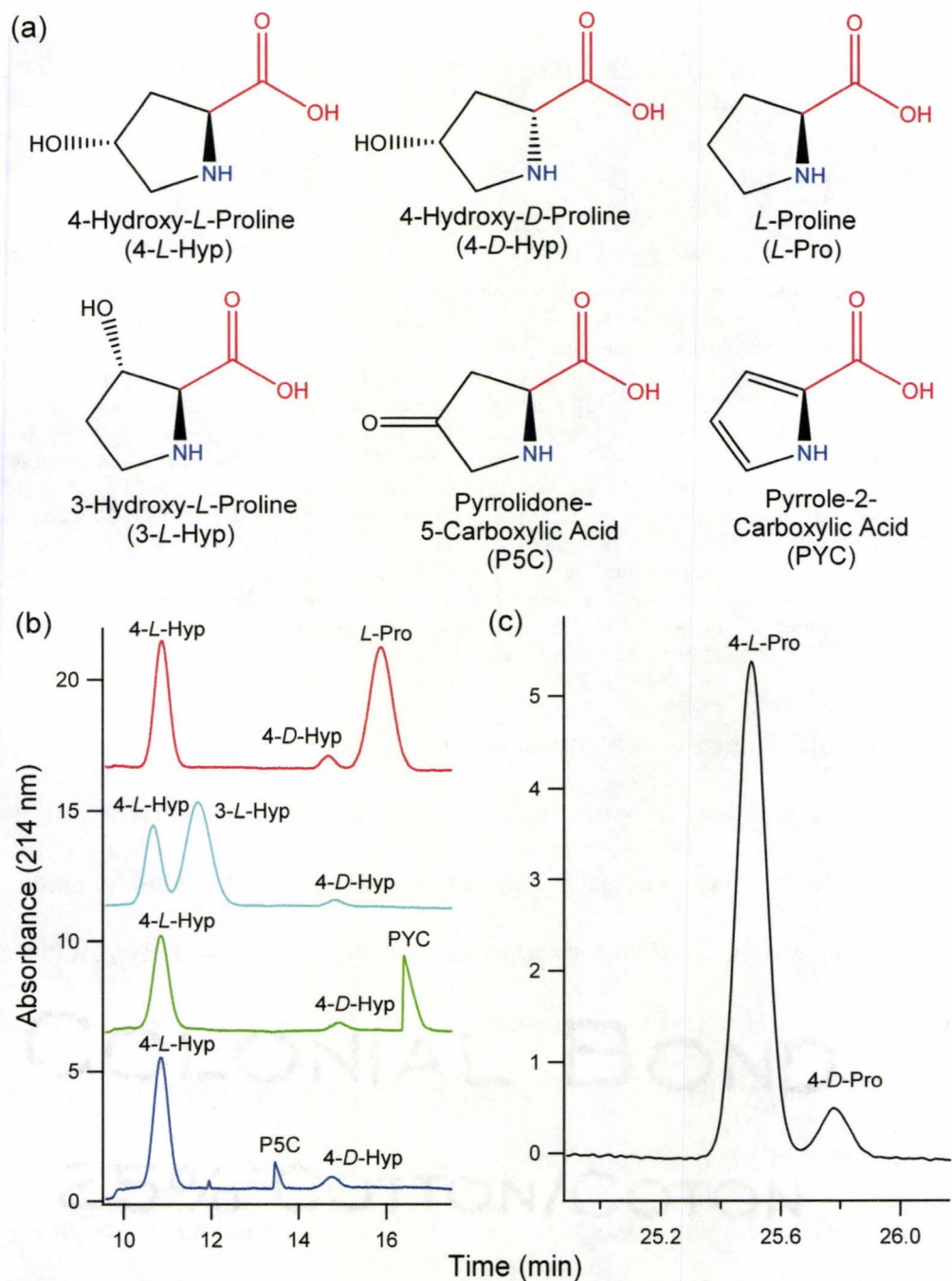
Figure 4.1. (a) 2D structures of major Hyp/Pro stereoisomers and structural analogues, where (b) and (c) demonstrate their selective resolution by CE under two buffer conditions (see Supplemental Information) required for unbiased screening of inhibitors with Hyp epimerase (HyPRE) and/or Pro racemase (PRAC) activity.
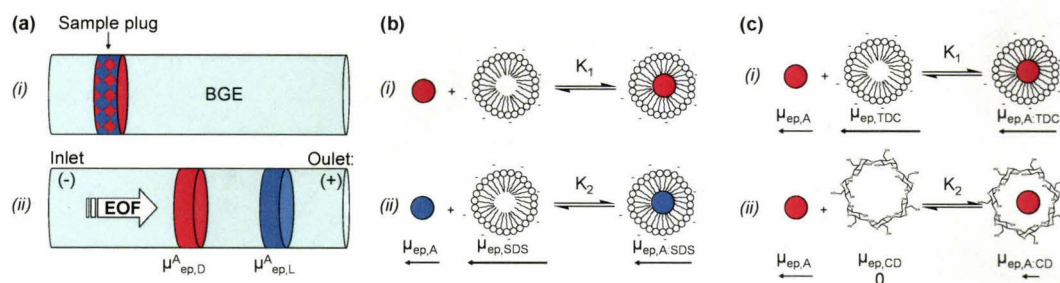
Figure 4.2. Tunable resolution of amino acid stereoisomers by CE where (a) quenched Fmoc-labeled enzyme reactions containing a mixture of 4-D/L-Hyp were injected into the capillary (*i*) followed by their resolution (*ii*), based on dynamic non-covalent interactions with specific additives (e.g., SDS, β-CD, TdC) in the BGE during electromigration. Buffer conditions for resolution of 4-D/L-Hyp diastereomers only required addition of SDS to the BGE (b) based on differences in their partition constants with the anionic micelle, where 4-D-Hyp (*i*) partitioned with SDS to a greater extent than 4-L-Hyp (*ii*) resulting in a greater negative apparent electrophoretic mobility (μ^A_{ep}) or longer migration time. However, enantioselective resolution of D/L-Pro required the use of multiple chiral selectors in the BGE as depicted in (c), namely (*i*) TdC and (*ii*) β-CD. In this case, resolution is achieved by differences in partitioning with anionic TdC micelles and/or complex formation with neutral β-CD, where increased affinity for binding to β-CD results in a slower apparent negative μ^A_{ep} or shorter migration time for Fmoc-labeled amino acids via *in-situ* formation of diastereomeric complexes. In this work, enantioselective resolution of most other Fmoc-labeled primary amino acids only required the addition of β-CD (c, *ii*) in conjunction with small amounts of isopropanol (5-15% v) as an organic solvent modifier as shown in Figure 4.3.

largely reversible, **Figure 4.4(b)** demonstrates that a statistically greater ($P <$ 0.05) maximum reaction velocity (V_{max}) for the forward reaction ($L \rightarrow D$) is favored despite similar Michaelis-Menten constants (K_M). This inherent stereospecificity can be attributed to a greater stability of the 4-D-Hyp:HyPRE relative to the 4-L-Hyp:HyPRE complex due to differences in V_{max}, which is consistent with the availability of extra-cellular pools of host L-Hyp that can utilized by opportunistic pathogens. The reversibility for D/L-Hyp interconversion by HyPRE measured in this work is contradictory to a previous study using polarimetry,[17] probably due to limitations in concentration sensitivity of the kinetic assay since it requires considerably higher enzyme/substrate reaction conditions (*e.g.,* 20 µg/mL protein, 10-160 mM substrate) relative to CE with UV
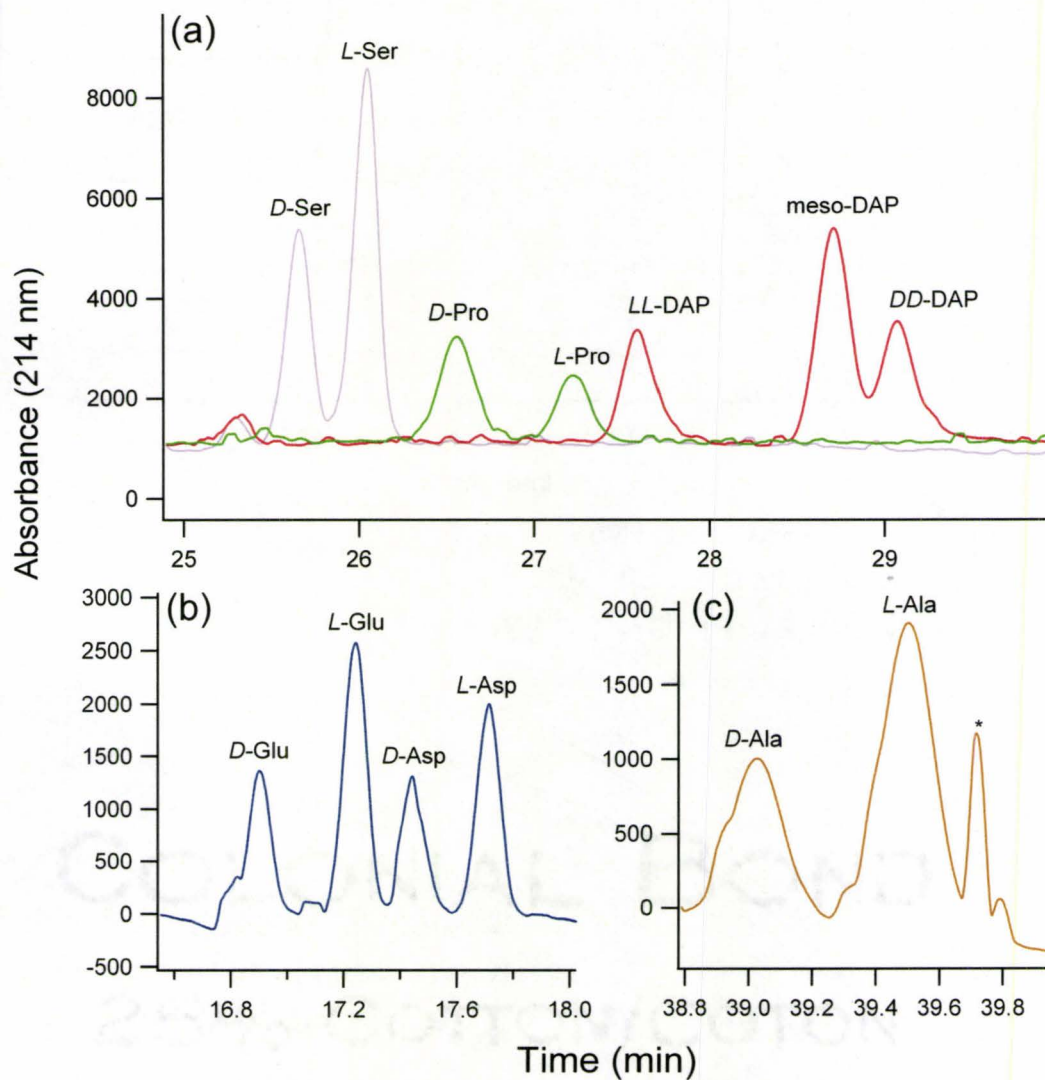
Figure 4.3. Stereoselective resolution of *D/L*-amino acids of biological significance for unbiased enzyme kinetic studies of isomerases. Samples consisted of 100 μM DAP or 100 μM D- and 200 μM L-Glu, Asp, Ser, Ala or 200 μM D-, 100 μM L-Pro labeled with Fmoc. All separations were performed at 20°C, 25 kV with a 50 μm i.d., 60 cm L_T, 50 cm L_d capillary. Separation buffer conditions for (a): 150 mM HEPES pH 8, 30 mM β-CD, 15% (v/v) isopropyl alcohol; (b): 125 mM HEPES pH 8, 15 mM β-CD, 7.5% (v/v) isopropanol; (c): 150 mM HEPES pH 8 + 30 mM β-CD, 30 mM TDC, 15% (v/v) isopropanol. Note that identification of DAP isomers is based on relative peak areas for stereoisomers based on reference.[22] *Denotes noise associated with use of ternary system.
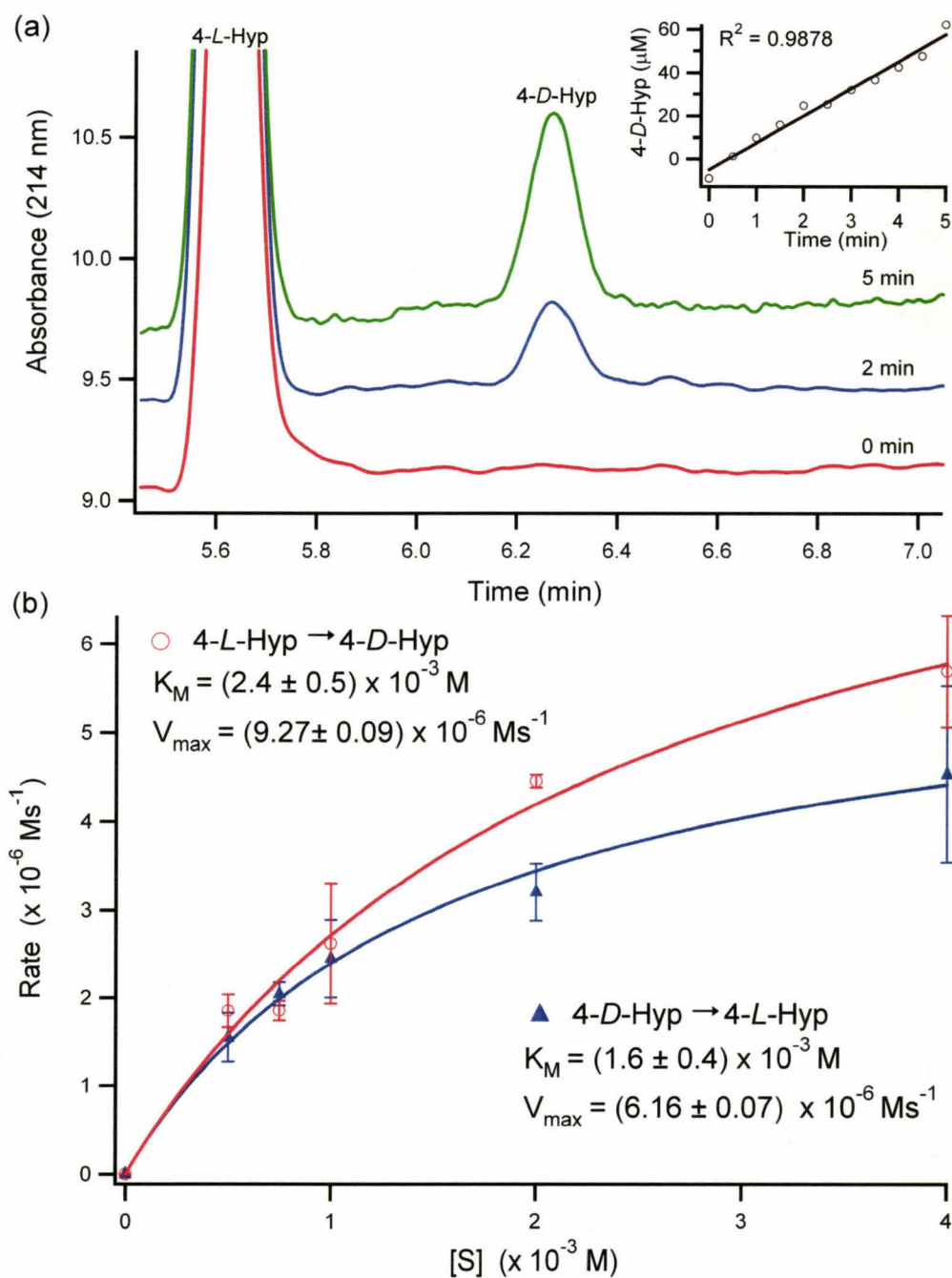
Figure 4. 4. Enzyme kinetic studies by CE using 10 nM HyPRE. (a) Electropherograms depicting quantification of micromolar levels of the diastereomeric product (4-D-Hyp) from 1 mM 4-L-Hyp as substrate ([S]) as a function of time. (b) Non-linear regression of Michaelis-Menten kinetics highlighting the intrinsic specificity of 4-D/L-Hyp interconversion.   Error represents $\pm 1\sigma$ involving three biological replicates (n = 3).   Refer to Supplemental Information for details regarding incubation/separation conditions.

detection. Indeed, both HyPRE and PRAC isomerases share high structural homology,[17] where *T. cruzi* PRAC has recently been shown to undergo closure of the catalytic cleft upon substrate binding involving an active homodimeric enzyme state with oligomeric species forming at higher protein concentrations.[23, 24]

The Hyp analogues used in this study (**Figure 4.1**) were selected to examine the stringency of the hydroxyl functional group in the 4-position (*i.e.,* 4-*L*-Pro, 3-*L*-Hyp, pyrrolidone-5-carboxylic acid (P5C)), as well as confirm the inhibitory effect of the transition-state analogue PYC.[17] To the best of our knowledge, the selectivity of the positional isomer (3-*L*-Hyp) and the ketone analogue (P5C) have not been reported to date. Although very similar in structure to the native substrates, *L*-Pro, 3-*L*-Hyp and P5C were not observed to be converted to their corresponding enantiomers or diastereomers by HyPRE. Moreover, these same analogues did not significantly inhibit *L*-Hyp→*D*-Hyp conversion during competitive inhibition studies by CE when using a 5-fold excess of competitor with incubation times over 5 min (refer to **Table 4.1**), which highlights the inherent selectivity of HyPRE. The specific recognition of 4-*D/L*-Hyp among other related Hyp/Pro structural analogues confirmed by this study is associated with a predicted hydrogen bond between the 4-hydroxyl group and the side-chain of His270 in the active site of *P. aeruginosa* HyPRE, which likely plays an important role in substrate binding discrimination.[17] As expected, our work confirmed that PYC acts as a competitive inhibitor of HyPRE as shown in

Table 4.1. Rate of 4-D-Hyp formation in competition assays with 1 mM 4-L-Hyp as substrate and 5 mM L-Pro, 3-L-Hyp, P5C or PYC as inhibitor.

Inhibitor	Rate of 4-D-Hyp Formation ($\times 10^{-6}$ Ms^{-1})	
	0 mM Inhibitor	5 mM Inhibitor
L-Pro	13 ± 1	14 ± 1
3-*L*-Hyp	14 ± 1	15 ± 2
P5C	14 ± 1	12 ± 1
PYC	12.7 ± 0.5	3.4 ± 0.2

Figure 4.5.[17] This transition-state analogue is a by-product of Hyp metabolism, which is also an inhibitor of *T. cruzi* PRAC.[25] In this work, PYC was determined to have a half-maximal inhibition concentration (*IC50*) of about 2.8 mM that is equivalent to an inhibition constant (K_I) of about 1.0 mM (refer to **Figure 4.6**) when using 1 mM 4-*L*-Hyp as substrate and 10 nM HyPRE during CE-based enzyme competition studies.

CE in conjunction with pre-column Fmoc derivatization offers a selective and sensitive method for assessing enzyme kinetics of isomerases associated with primary and secondary amino acid metabolism when using low amounts of recombinant protein (*i.e.,* < 0.5 ng per assay at 6 different substrate concentration levels with 3 biological replicates). Changes in buffer composition can be used to readily tune the selectivity of separations in CE for a wide variety of enantiomers, diastereomers and structural analogues required for competitive inhibition studies, such as HyPRE and/or PRAC. In addition, direct photometric detection and simultaneous resolution of substrate, product and competitor by CE avoids bias associated with coupled enzyme assays and the poor concentration sensitivity of
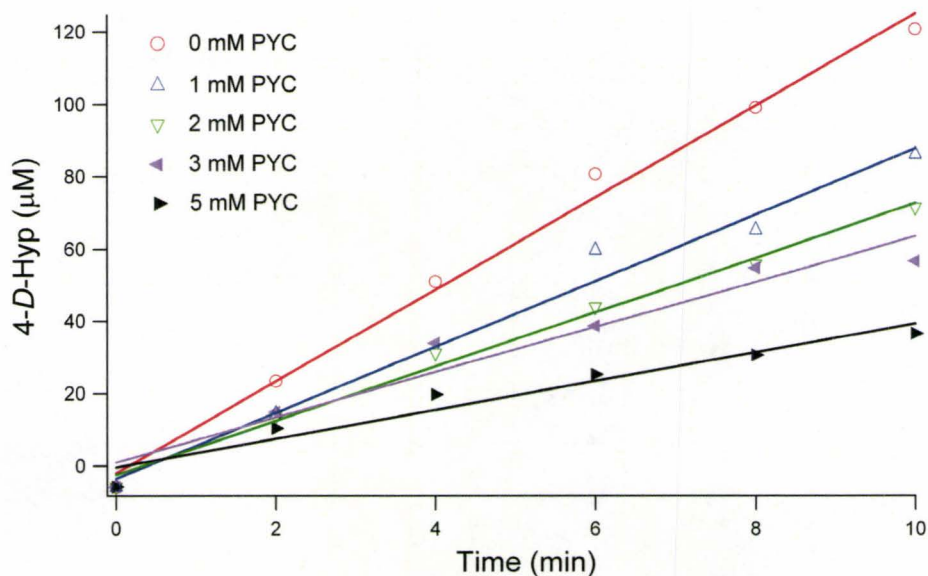
Figure 4.5. Competitive inhibition studies of HyPRE using 1 mM 4-*L*-Hyp as substrate in the presence of increasing PYC concentration (0-5 mM). Concentration of the reaction product (4-*D*-Hyp) was determined by CE as a function of incubation time (*n* = 3). Refer to Supplemental Information for assay conditions.

polarimetry that can result in oligomerization at higher protein concentrations. Our work confirmed the intrinsic selectivity of HyPRE for enzyme-catalyzed 4-*D/L*-Hyp interconversion, including two previously uncharacterized Hyp analogues, 3-*L*-Hyp and P5C, which lacked activity unlike the competitive inhibitor, PYC. Although this study was focused on the characterization of HyPRE and/or PRAC, it is also applicable to inhibitor screening of other classes of amino acid isomerases, such as Ser[20] and Glu racemases,[26] as well as DAP epimerases.[26] In summary, CE offers a convenient stereoselective microseparation technique for enzyme kinetic studies of isomerases associated with *D/L*-amino acid metabolism. Future work is aimed at developing high-quality screening assays based on CE for thermodynamic and kinetic characterization of allosteric modulators of enzyme activity.[27]
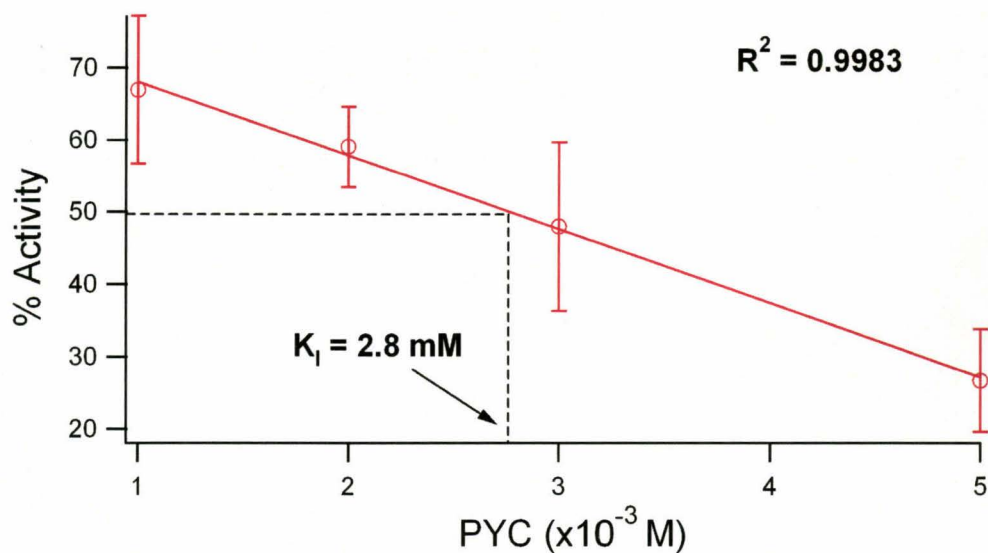
Figure 4.6. Determination of IC_{50} from inhibition of HyPRE by PYC using 1 mM of 4-*L*-Hyp as substrate and increasing concentrations of inhibitor. Activity (%) was determined by comparing the rate of 4-*D*-Hyp formation in the presence of PYC to the formation of 4-*D*-Hyp in the control (0 mM PYC).

4.4. Supplemental Information

4.4.1. Chemicals and Reagents

Deionized water for buffer and sample preparations was obtained using a Barnstead EASYpure® II LF ultrapure water system (Dubuque, IA, USA). *Trans*-4-hydroxy-*L*-proline (4-*L*-Hyp), *cis*-4-hydroxy-*D*-proline (4-*D*-Hyp), *trans*-3-hydroxy-*L*-proline (3-*L*-Hyp), pyrrole 2-carboxylic acid (P2C), pyrrolidone 5-carboxylic acid (P5C), *D*-proline (*D*-Pro), L-proline (*L*-Pro), sodium hydroxide (NaOH), taurodeoxycholate (TDC), sodium dodecyl sulphate (SDS), 9-Fluorenylmethyl chloroformate (Fmoc-Cl), acetonitrile (ACN), glycerol, and β-mercaptoethanol (β-ME) were obtained from Sigma Aldrich (St. Louis, MO, USA). 4-(2-Hydroxyethyl)piperazine-1-ethanesulfonic acid (HEPES) was

obtained from BioShop Canada Inc.(Burlington, ON, Canada). Ethanolamine

NH$_2$OH) was obtained from Fisher Scientific (Pittsburgh, PA, USA). Caffeine, β-

cyclodextrin (β-CD), ethylenediaminetetraacetic acid (EDTA) and 2-nitrophenol

were acquired from Alfa Aesar (Ward Hill, MA, USA). Stock solutions of

reagents were prepared in ultrapure water or HPLC grade solvent.

4.4.2. Expression and Purification of *Pseudomonas aeruginosa* HyPRE

A plasmid expressing the *P. aeruginosa* HyPRE protein with a C-terminal

6-histidine tag from the T7 promoter was kindly provided by Paola Minoprio.[17]

The plasmid was introduced into *Escherichia coli strain* BL21/DE3 (Novagen),

which was then cultured with aeration at 30°C to mid-log phase in 1 L of Luria-

Bertani medium supplemented with 200 ug/mL of ampicillin; at which point

expression of the recombinant protein was induced by addition of isopropyl-ß-D-

thiogalactopyranoside to 0.5 mM. The culture was incubated for an additional 4

hours at the above conditions, and cells were then harvested and resuspended in

buffer (20 mM HEPES, pH 7.5; 150 mM KCl, 7.5% glycerol). Cells were

disrupted by french press, and the lysate was cleared by centrifugation at 40,000

rpm for 20 minutes. The recombinant protein was purified from the cleared lysate

using HisPur Cobalt Resin (Thermo Scientific), using batch elution as described

in the manufacturer's instructions. The concentrated fractions of purified protein

were then dialysed against storage buffer (20 mM HEPES, pH 7.5; 150 mM KCl,

50% glycerol, 1 mM DTT, 1 mM EDTA), and stored at –80°C. Protein

concentration was determined using BioRad Protein Assay Reagent (BioRad) and bovine serum albumin as a standard. The recombinant HyPRE protein (335 residues, 35.8 kDa, isolectric point: 5.8) was purified to approximately 95% homogeneity, and stored as a 78 μM stock.

4.4.3. Capillary Electrophoresis

Separations were performed on a P/ACE MDQ CE system equipped with UV absorbance detection (Beckman-Coulter Inc., Fullerton, CA, USA) using a 50 μm i.d., 360 μm o.d. uncoated fused-silica capillary (Polymicro Technologies, Phoenix, USA). All separations were thermostatted to $20^{\circ}C$ and electropherograms were collected at 214 nm. New capillaries were first conditioned by rinsing with methanol for 5 min, water for 5 min, 1 M NaOH for 5 min, background electrolyte (BGE) for 15 min, which were then left to equilibrate for at least 30 min prior to usage. At the beginning of each day, the capillary was rinsed for 5 min with 0.1 M NaOH and BGE for 5 min. All separations began by rinsing the capillary for 2 min with 0.1 M NaOH followed by 4 min with BGE. Samples were injected by application of 0.5 psi pressure for 5 s. At the end of the day, the capillary was rinsed for 5 min with 0.1 M NaOH and 5 min with BGE and stored overnight in BGE. For longer storage, the capillary was rinsed for 5 min with 0.1 M NaOH, 5 min water and then stored in air. Modifications to the BGE composition and separation conditions were performed for optimization of the resolution of various *D/L*-amino acid stereoisomers (diastereomers,

enantiomers) and structural isomers for enzyme kinetics studies. Prior to CE separations, all enzyme reaction samples were reacted off-line with a 2-fold mole excess of Fmoc relative to substrate concentration in ACN for 2 min, followed by quenching with 20-fold excess NH_2OH which also contained *p*-nitrophenol or caffeine as the internal standard (IS).

4.4.4. Separation Optimization

Separations were performed by micellar electrokinetic chromatography (MEKC) using a negatively charged surfactant (SDS) in the BGE in conjunction with chiral selector(s) when necessary as shown schematically in **Figure 4.2**. Typical separation conditions for enzyme kinetic studies of HyPRE were performed using 100 mM HEPES, pH 8 with 10 mM SDS, which allowed for resolution of 4-*D/L*-Hyp diastereomers under a minimal analysis time, whereas 30 mM SDS was required for improved resolution of all other Hyp structural isomers and their analogues for competitive enzyme inhibition studies. As shown in Figure **4.2(b)**, anionic Hyp diastereomers (as their Fmoc adducts) and their structural analogues are resolved based on differences in their partitioning constant (*K*) with SDS during their electromigration in the capillary, where the diastereomer with a greater *K* tends to migrate with longer apparent times (*i.e., D*-Hyp) due to the larger negative mobility of anionic SDS micelles that is superimposed on the strong cathodic electroosmotic flow (EOF). For enantiomeric resolution of *D/L*-Pro, chiral resolution was achieved with

cyclodextrin-mediated MEKC with a BGE of 140 mM HEPES pH 8 containing two discrete chiral selectors, namely 30 mM taurodeoxycholate (TdC, a chiral bile salt surfactant) and 30 mM β-cyclodextrin (β-CD, a chiral oliogosaccharide macrocyle). As depicted in **Figure 4.2(c)**, in this case a competitive equilibrium process involving dynamic interactions with anionic TdC and neutral β-CD impacts the apparent migration times of *D/L*-Pro via *in-situ* formation of diastereomeric complexes. However, resolution of most other amino acid enantiomers (refer to **Figure 4.3**) was achieved by CE using isopropanol as an organic solvent modifier with β-CD as a single chiral selector in the BGE since optimal conditions for *D/L*-Pro resolution using TdC with β-CD was not applicable for their separation. In addition, baseline resolution of *D/L*-Ala enantiomers was realized by use of a ternary system with all three additives in the BGE, namely β-CD, TdC and isopropanol. Indeed, simultaneous resolution of all amino acid stereoisomers under a single buffer condition is challenging given significant differences in side-chain structure of amino acids that impacts their non-covalent interactions with additives in the BGE. Nevertheless, CE offers a versatile format for stereoselective resolution of various classes of amino acids based on simple changes in the composition of the BGE using single or multiple additives in free solution unlike LC that requires the use of expensive immobilized chiral stationary phases.

4.4.4. Pre-Column Fmoc Labeling

Derivatization of secondary amino acids by Fmoc is commonly used to improve photometric detection of amino acids and was performed *off-line* prior to analysis by CE following enzyme incubation reactions. Although labelling efficiency has been shown to be increased under more alkaline conditions,[28-30] the buffer pH was selected in order to avoid sample matrix interferences in the separation (*e.g.*, β-mercaptoethanol, β-ME). In our study, chemical derivatization was shown to be complete within 2 min with a 2-fold mole excess of Fmoc relative to total concentration of substrate. Higher excess Fmoc concentrations hindered separations due to the limited solubility of Fmoc in aqueous solution. Quenching of the derivatization reaction with ethanolamine decreased the presence of Fmoc hydrolysis product(s) which also increased the long-term stability of amino acid adducts for up to ~7 hours after chemical derivatization.

4.4.5. Kinetic Assays

All reactions were performed in an assay buffer (50 mM HEPES pH 8 with 2 mM β-ME, 1 mM EDTA) with 0 to 4 mM substrate and 10 nM HyPRE in a 200 μL reaction volume. Although previous assay[17] used Tris buffer, Tris was excluded due interference with Fmoc labeling. Reactions were carried out at 37°C and initiated by addition of HyPRE. Aliquots (20 μL) were withdrawn from the bulk reaction mixture at 30 s intervals and quenched by irreversible thermal denaturation of the enzyme at 90°C for 30 min. Competition studies were

performed under the same conditions where 1 mM 4-*L*-Hyp was used as substrate and the competitor was added at 0, 1, 2, 3 or 5 mM. Representative apparent reaction rates for formation of 4-*D*-Hyp in these studies are shown in Table S1. The linear range for epimerase activity over time was determined for 20 nM HyPRE with 1 mM 4-*L*-Hyp as per the assay described above. Aliquots were withdrawn at t = 0, 2, 5, 10, 15, 20, 25, 30, 45, 60 min. Activity was linear within a 10 min interval. To determine the kinetic parameters for active substrates of HyPRE, enzymatic assays analyzed by CE with UV detection as described above.

4.4.6. Data Analysis

Calibration curves were constructed for 4-*D*-Hyp and 4-*L*-Hyp by measuring the average peak area response normalized against the internal standard. Calibration solutions were prepared independently for each isomer in a 10-fold excess of the other in conditions mimicking those of the kinetic assay in order to account for effects of the assay buffer and labeling reaction on detection sensitivity. Samples were labelled with Fmoc and analyzed by CE as described above. Responses were linear based on triplicate measurements of 6 points over a 10-fold concentration range from 0-100 μM as reflected by R^2 values of 0.9900 and 0.9914. For 4-*D*-Hyp normalized to *p*-nitrophenol as internal standard [y = (0.0081 ± 0.0004) x + (0.07 ± 0.02), μM], the limit of detection was found to be anout 4 μM with an average coefficient of variance of 8%. For *D*-Hyp normalized to caffeine as the internal standard [y = (0.019 ± 0.001) x + (0.11 ±

0.08), µM], the limit of detection was found to be 4 µM with an average coefficient of variance of of 6%. *D*- and *L*-isomers were found to have similar UV responses at 214 nm. Recovery studies was performed at three different concentrations of 4-*D*-Hyp (10, 50, 90 µM) in the presence of 1 mM 4-*L*-Hyp for assessing accuracy. The average error for intraday triplicate measurements was within 10%. Kinetic parameters K_M, V_{max}, IC50 and K_I were calculated using non-linear and linear regression by Igor Pro 5.0 software (Wavemetrics Inc., Lake Oswego, OR, USA).

4.5. References

1.   Adams, E., *Mol. Cell. Biochem.* **1973,** *2*, 109.

2.   Adams, E.; Norton, I. L., *J. Biol. Chem.* **1964,** *239*, 1525.

3.   Gryder, R. M.; Adams, E., *J. Bacteriol.* **1969,** *97*, 292.

4.   Chamond, N.; Gregoire, C.; Coatnoan, N.; Rougeot, C.; Freitas-Junior, L. H.; da Silveira, J. F.; Degrave, W. M.; Minoprio, P., *J. Biol. Chem.* **2003,** *278*, 15484.

5.   Adams, E., *J. Biol. Chem.* **1959,** *234*, 2073.

6.   Singh, R. M. M.; Adams, E., *J. Biol Chem.* **1965,** *240*, 4344.

7.   Yoneya, T.; Adams, E., *J. Biol. Chem.* **1961,** *240*, 236.

8.   Murray, T. S.; Egan, M.; Kazmierczak, B. I., *Curr. Opin. Ped.* **2007,** *19*, 83.

9.   Ramaswamy, S., *J. Biol. Chem.* **1984,** *259*, 249.

10.   Finlay, T. H.; Adams, E., *J. Biol. Chem.* **1970,** *245*, 5248.

11.   Chamond, N.; Goytia, M.; Coatnoan, N.; Barale, J. C.; Cosson, A.; Degrave, W. M.; Minoprio, P., *Mol. Microbiol.* **2005,** *58*, 46.

12.   Reina-San-Martin, B.; Degrave, W.; Rougeot, C.; Cosson, A.; Chamond, N.; Cordeiro-Da-Silva, A.; Arala-Chaves, M.; Coutinho, A.; Minoprio, P., *Nat. Med.* **2000,** *6*, 890.

13.   Gubitz, G.; Schmid, M. G., *J. Chromatogr. A* **1997,** *792*, 179.

14.   Terabe, S.; Otsuka, K.; Nishi, H., *J. Chromatogr. A* **1994,** *666*, 295.

15.   Stecher, H.; Hermetter, A.; Faber, K., *Biotechnol. Techniques* **1998,** *12*, 257.

16.   Gallo, K. A.; Knowles, J. R., *Biochemistry (Mosc).* **1993,** *32*, 3981.

17.   Goytia, M.; Chamond, N.; Cosson, A.; Coatnoan, N.; Hermant, D.; Berneman, A.; Minoprio, P., *PLoS One* **2007,** *2*, e885.

18.   Koval, D.; Jiraskova, J.; Strisovsky, K.; Konvalinka, J.; Kasicka, V., *Electrophoresis* **2006,** *27*, 2558.

19.   Ptolemy, A. S.; Tran, L.; Britz-McKibbin, P., *Anal. Biochem.* **2006,** *354*, 192.

20.   Wolosker, H.; Sheth, K. N.; Takahashi, M.; Mothet, J. P.; Brady, R. O.; Ferris, C. D.; Snyder, S. H., *PNAS* **1999,** *96*, 721.

21.   Yoshimura, T.; Esak, N., *J. Biosci. Bioeng.* **2003,** *96*, 103.

22.   Ptolemy, A. S.; Le Bilhan, M.; Britz-McKibbin, P., *Electrophoresis* **2005,** *26*, 4206.

23.   Buschiazzo, A.; Goytia, M.; Schaeffer, F.; Degrave, W.; Shepard, W.; Gregoire, C.; Chamond, N.; Cosson, A.; Berneman, A.; Coatnoan, N.; Alzari, P. M.; Minoprio, P., *PNAS* **2006**, *103*, 1705.

24.   Wang, Y.; Addess, K. J.; Chen, J.; Geer, L. Y.; He, J.; He, S.; Lu, S.; Madej, T.; Marchler-Bauer, A.; Thiessen, P. A.; Zhang, N.; Bryant, S. H., *Nucleic Acids Res.* **2007**, *35*, D298.

25.   Buschiazzo, A.; Goytia, M.; Schaeffer, F.; Degrave, W.; Shepard, W.; Gregoire, C.; Chamond, N.; Cosson, A.; Berneman, A.; Coatnoan, N.; Alzari, P. M.; Minoprio, P., *PNAS* **2006**, *103*, 1705.

26.   Pillai, B.; Cherney, M.; Diaper, C. M.; Sutherland, A.; Blanchard, J. S.; Vederas, J. C.; James, M. N. G., *Biochem. Biophys. Res. Commun.* **2007**, *363*, 547.

27.   Gavina, J. M. A.; Mazhab-Jafari, M. T.; Melacini, G.; Britz-McKibbin, P., *Biochemistry (Mosc).* **2009**, *48*, 223.

28.   Ptolemy, A. S.; Britz-McKibbin, P., *Analyst* **2005**, *130*, 1263.

29.   Jambor, A.; Molnar-Perl, I., *J. Chromatogr. A* **2009**, *1216*, 3064.

30.   Han, Y. L.; Zuo, M.; Qi, L.; Liu, K.; Mao, L. Q.; Chen, Y., *Electrophoresis* **2006**, *27*, 4240.

(Intentionally Blank)

Chapter V:

Characterization of the Thermodynamic Stability and Enzymatic Activity of

4-Hydroxyproline-2-Epimerase Mutants by Capillary Electrophoresis:

Revealing the Function of an Active-Site Cysteine Dyad

V. Characterization of the Thermodynamic Stability and Enzymatic Activity of 4-Hydroxyproline-2-Epimerase Mutants by Capillary Electrophoresis: Revealing the Function of an Active-Site Cysteine Dyad

5.1. Abstract

Hydroxyproline-2-epimerase (HyPRE) is a pyridoxal phosphate-independent enzyme relevant to bacterial metabolism, which involves a dual Cys paired mechanism in the active site for epimerization of 4-D/L-hydroxyproline (D/L-Hyp). Herein, an integrated platform based on capillary electrophoresis (CE) is presented for the characterization of the thermodynamic stability and enzymatic activity of HyPRE variants from *Pseudomonas aeruginosa* and *Sinorhizobium meliloti*. A comparison study of the thermodynamics of urea-induced protein unfolding demonstrated that HyPRE from *P. aeruginosa* and *S. meliloti* possess similar conformational stabilities and unfolding cooperativities (*m*) which are not impacted by substrate and/or orthosteric inhibitor binding. Further analysis of Cys90 and Cys253 to Ser mutants of *S. meliloti* HyPRE confirmed that both mutants lacked epimerization activity while having similar thermodynamic stability under neutral buffer pH conditions relative to the wild-type enzyme. However, the pH-dependence of protein unfolding revealed that each mutant can be readily distinguished from wild-type *S. meliloti* HyPRE under alkaline buffer conditions based on relative differences in their conformational stability, such as apparent mid-point for urea denaturation (C_M) and standard free

energy change of unfolding $(\Delta G_U{}^\circ)$.   These studies clearly demonstrate that

Cys90 within the active site of *S. meliloti* HyPRE was more acidic relative to

Cys253 site and that these Cys residues functioned as the catalytic dyad. CE

offers a versatile biophysical technique for characterization of the

thermodynamics and kinetics of isomerases associated with *D/L*-amino acid

metabolism, which is useful for elucidation of the mechanism of catalysis

involving recombinant enzyme mutants.

5.2. Introduction

Uncovering the functional link between folding, binding, activity and

allostery represents one of the most challenging tasks in fundamental mechanistic

study of proteins.[1, 2] Most investigations to date rely on a variety of techniques to

characterize protein conformational changes using circular dichroism,

fluorescence, NMR, MS and X-ray crystallography.[3, 4] Capillary electrophoresis

(CE) represents a versatile microseparation format applicable to the analysis of

complex mixtures of protein and small molecules,[5,6] including characterization of

biomolecular interactions.[7, 8] Both thermodynamic and kinetic studies of enzymes

can be performed by CE with lower sample/reagent consumption and reduced

sample handling/pretreatment as compared to traditional methods.[3, 9, 10]

Moreover, CE allows integration of sample pre-treatment steps such as *in-situ*

generation of highly labile *apo*-protein and ligand-exchanged *holo*-protein states

in-capillary during electromigration.   CE is thus an ideal platform evaluating

recombinant proteins, particularly the effect of single-point mutations on enzymes.[11] For instance, Rochu et al.[12] demonstrated that CE can be used to assess metalloenzyme stability and activity by comparing the effect of cation substitutions in the active site heme moiety of a series of phosphotriesterase mutants. However, future work is needed to examine the usefulness of CE for characterizing the thermodynamic stability and kinetic activity of mutant enzymes as a way to elucidate the mechanism of catalysis.

There is growing interest in characterizing isomerase enzymes associated with D-amino acid metabolism given their relevance in drug development.[13] In eukaryotes, L-amino acids are the dominant component of proteins and only a few instances have been reported where D-amino acids are found, such as neurosignalling involving D-Ser that is generated by Ser racemase.[14] Since D-amino acids are widely known components of the peptidoglycan layer of bacterial cell walls, the presence of D-amino acids biological samples is often associated with bacterial contamination or infectious disease.[15, 16] The unique ability of bacteria to actively utilize and produce D-amino acids makes enzymes involved in these processes valuable therapeutic targets for drug development. Such efforts have been made to demonstrate the therapeutic potential in developing inhibitors targeting the proline racemase of *Trypanosoma cruzi* (*Tc*PRAC), the organism responsible for Chagas' disease in humans.[17-19] Similarly, hydroxyproline-2-epimerase (HyPRE) represents another important isomerase which enables microorganisms such as *Pseudomas aeruginosa* and *Sinorhizobium meliloti* to

utilize hydroxyproline (Hyp), which can potentially be derived from collagen as sources of energy.[20-22] *P. aeruginosa* HyPRE (*Pa*HyPRE) consists of a 36 kDa monomer that exists as a homodimer in solution as indicated by size exclusion studies.[23]   The crystal structure for *Pa*HyPRE reveals that each monomer contributes one active site located away from the dimer interface.[17, 24] Although each monomer has the potential to perform catalysis, no studies have been performed to date to determine whether dimerization is essential for catalysis or whether the monomers can function independently. The crystal structure for *S. meliloti* HyPRE (*Sm*HyPRE) has not yet been solved; however sequence homology suggests similar dimerization capability of the 38 kDa monomer. Stereoinversion of the chiral α-carbon center of *D/L*-Hyp is mediated in HyPRE by a dual acid/base-paired mechanism.[25] Two sulfhydryl moieties form a catalytic dyad with one Cys being donated from each domain. The two-base mechanism utilizing paired Cys residues is also conserved in other pyridoxyl phosphate-independent isomerases such as Pro, Glu, Asp racemases and DAP epimerase.[17, 26-28] In the absence of crystal structures, site-directed mutagenesis is often performed to evaluate the contribution of particular amino acids to catalytic activity and/or conformational stability. In *Tc*PRAC, the catalytic dyad has been identified as Cys130 and Cys300.[29] The Cys dyad corresponds to Cys88 and Cys236 in *Pa*HyPRE based on crystal structure comparison and mutation studies,[24] whereas in *Sm*HyPRE sequence comparison suggests that Cys90 and Cys253 behave as the catalytic acid/base pair for epimerization.

In this work, CE is used as a versatile platform for characterization of the conformational stability and enzyme activity of wild-type (*wt-*) HyPRE enzymes from *P. aeruginosa* and *S. meliloti,* as well as two Cys mutants of *Sm*HyPRE, C90S and C253S. To the best of our knowledge, this is the first report examining protein unfolding of HyPRE and/or their mutants to date. The effect of substrate, inhibitor and other Hyp analogues were evaluated by CE in order to determine the thermodynamic and kinetic parameters associated with enzyme conformational stability and activity. Noteworthy, Cys90 and Cys253 to Ser *Sm*HyPRE mutants exhibited complete loss activity as compared to the wild-type providing direct evidence for the key role these residues play in catalysis. For *Sm*HyPRE C90S and C253S mutants, the pH-dependence of protein unfolding parameters revealed the contribution of each residue to the active site environment, by differential changes in global conformational stability, which allowed the relative acidity of each Cys moiety to be evaluated. CE thus offers an integrated platform for characterizing both the thermodynamic stability and enzyme activity of isomerases and their mutants, which can provide deeper insight into the catalytic mechanisms associated with *D/L*-amino acid metabolism.

5.3. Experimental

5.3.1. Chemicals and Reagents

Deionized water for buffer and sample preparations was obtained using a Barnstead EASYpure®II LF ultrapure water system (Dubuque, IA, USA). *Trans-*

4-hydroxy-*L*-proline (4-*L*-Hyp), *cis*-4-hydroxy-*D*-proline (4-*D*-Hyp), pyrrole 2-carboxylic acid (PYC), *trans*-3-hydroxy-*L*-proline (3-*L*-Hyp), pyrrolidone 5-carboxylic acid (P5C), *D*-proline (*D*-Pro), *L*-proline (*L*-Pro), sodium hydroxide (NaOH), sodium dodecyl sulphate (SDS), 9-fluorenylmethyl chloroformate (Fmoc-Cl), N-cyclohexyl-2-aminoethanesulfonic acid (CHES), *tris*(hydroxymethyl)aminomethane hydrochloride (Tris-HCl), acetonitrile (ACN), glycerol, and β-mercaptoethanol (β-ME) were obtained from Sigma Aldrich (St. Louis, MO, USA). Urea and 4-(2-Hydroxyethyl)piperazine-1-ethanesulfonic acid (HEPES) were obtained from BioShop Canada Inc.(Burlington, ON, Canada). Ethanolamine (NH$_2$OH) was obtained from Fisher Scientific (Pittsburgh, PA, USA). Ethylenediaminetetraacetic acid (EDTA) and *m*-nitrophenol were acquired from Alfa Aesar (Ward Hill, MA, USA). Stock solutions of reagents were prepared in ultrapure water or HPLC grade solvent.

5.3.2. Expression and Purification of *Pseudomonas aeruginosa* and *Sinorhizobium meliloti* HyPRE

The plasmid expressing the *P. aeruginosa* HyPRE protein was previously provided by Paola Minoprio.[29] Protein expression and purification was performed in collaboration by White & Finan as follows.[30] A plasmid expressing the with *P. aeruginosa* or *S. meliloti* HyPRE protein with a C-terminal 6-histidine tag from the T7 promoter was introduced into *Escherichia coli* strain BL21/DE3 (Novagen), which was then cultured with aeration at 30°C to mid-log phase in 1 L

of Luria-Bertani medium supplemented with 200 µg/mL of ampicillin; at which point expression of the recombinant protein was induced by addition of isopropyl-ß-D-thiogalactopyranoside to 0.5 mM. The culture was incubated for an additional 4 hours at the above conditions, and cells were then harvested and resuspended in buffer (20 mM HEPES, pH 7.5; 150 mM KCl, 7.5% glycerol). Cells were disrupted by french press, and the lysate was cleared by centrifugation at 40,000 rpm for 20 minutes. The recombinant protein was then purified from the cleared lysate using HisPur Cobalt Resin (Thermo Scientific), using batch elution as described in the manufacturer's instructions. The concentrated fractions of purified protein were then dialysed against storage buffer (20 mM HEPES, pH 7.5; 150 mM KCl, 50% glycerol, 1 mM DTT, 1 mM EDTA), and stored at –80°C. Protein concentration was determined using BioRad Protein Assay Reagent (BioRad) and bovine serum albumin as a standard. The recombinant *Pa*HyPRE protein (335 residues, 35.8 kDa, isolectric point (*pI*): 5.8) was purified to approximately 95% homogeneity, and stored as a 78 µM stock. The recombinant *Sm*HyPRE protein (346 residues, 37.8 kDa, *pI*: 6.3) was purified to approximately 95% homogeneity, and stored as a 98 µM stock. Mutants containing single point mutations of the active site Cys residues of *Sm*HyPRE, C90S and C253S, where prepared similarly,[30] prepared as 30 and 35 µM stock solutions respectively.

5.3.3. Capillary Electrophoresis

Separations were performed on a P/ACE MDQ Capillary Electrophoresis System equipped with UV detection (Beckman-Coulter Inc., Fullerton, CA, USA) in a 50 μm i.d., 360 μm o.d. uncoated fused-silica capillary (Polymicro Technologies, Phoenix, USA). All separations were thermostatted to 20°C and electropherograms were collected at 214 nm. New capillaries were conditioned by rinsing with methanol for 8 min, water for 8 min, 8 M NaOH for 5 min, background electrolyte (BGE) for 16 min and were left to equilibrate for at least 30 min. At the beginning of each day, the capillary was rinsed for 8 min with 0.1 M NaOH and BGE for 8 min. All separations began by rinsing the capillary for 2 min with BGE. Between replicate measurements the capillary was rinsed with 0.1 M NaOH for 2 min and BGE for an additional 3 min. Samples were injected by application of 0.5 psi pressure. At the end of each day, the capillary was rinsed for 8 min with 0.1 M NaOH and 8 min with BGE and stored overnight in BGE. For longer storage, the capillary was rinsed for 8 min with 0.1 M NaOH, 8 min water and then stored in air. For protein unfolding experiments, frequent cleaning of electrodes and inlet/outlet lifts was necessary due to build-up of urea. The capillary was additionally cleaned of adsorbed protein by rinsing the capillary with 50:50 EtOH: 1 M NaOH for 8 min followed by rinsing with water for 8 min between unfolding experiments (*i.e.* collection of a full unfolding curve).

5.3.4. Protein Unfolding

Protein unfolding studies were performed in 100 mM electrolyte (pH adjusted by 0.1 M NaOH) buffer with or without 0.5 mM 4-*L*-Hyp or PYC and/or urea. HEPES was used as the electrolyte for pHs 7 and 8, Tris-HCl for ph 8.75 and CHES for pH 9.5. Separation buffers containing 0.5 mM 4-*L*-Hyp, PYC or urea were prepared from stock solutions of 50 mM 4-L-Hyp in water, 50 mM PYC in buffer and/or 8 M urea in 100 mM of the appropriate electrolyte, pH adjusted. Urea stock solutions were prepared fresh daily. Buffer and other stock solutions were stored at 4°C. CE experiments required less than 0.5 nmol of HyPRE (20 μM *Pa*HyPRE or 50 μM *Sm*HyPRE in 10 μL) which was prepared by diluting the stock solution in 100 mM HEPES (pH 7, filter sterilized). Separations were performed using short-end injections (effective capillary length, 10 cm; total length 60 cm) where the sample was introduced into the capillary by hydrodynamic injection at the outlet using low pressure (0.5 psi or 3.5 kPa) for 10s. Separations were performed under reverse polarity at -20 kV. Unfolding studies were carried out in separation buffer containing increasing concentrations of urea (x). The relative viscosity correction factor [$v = (0.0108 \pm 0.0008) x^2 + (1.02 \pm 0.02)$], required to normalize the apparent protein mobilities, was calculated by CE by the average time ($n = 5$) required for a sample plug to travel to the detector window under low pressure, which was fitted using non-linear regression analysis as described previously.[31]

Change in the hydrodynamic size of proteins during unfolding permits observation of protein unfolding via changes in apparent electrophoretic mobility ($\nu\mu_{ep}{}^{A}$). Under certain conditions, enzyme samples displayed heterogeneity in the transition region which may relate to the presence of partially unfolded intermediates[32] or may be attributed to HyPRE unfolding according to an intermediate time-regine.[33] In these cases peak shape was no longer Gaussian and instead resembled two overlapping unresolved peaks (refer to **Figure 2(a)**). Attempts to enhance resolution were unsuccessful, presumably due to the dynamic nature of the equilibria established by these two (or more) populations. In cases where non-Gaussian peaks where observed, $\nu\mu_{ep}{}^{A}$ was calculated as a weighted average based on heights of the overlapping peaks in order to account for shifts in population equilibria. Triplicate measurements using weighted average $\nu\mu_{ep}{}^{A}$ showed good precision with typical CV < 1%. The fraction of unfolded protein (F_{U}) was determined from changes in the average viscosity corrected apparent electrophoretic mobility ($\nu\mu_{ep}{}^{A}$) as a function of the urea concentration (c) assuming an ideal two-state unfolding system:

$$F_{U} = \frac{\nu\mu_{ep}{}^{A} - \mu_{ep,F}}{\mu_{ep,U} - \mu_{ep,F}} \tag{5-1}$$

where $\mu_{ep,\,F}$ and $\mu_{ep,\,U}$ represent the mobility of fully folded and unfolded protein states, respectively, and determined experimentally from the pre- and post-transition baselines of the $\nu\mu_{ep}{}^{A}$ expressed unfolding curves. The standard free

nergy of unfolding (ΔG_U^0) and the dependence of ΔG_U on urea concentration (m) were determined by non-linear regression of the F_U expressed unfolding curves:

$$F_U = \frac{\exp\left(-\dfrac{\Delta G_U^0 - mc}{RT}\right)}{1 + \exp\left(-\dfrac{\Delta G_U^0 - mc}{RT}\right)} \qquad (5\text{-}2)$$

where R and T respectively correspond to the gas constant and temperature, respectively.   Further preliminary work was performed to demonstrate that HyPRE was a suitable protein for dynamic unfolding experiments by CE with urea based on a two-state regime. Assumptions of fast and reversible unfolding were experimentally validated by CE. HyPRE was found to establish unfolding equilibria within the timescale of the separation (< 3 min) as supported by time-dependant protein unfolding experiments at 0, 2, 4, 6 and 7 M urea since no significant change in $\nu\mu_{ep}^A$ occurred from 0-3 hours after initial denaturation *off-line* at room temperature. The reversibility of the unfolding reaction was also evaluated by CE based on dynamic refolding experiments. In this case, the enzyme was unfolded *off-line* in 7 M urea and then analyzed by CE with the BGE containing 0-7 M urea. These studies demonstrated that HyPRE unfolding to be reversible as the thermodynamic parameters associated with refolding were statistically equivalent to unfolding ($\Delta G_U^0 = 3.0 \pm 0.6$ kcal/mol; $m = 1.0 \pm 0.2$ kcal·mol^{-1}·M; $C_M = 3 \pm 1$ M). In this work, thermodynamic parameters for protein unfolding, ΔG_U^0 and m, were determined using non-linear regression analysis with Igor Pro 5.0 (Wavemetrics Inc., Lake Oswego, OR, USA), whereas the

concentration midpoint for urea denaturation (C_M) was calculated based on rearrangement of **Eq. 5-2** where $F_U = 0.5$:

$$C_M = \frac{\Delta G_U^0}{m}$$ (5-3)

5.3.5. Kinetic Assays

All reactions to assess *Sm*HyPRE activity were conducted in an assay buffer (50 mM HEPES pH 8 with 2 mM β-ME, 1 mM EDTA) with 0 to 8 mM substrate and 50 nM HyPRE in a 210 μL reaction volume. Although previous assays with *Pa*HyPRE had been conducted in Tris buffer,[29] it was excluded due to interferences with Fmoc-Cl labelling required necessary for improved concentration sensitivity of amino acids with micromolar detection limits. Reactions for *Sm*HyPRE were carried out at 30°C and initiated by enzyme addition. Aliquots (20 μL) were withdrawn from the bulk reaction mixture at 30 s intervals from 0 to 5 min and quenched by irreversibly denaturing the enzyme at 90°C for 30 min. Epimerase activity was found to be linear within a 10 min sampling interval (t = 0, 2, 3, 5, 10 min). In this study, *on-line* Fmoc chemical derivatization was performed on quenched enzyme samples containing *D/L*-Hyp diastereomers by CE unlike our previous report that used *off-line* labeling (refer to **Chapter IV**). Prior to analysis by CE, 1 μL of 5 mM *m*-nitrophenol was added as the internal standard (IS) to 10 μL aliquots of quenched enzyme reaction. On-line labeling with Fmoc-Cl was accomplished by first injecting a spacer plug (100 mM HEPES pH 9.5) for 5 s under low pressure to the capillary inlet. The sample was

then introduced as a 5 s plug under low pressure. A solution of Fmoc-Cl, prepared in ACN at a concentration 10-fold higher than the concentration of substrate used in the kinetic assay was then introduced for 5 s under low pressure. The plugs were mixed by a low pressure injection of another spacer plug and allowed to react for 2 min in-capillary with the absence of an external electric field. All injection sequences were automated using 32 Karat Software v.5.0 by Beckman-Coulter Inc. All separations were performed in normal cathodic mode using a voltage of +25 kV. *On-line* Fmoc chemical derivatization was found to provide comparable analytical performance relative to the *off-line* labelling in terms of linearity and sensitivity, while offering a more convenient format for enzyme kinetic studies with greater sample throughput and automation. The concentration of product formed was determined by its average normalized peak area relative to the IS. Calibration solutions were prepared for 4-*D*-Hyp in a 10-fold excess of 4-*L*-Hyp in conditions mimicking those of the kinetic assay in order to account for effects of the assay buffer and labeling reaction on detection sensitivity. Solutions were labeled with Fmoc and analyzed by CE as described above. Responses were linear based on triplicate measurements of 8 points over a 25-fold concentration range from 10-250 μM as reflected by an R^2 value of 0.9987. Similarly 4-*D*-Hyp normalized to *m*-nitrophenol [y = (0.0098±0.0001) x + (0.0195± 0.02), μM], the limit of detection was found to be 3 μM with triplicate measurements possessing an average coefficient of variation of 4%. Fmoc-labeled *D*- and *L*-isomers were found to have similar UV responses at 214 nm.

Recovery was calculated at three different concentrations of 4-D-Hyp (30, 70, 500 µM) in the presence of 1 mM 4-L-Hyp. Average error for intraday triplicate measurements was under 10%. Enzyme kinetic parameters K_M and V_{max} were calculated using non-linear regression by Igor Pro 5.0.

5.4. Results and Discussion

5.4.1. Unfolding of *Pa*HyPRE: Evaluation of Substrate Binding on Enzyme Conformational Stability

Unfolding experiments were performed dynamically in the absence and with the presence of Hyp and various structural analogues as described previously.[31, 34] All experiments with *Pa*HyPRE were performed at pH 8, the optimal pH for enzyme activity,[29, 30] in order to make appropriate interpretation of apparent changes in protein conformational stability to catalysis. **Figure 5.1** depicts the unfolding curves of the *apo*-enzyme in its substrate/inhibitor-free state, compared to unfolding in the presence of the native substrate L-Hyp as well as various isomers and structural analogues. The thermodynamic parameters derived from non-linear regression of the unfolding curves of various *apo/holo*-enzyme states are summarized in **Table 5.1**. For all the Hyp analogues examined, the midpoint of urea-induced unfolding (C_M = 3-4 M urea) and standard free energy change for unfolding (ΔG_U^0 ~ 3 kcal/mol) were statistically equivalent to *apo*-*Pa*HyPRE. The similarity to the *apo*-protein state indicates that *Pa*HyPRE does not undergo any significant conformational changes
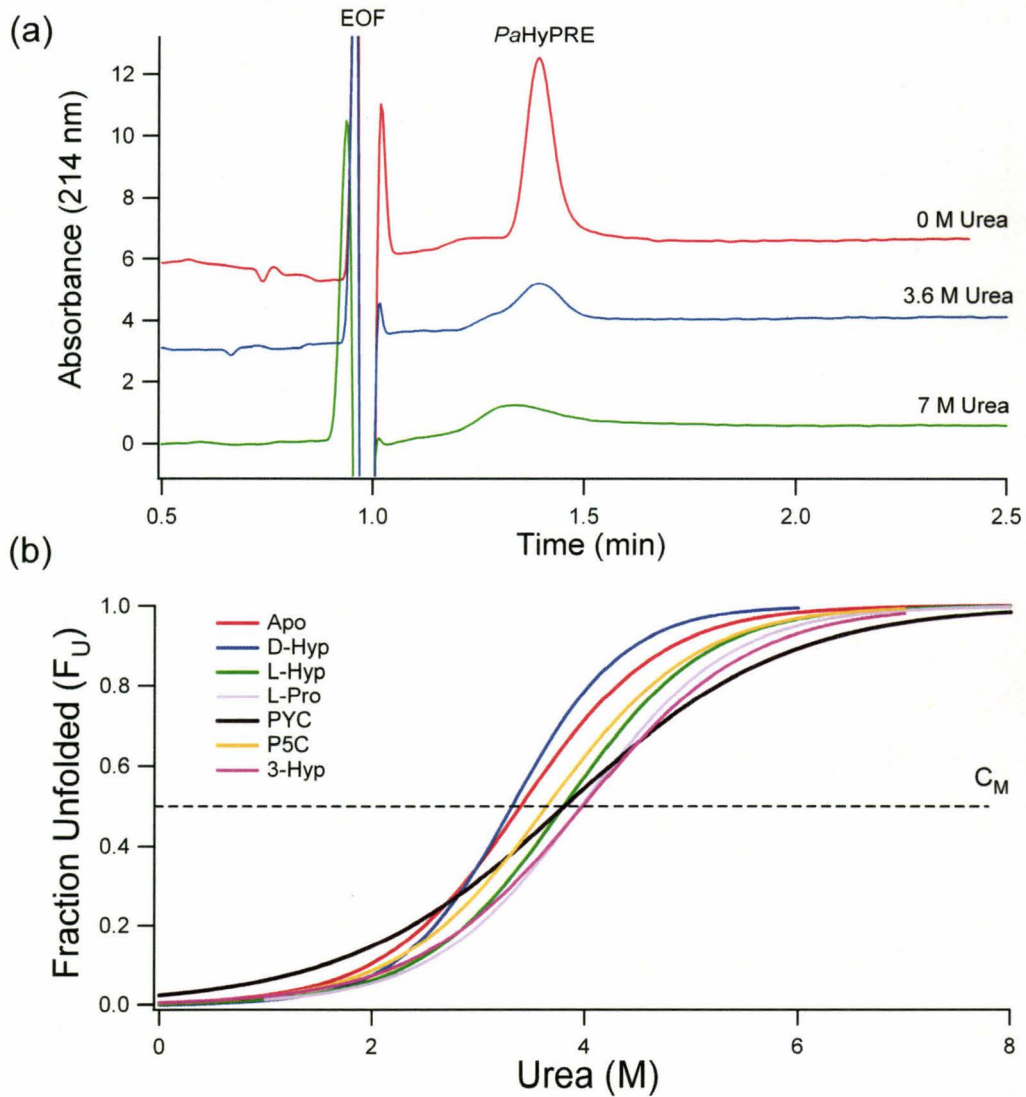
Figure 5.1. Dynamic denaturation of *Pa*HyPRE by CE where (a) depicts representative electropherograms for the unfolding of *apo*-PaHyPRE; and (b) represents the corresponding unfolding curves. Traces in (a) are aligned to the EOF. Samples containing 20 μM HypRE were unfolded in 100 mm HEPES pH 8 containing urea with no substrate/inhibitor or a 10-fold excess of Hyp analogue.

Table 5.1. Comparison of the thermodynamic parameters for conformational stability of
*Pa*HyPRE with various Hyp analogues.

Analogue	ΔG_U^0 (kcal/mol)	m (kcal/molM)	C_M (M)
Apo	3.0 ± 0.7	0.9 ± 0.2	4 ± 1
4-*L*-Hyp	3.7 ± 0.4	1.0 ± 0.1	3.8 ± 0.5
4-*D*-Hyp	3.7 ± 0.5	1.1 ± 0.1	3.4 ± 0.5
L-Pro	3.3 ± 0.5	0.84 ± 0.07	4 ± 0.4
3-*L*-Hyp	3.0 ± 0.2	0.74 ± 0.06	4 ± 0.4
P5C	3.0 ± 0.3	0.83 ± 0.07	3.6 ± 0.5
PYC	2.1 ± 0.2	0.56 ± 0.05	3.8 ± 0.5

upon diastereomers or inhibitor in an allosteric manner, including the active

substrates 4-*L*-Hyp and 4-*D*-Hyp. A marginal decrease in destabilization of

*Pa*HyPRE was observed when comparing the active substrates (4-*L*-Hyp and 4-*D*-

Hyp) with the competitive transition-state inhibitor PYC [$\Delta\Delta G_U^0$(4-*L*-Hyp-PYC) ~1.6 ±

0.3 kcal/mol]. This slight reduction in *holo*-enzyme stability is associated with a

decrease in the cooperativity coefficient (*m*) which has been shown to be related

to changes in protein solvent accessible surface area.[35] Binding of PYC may

therefore affect the solvent-accessible surface area in the active site relative to the

native substrates *D/L*-Hyp. Further interpretation of the thermodynamic data

can be made by considering the structure and mechanism of catalysis by HyPRE.

Early literature reports a discrepancy between a lower and higher molecular

weight for HypRE,[36-38] which was later confirmed by Ramaswamy[23] to

correspond to the monomeric and dimeric forms of HyPRE. While the crystal

structure of dimeric HyPRE for *P. aeruginosa* is unavailable, useful interpretation

of the conformational changes implied by the unfolding thermodynamic data can

be inferred from examination of the crystal structures of other related PLP-

independent isomerases such as diaminopimileate epimerase (DAP)[27] and PRAC.[17,39]

Like HyPRE, DAP and PRAC are homodimers with each monomer composed of two structurally similar domains that contribute one Cys each to the active site at the domain interface. The interdomain space is solvent accessible and contains two interdomain connections.[27, 29] Both DAP and PRAC have been shown to undergo substrate/inhibitor-promoted closure of the cleft around the active site which results in exclusion of water and burial of ligand from bulk solution. It should be noted that water is nearly completely excluded from the active site during catalysis and only 2 molecules are reported in the closed active site of DAP.[40] Exclusion of water reduces the dielectric constant of the active site pocket and aids in stabilization of the transition-state carbanionic species which is ultimately the driving force for deprotonation of the Hyp C_α.[40] For DAP, ligand-promoted closure was demonstrated by comparison of Cys→Ser single active site mutations at positions 73 or 217, which was done to allow crystallization of a native-like enzyme. This was compared to the inactivated disulphide-linked (Cys73-Cys217) crystal structure. Oxidation to a disulphide linkage was reported to occur spontaneously during crystallization of the wild-type enzyme. For TcPRAC crystallization was done in the presence of the inhibitor PYC. Crystal structures for TcPRAC were obtained for the fully bound and a half-site occupied enzyme. Both DAP and TcPRAC show that in the absence of substrate/inhibitor, the monomers display a more "open" conformation; where the channel at the

subunit interface connects the active site to bulk solution. The fact that 4-*L/D*-Hyp failed to produce the anticipated increase in unfolding stability expected by a ligand induced closure event can be attributed to the fact that no allosteric regulation is known for HyPRE and the transient nature of enzyme-substrate complexes. Since the active site is buried, it is plausible that the catalysis does not result in a large change in global protein conformation. It is also feasible that if a conformational change does occur during catalysis, that the catalytic state is too short-lived to be detected by equilibrium unfolding studies. Therefore, the equilibrium studies largely measure the *"apo"* conformation. In this the case, methods which allow for time resolved analysis, such as stopped-flow spectroscopy[41] or pulsed H/D exchange ESI-MS,[42, 43] would be required to probe the short-lived catalytic conformation.

PYC is known to be a transition state analog of the enzyme *Tc*PRAC and is therefore assumed to inhibit HyPRE by the same mechanism.[29] However, there are differences in the amino acids composition of the active site between these enzymes. Goytia *et al.* highlighted several amino acid differences which allowed for the bulky –OH group to be accommodated into the active site of HyPRE, stressing a predicted hydrogen bond between His270 and the 4-hydroxyl of the substrate.[29] Previous work (refer to **Chapter IV**) confirmed the key role of the hydroxyl in the 4-position in substrate recognition by the enzyme. As compared to *Tc*PRAC, the active site pocket of HyPRE is poorly suited to bind PYC due to additional difference in active site residues. **Figure 5.2** highlights differences in
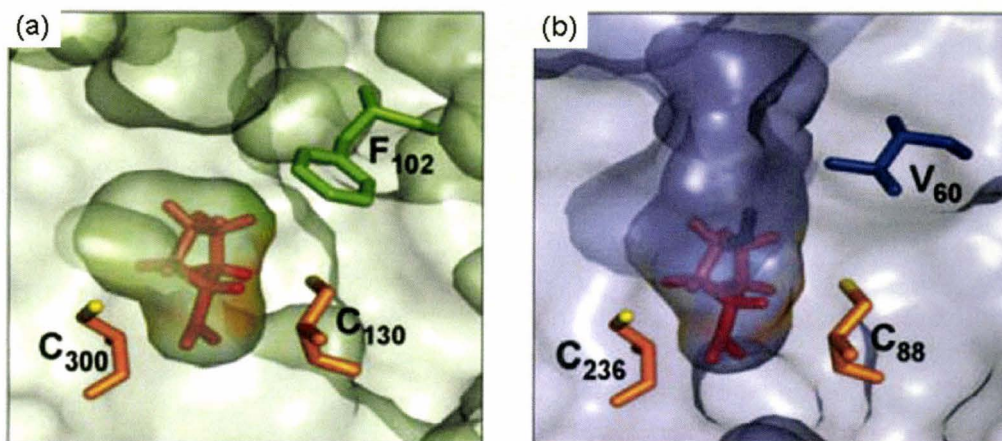
Figure 5.2. 3D model of the active sites of (a) *Tc*Prac and (b) *Pa*HyPRE with bound substrate (*L*-Pro or 4-*L*-Hyp) highlighting the paired catalytic cysteines and differences in hydrophobic contact. Reprinted from Goytia, *et al.*[29]

the contacts made in the active site between *Pa*HyPRE and *Tc*PRAC with their substrates, *L*-Hyp and *L*-Pro. Key amino acids in *Pa*HyPRE recognition of *D/L*-Hyp are His270 and Val60 which interact favorably with the substrate. In *Tc*PRAC, a Cys or Leu residue replaces His270 and an important Phe is present at position 102 making hydrophobic contacts with the Pro ring. These same residues are also attributed to steric hindrance of Hyp catalysis by *Tc*PRAC. As depicted in **Figure 5.2**, PYC, which better resembles Pro, would not be able to make favorably contacts in HyPRE. This not only accounts for its decreased function as an inhibitor,[29] but also may contribute altered closure of the catalytic cleft. As a consequence, removal of water during closure may be incomplete which may account for the relative reduction in unfolding free energy due to disruption of hydrogen-bonding between polar residues in the active site and the substrate that typically stabilizes the substrate during catalysis.[17, 29]
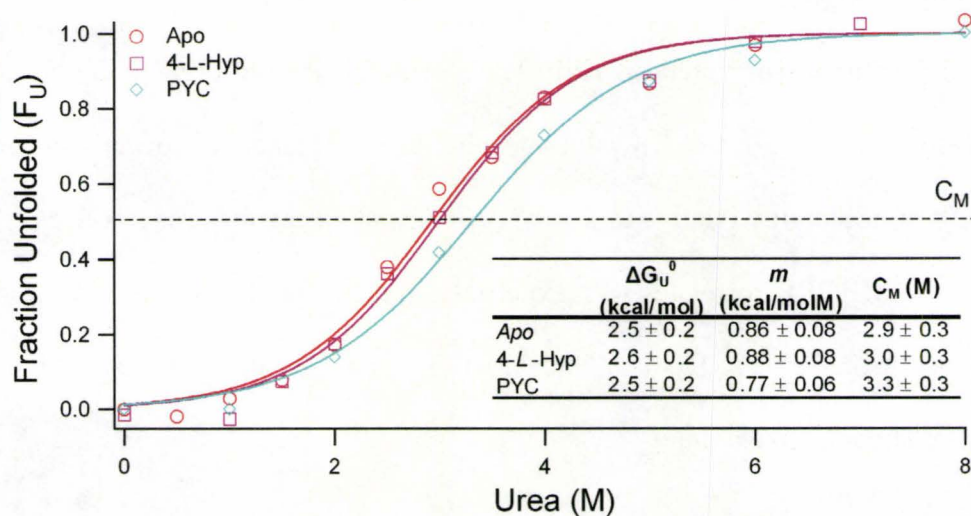
Figure 5.3. Dynamic denaturation of *Sm*HyPRE by CE. Samples containing 50 μM HypRE were unfolded in 100 mM HEPES pH 8 containing urea with or without a 10-fold excess of 4-*L*-Hyp or PYC. Fraction of unfolded protein was calculated based on changes in $v\mu_{ep}^{A}$. The inset shows the thermodynamic parameters associated with unfolding of *wt*-SmHyPRE, in the absence and presence of substrate, 4-*L*-Hyp, and the competitive inhibitor, PYC.

5.4.2. Unfolding of *Sm*HyPRE: Evaluation of Substrate Binding on Enzyme Conformational Stability

The epimerase from *S. melioiti* was also characterized by dynamic protein unfolding using CE. Although no crystal structure is available for *Sm*HyPRE, sequence similarity and preliminary kinetic studies confirms that *Sm*HyPRE is very alike to *Pa*HyPRE in both structural homology and catalytic mechanism. It was therefore of interest to assess whether the two enzymes also possessed similar conformational changes with substrate/inhibitor binding. **Figure 5.3** shows that, like *Pa*HyPRE, the substrate 4-*L*-Hyp and the inhibitor PYC do not impact the global conformation of *Sm*HyPRE under these conditions. PYC appears to exhibit marginal increase in stability against denaturation, however it is clear that

this modest change is within error of 4-L-Hyp (**Figure 5.3** inset). Comparison of the thermodynamic parameters of HyPRE isoforms of the two organisms shows statistically similar ΔG_U^0 and C_M values despite the slight tendency towards lower thermodynamic stability relative to *S. meliloti*. This tendency towards lower ΔG_U^0 and C_M for *Sm*HyPRE correlates with experimental observation that the enzyme is more labile than *Pa*HyPRE since SmHypRE is more sensitive to deactivation from shear stress or freeze-thaw.[30]

5.4.3. Characterization of *Sm*HyPRE Mutants: C90S and C253S

Site-directed mutagenesis based on the introduction of a single-point mutation is widely used in molecular biology and biochemistry to study protein function.[44,45] Mutations are performed in order to assess the contribution of a particular amino acid to a recognition process, catalytic event or overall protein stability.[46] Protein engineering is therefore often performed to enhance both the activity and the stability of proteins for therapeutic use.[47, 48] Based on the sequence alignments with *Tc*PRAC and *Pa*HyPRE, it is proposed that the Cys residues 90 and 253 form the catalytic dyad in the active site (refer to **Chapter IV**). Mutational analysis of the catalytic Cys with related isomerase enzymes have shown that they are both required for optimal enzymatic activity.[29] In some cases, enzyme function is completely abolished (*e.g.* DAP), whereas mutants of glutamate racemase (GluRAC) show diminished activity, suggesting that mutations are compensated by other amino acids.[26, 49]
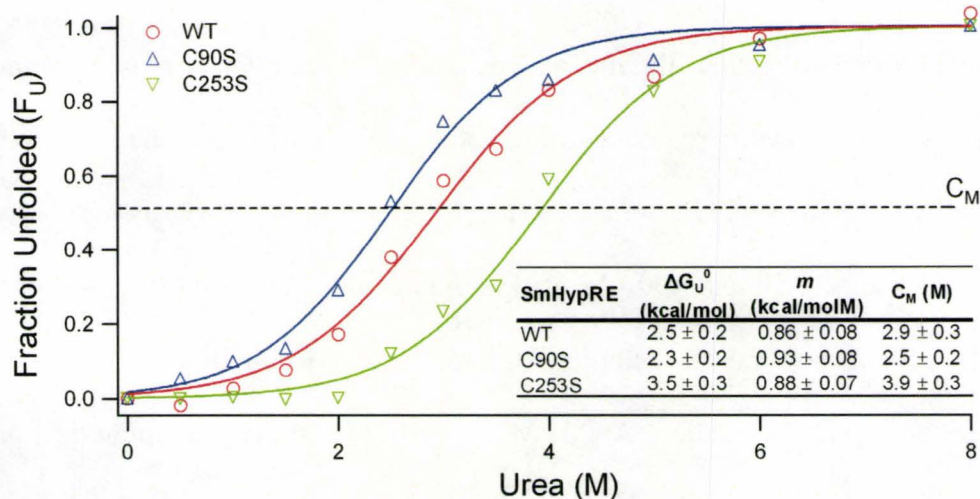
Figure 5.4. Impact of single amino acid mutations of cysteines in the catalytic dyad on the conformational stability of *Sm*HyPRE upon urea denaturation by CE. Samples containing 50 µM HypRE were unfolded in 100 mM HEPES pH 8 containing urea. Fraction of unfolded protein was calculated as in **Fig. 5.3.** The thermodynamic parameters associated with unfolding are provided in the inset.

Nonetheless, when assessing mutant enzymes for function it is important to evaluate the effect of the mutation on the global conformation of the enzyme in order to differentiate its contribution to structure from its contribution to function.

Figure 5.4 depicts the unfolding curves for single-point Cys mutations in *Sm*HyPRE under buffer pH conditions required for optimum enzyme activity (pH 8). Both the *wt* and C90S possess similar conformational stabilities as reflected by the similarities in ΔG_U^0, m and C_M. Interestingly, the mutation at C253S leads to a relative increase in ΔG_U^0 of about 1 kcal/mol and a corresponding increase in C_M of 1 M relative to the *wt-Sm*HyPRE. These results suggest that the C90S mutant folds in a manner similar to the wild-type enzyme, but that the C253 mutation leads to an increasingly stable conformation more resistant to urea denaturation.

5.4.4. Enzyme Kinetics

In order to relate thermodynamic unfolding parameters to enzyme function, kinetic assays were performed to determine activity based on assessment of Michaelis-Menten parameters (K_M and V_{max}). Preliminary assays were performed with 20, 50 and 100 nM of wild-type SmHyPRE using 0, 1, 4 and 8 mM 4-L-Hyp as substrate to determine the minimal concentration that could be used to assess enzyme kinetics. At 20 nM wt-SmHyPRE, the rate of epimerization was found to be ~ 1 x 10^{-7} Ms^{-1} for the highest concentration of substrate evaluated (8 mM). This corresponded to a concentration increase of only 3 μM 4-D-Hyp (per 30s sampling interval) which was at the limit of detection of the method. An enzyme concentration of 50 nM, which corresponds to a V_0 of (66 ± 2) x 10^{-8} Ms^{-1} at 8 mM 4-L-Hyp as substrate (~20 μM for t = 30s), was therefore chosen to perform the kinetic assays.

Wt-SmHyPRE was found to be fully reversible for the epimerization of 4-D/L-Hyp as shown in **Figure 5.5.** Activity for SmHyPRE was observed to be lower as compared to PaHyPRE [K_M = (2.0 ± 0.5) x 10^{-3} M; V_{max} = (9.27 ± 0.09) x 10^{-6} Ms^{-1} for 4-L-Hyp as substrate, refer to **Chapter IV**]. Additionally, the activity of PaHyPRE could be quantified accurately with only 10 nM enzyme where a change of ~20 μM over 30 s could be observed with only 4 mM of substrate. Assays for $S.$ $meliloti$ were performed at 30°C which is the typical environmental temperature for $S.$ $meliloti$ whereas assays for $P.$ $aeruginosa$ were
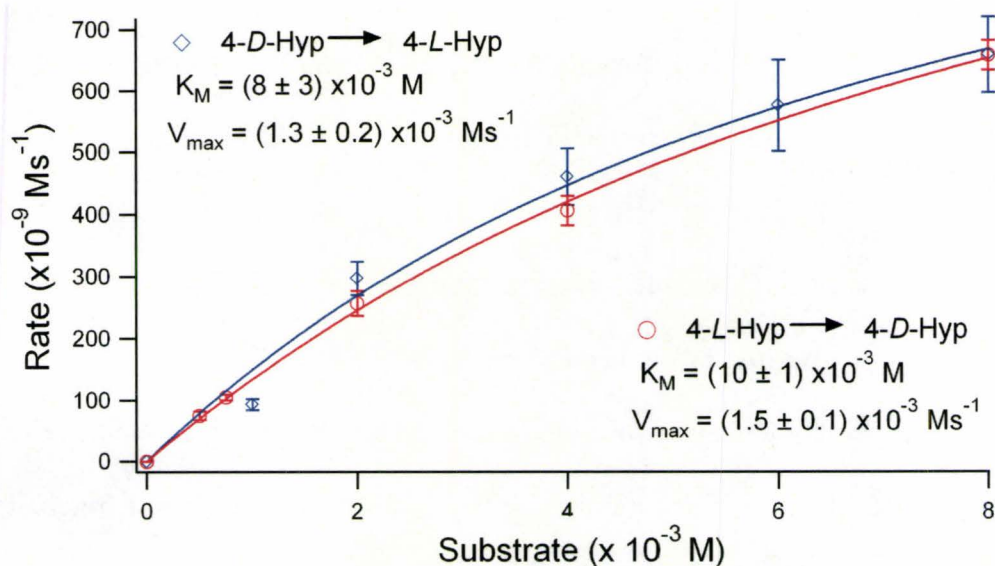
Figure 5.5. Nonlinear regression of Michaelis-Menten kinetics highlighting the reversibility of 4-*D/L*-Hyp conversion by SmHyPRE. Reactions were performed with 50 nM enzyme at 30°C and heat quenched prior to CE analysis. Error represents the standard error of the initial rate measurements.

performed at $37°$C (refer to **Chapter IV**). The lower apparent activity for *S. meliloti* as compared to *P. aeruginosa* can thus be attributed to temperature of the assay. Assays conducted for *Pa*HyPRE at 30°C confirmed this difference was largely due to temperature of the assay. In fact, at 30°C the K_M of *Pa*HyPRE [(3.2 ± 0.3) x 10^{-3} M] was found to be within error of *Sm*HyPRE, but *Sm*HyPRE exhibited the higher V_{max} [(1.16 ± 0.02) x 10^{-6} Ms^{-1} for *Pa*HyPRE]. Our results show that *Sm*HyPRE is actually the more active of the two enzymes which is further accentuated by comparison of turnover number and catalytic efficiency (k_{cat}/K_M) respectively: k_{cat} ~ 1 x 10^3 s^{-1}, efficiency ~ 8 x 10^5 Ms^{-1} for *Pa*HyPRE at 37°C; and k_{cat} ~ 2 x 10^4 s^{-1}, efficiency ~ 3 x 10^6 Ms^{-1} for *Sm*HyPRE. This result is

in contrast to experimental observation,[30] which can be attributed to the previous use of a colorimetric coupled enzyme assay with *D*-amino acid oxidase. The coupled assay suffers from bias as the inhibitor, PYC, is produced as a by-product and inhibits both HyPRE and the coupled enzyme. In comparison, the CE assay alleviates reliance on the coupled enzyme allowing for bias-free evaluation of kinetics (refer to **Chapter IV**). The Cys mutants of *S. meliloti* were also tested for epimerase activity at similar reaction conditions to the wild-type. No activity was observed after 5 min, therefore reaction was tested over a longer time interval (up to 60 min) as shown in **Figure 5.6.** The loss of enzyme activity of Cys90 and Cys253 mutations confirm that both sites are essential for the *D/L*-Hyp epimerization reaction with no other amino acids present in the active site cavity able to function as an acid/base donor/acceptor. This experimental observation is consistent with results from quantum mechanic-molecular mechanic studies performed with PRAC that conclude no other active site residues other than the Cys dyad are involved in catalysis.[50] Furthermore, this result cautions against correlating enhanced thermodynamic stability (refer to **Fig. 5.4**) to increased activity since the more stable C253S mutant was functionally inactive.

5.4.5. pH-dependence of the *Sm*HyPRE Conformational Stability

The thermodynamic stability of *Sm*HyPRE was enhanced by the C253S mutation but resulted in loss of activity. However, the thermodynamic stability of the C90S mutant was similar to the *wt*-HyPRE, but epimerization activity was still
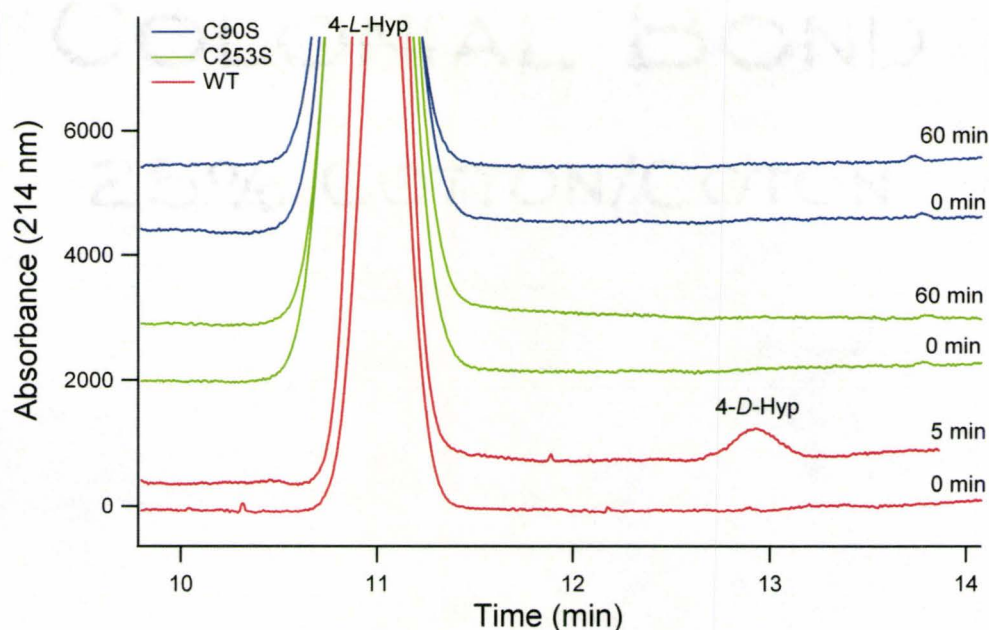
Figure 5.6. Representative electropherograms from kinetic evaluation of the C90S and C253S mutants of SmHyPRE compared to the wild-type. The standard trace represents an abiotic control spiked with 100 μM 4-D-Hyp. Assays were performed with 50 nM enzyme and 8 mM 4-L-Hyp as substrate at 30°C.

abolished. Clearly, the Cys residues are essential in the active site for the enzyme to function properly; however results from the unfolding studies also suggest that they do not necessarily contribute to the most stable global conformation for SmHyPRE. The Cys→Ser mutation introduces a hydroxyl group in place of the thiol which alters the electrostatic environment of the active site since the thiol from Cys is ionizable.[51] In order to determine the extent of the electrostatic contribution of Cys90 and Cys253, unfolding was performed under neutral and alkaline conditions at three additional buffer pH: 7, 8.75 and 9.5. At neutral pH, the two mutants possess similar conformational stabilities to the wt-SmHyPRE as shown by the similar C_M values in **Figure 5.7(a).** While this was observed at pH
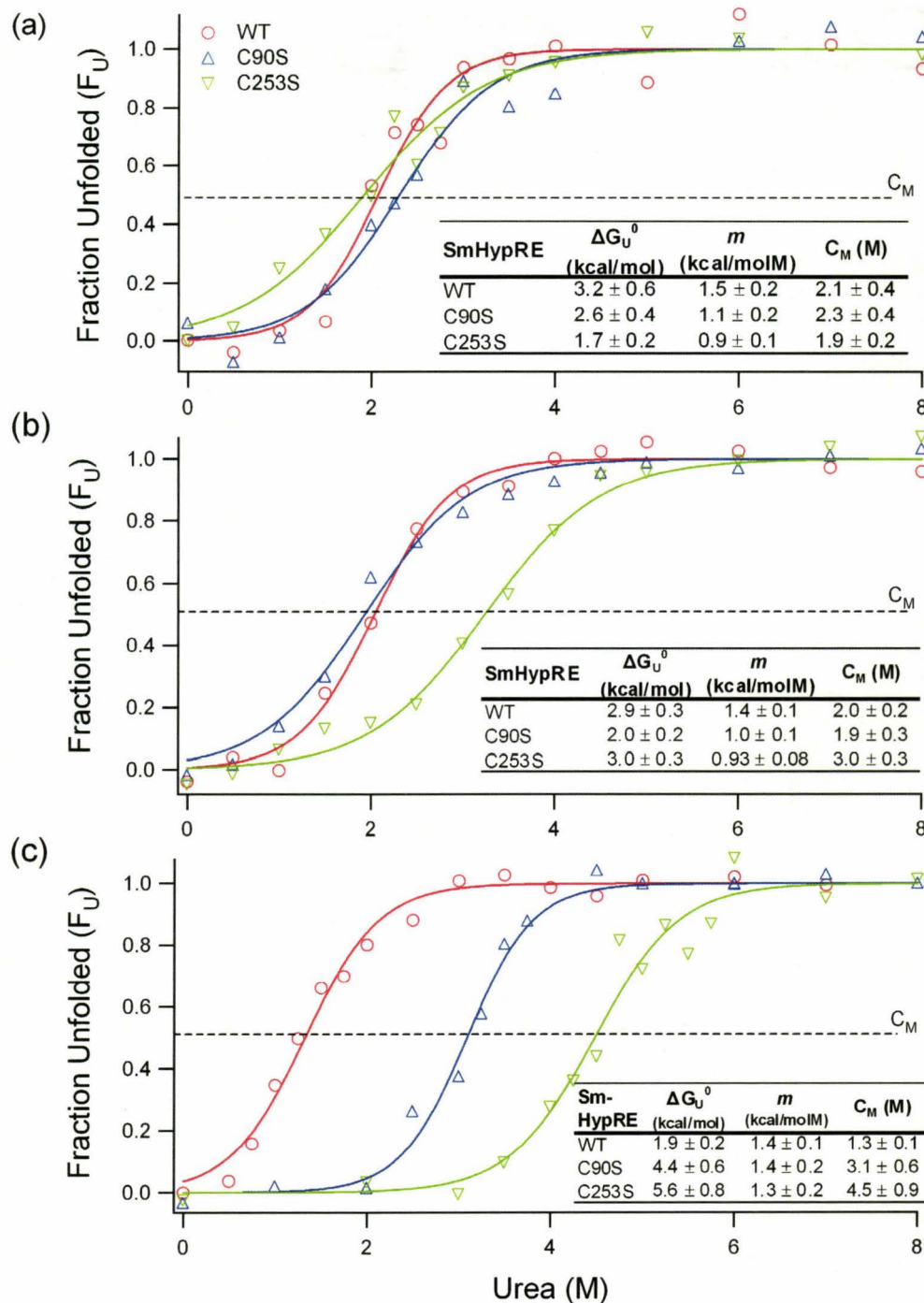
Figure 5.7. Comparison of the conformational stability of *wt-Sm*HyPRE and mutants C90S and C253S, as a function of increasing pH buffer from pH 7 (a) to pH 8.75 (b) and pH 9.5(c).
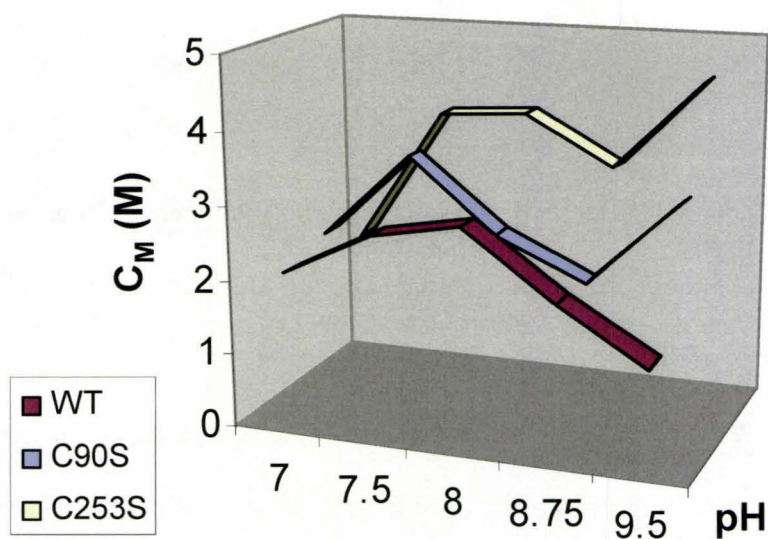
Figure 5.8. Impact of pH on the conformational stability of C90S and C253S relative to *wt-Sm*HyPRE where C_M is the mid-point of urea denaturation.

8 for the wild-type and C90S (refer to **Fig. 5.3**), C253S exhibited a higher conformational stability. Therefore, in order to elicit a conformation state more similar to the wild-type, a decrease in pH is required for C253S in order to fully protonate the more acidic Cys residue. As pH is increased, C253S gains additional stability reflected by higher ΔG_U^0 and C_M values relative to the wild-type enzyme. Of note, C90S becomes more stable at pH 9.5, whereas the wild-type becomes more destabilized relative to neutral pH conditions, reflected by differences in apparent ΔG_U^0 and C_M. This is more clearly summarized in **Figure 5.8** where it can be seen that the C90S mutant is thermodynamically similar to the wild-type from pH 7-8.75, but gains greater stability at pH 9.5. In contrast, C253S only behaves similarly to the wild-type at pH 7 with much greater conformational stability under alkaline pH conditions.

The relationship between the pH-dependence of unfolding of enzyme mutants examined in this study can be related to the apparent pK_a of the specific Cys residues in the active site of the enzyme. Under strongly alkaline conditions, both Cys residues in *wt-Sm*HyPRE are completely ionized, which results in significant electrostatic repulsion in the active site with decreased overall conformational stability. However, in the case of protein mutants, the replacement of Cys with Ser reduces the extent of Columbic repulsion in the active site leading to greater stability at high pH. At neutral pH, the Cys residues are largely unionized resulting in similar thermodynamic stability for all three proteins. Under weakly alkaline pH conditions, the contribution of each Cys residue to conformational stability can be attributed to differences in the pK_a of the corresponding Cys and the resulting changes to the electrostatic environment of the active site pocket. Since C90S has similar stability to the wild-type from pH 7-8.75, Cys253 must be in the same ionization state in both proteins, only becoming fully ionized at pH 9.5. This implies it functions as the more basic Cys residue in the active site. Conversely, C253S only behaves similarly to the wild-type enzyme at pH 7 suggesting that Cys90 possess a lower pK_a (more acidic) than Cys253. The pK_a of the thiol in a typical Cys residue is ~9,[52] however surrounding resides can significantly alter its acidity. The pH-dependence of *Sm*HyPRE unfolding is consistent with the pK_a values of 6.1 and 7.0 that have been reported for *Arabidopsis thaliana* DAP epimerase that correspond to Cys99 and Cys254, respectively.[40] The Cys dyad of isomerase enzymes therefore

represents a unique model where the comparative pH dependence of protein unfolding parameters can be used to evaluate the relative acidity of each residue in the acid/base pair since ionization results in protein destabilization of the wild-type relative to the Cys mutants. To the best of our knowledge, the relationship between protein unfolding and pK_a of amino acids involved in acid/base catalysis has not been previously demonstrated. In fact, pK_a determination for amino acid residues in enzyme active sites is often not determined directly, but rather through modeling and simulation of enzyme crystal structure data.[53, 54] The study of site-directed mutants by protein unfolding at different pH on a CE platform therefore represents a novel approach to directly measuring pK_a of residues involved in enzyme catalysis.

5.5. Conclusions

CE provides a convenient platform for the thermodynamic and kinetic assessment for mutant isomerase enzymes for elucidation of catalysis mechanisms. The thermodynamic properties of wild-type and mutant HyPREs were characterized by CE via dynamic unfolding. The conformational stability of *apo-wt*-HyPRE from *P. aeruginosa* and *S. meliloti* were found to be similar; both in the presence of substrate/inhibitor and to each other, which indicates similar global conformations between the two HyPREs. Thermodynamic analysis of single point mutants, C90S-, C253S-*Sm*HyPRE, confirmed similar global conformation to the wild type at neutral pH. Kinetic analysis demonstrated that no

activity was observed for these mutants providing direct evidence that these Cys residues comprise the catalytic dyad. pH-dependent unfolding studies further demonstrated the contribution of each Cys to the electrostatic environment of the active site pocket. This was inferred from differential shifts in thermodynamic stability of the mutants relative to the wild-type at increasing buffer pH attributed to decreased coloumbic repulsion in the active site. Future work is aimed at confirming the role of each residue in recognition of 4-L/D-Hyp and comparative inhibition studies with PYC to determine the impact of species differences on HyPRE activity as well as better understand the phylogenic relationship between related bacteria. To the best of our knowledge, this work represents the first direct assessment of the apparent pK_a of active site residues that does not require crystal structure data. CE represents a convenient format to quantifying the contribution of individual amino acid residues to enzyme activity and conformational stability. Given the important relationship between protein structure and function, CE based assessment of thermodynamic stability has promising application in the differentiation of diseased protein states,[55] genetic polymorphisms,[56] and allostery.[57] It is anticipated that CE will play an increasing role as an integrative platform for elucidating catalytic mechanism in recombinant proteins.

5.6. References

1.   Wright, P. E.; Dyson, H. J., *Curr. Opin. Struct. Biol.* **2009,** *19*, 31.

2.   Goodey, N. M.; Benkovic, S. J., *Nat. Chem. Biol.* **2008,** *4*, 474.

3.   Martin, S. R.; Schilstra, M. J., Circular dichroism and its application to the study of biomolecules. In *Biophysical Tools for Biologists: Vol 1 in Vitro Techniques*, 2008; Vol. 84, pp 263.

4.   Cai, X. M.; Dass, C., *Curr. Org. Chem.* **2003,** *7*, 1841.

5.   Dolnik, V., *Electrophoresis* **2008,** *29*, 143.

6.   Glatz, Z., *J. Chromatogr. B.* **2006,** *841*, 23.

7.   Heegaard, N. H. H.; Nilsson, S.; Guzman, N. A., *J. Chromatogr. B* **1998,** *715*, 29.

8.   Monnig, C. A.; Kennedy, R. T., *Anal. Chem.* **1994,** *66*, R280.

9.   Bao, J. J.; Fujima, J. M.; Danielson, N. D., *J. Chromatogr. B* **1997,** *699*, 481.

10.   Righetti, P. G.; Verzola, B., *Electrophoresis* **2001,** *22*, 2359.

11.   Denton, K. A.; Tate, S. A., *J. Chromatogr. B* **1997,** *697*, 111.

12.   Rochu, D.; Viguie, N.; Renault, F.; Crouzier, D.; Froment, M. T.; Masson, P., *Biochem. J.* **2004,** *380*, 627.

13.   Imai, K.; Fukushima, T.; Santa, T.; Homma, H.; Hamase, K.; Sakai, K.; Kato, M., *Biomed. Chromatogr.* **1996,** *10*, 303.

14.   Yoshimura, T.; Goto, M., *Febs J.* **2008,** *275*, 3527.

15.   Corrigan, J. J., *Science* **1969,** *1964*, 142.

16.   Fuchs, S. A.; Berger, R.; Klomp, L. W. J.; de Koning, T. J., *Mol. Genet. Metab.* **2005**, *85*, 168.

17.   Buschiazzo, A.; Goytia, M.; Schaeffer, F.; Degrave, W.; Shepard, W.; Gregoire, C.; Chamond, N.; Cosson, A.; Berneman, A.; Coatnoan, N.; Alzari, P. M.; Minoprio, P., *PNAS* **2006**, *103*, 1705.

18.   Chamond, N.; Cosson, A.; Coatnoan, N.; Minoprio, P., *Mol. Biochem. Parasitol.* **2009**, *165*, 170.

19.   Chamond, N.; Goytia, M.; Coatnoan, N.; Barale, J. C.; Cosson, A.; Degrave, W. M.; Minoprio, P., *Mol. Microbiol.* **2005**, *58*, 46.

20.   Adams, E., *J. Biol. Chem.* **1959**, *234*, 2073.

21.   Singh, R. M. M.; Adams, E., *J. Biol. Chem.* **1965**, *240*, 4344.

22.   Yoneya, T.; Adams, E., *J. Biol. Chem.* **1961**, *236*, 3272.

23.   Ramaswamy, S., *J. Biol. Chem.* **1984**, *259*, 249.

24.   Wang, Y.; Addess, K. J.; Chen, J.; Geer, L. Y.; He, J.; He, S.; Lu, S.; Madej, T.; Marchler-Bauer, A.; Thiessen, P. A.; Zhang, N.; Bryant, S. H., *Nucleic Acids Res.* **2007**, *35*, D298.

25.   Tanner, M. E., *Accounts Chem. Res.* **2002**, *35*, 237.

26.   Glavas, S.; Tanner, M. E., *Biochemistry* **1999**, *38*, 4106.

27.   Pillai, B.; Cherney, M.; Diaper, C. M.; Sutherland, A.; Blanchard, J. S.; Vederas, J. C.; James, M. N. G., *Biochem. Biophys. Res. Commun.* **2007**, *363*, 547.

28.   Yamauchi, T.; Choi, S. Y.; Okada, H.; Yohda, M.; Kumagai, H.; Esaki, N.; Soda, K., *J. Biol. Chem.* **1992,** *267*, 18361.

29.   Goytia, M.; Chamond, N.; Cosson, A.; Coatnoan, N.; Hermant, D.; Berneman, A.; Minoprio, P., *PLoS One* **2007,** *2*, e885.

30.   White, C. E.; Finan, T. E., Unpublished result. McMaster University: Hamilton, 2009.

31.   Segui-Lines, G.; Gavina, J. M. A.; D'Amaral, J. C.; Britz-McKibbin, P., *Analyst* **2007,** *132*, 741.

32.   Privalov, P. L., *J. Mol. Biol.* **1996,** *258*, 707.

33.   Hilser, V. J.; Freire, E., *Anal. Biochem.* **1995,** *224*, 465.

34.   Gavina, J. M. A.; Mazhab-Jafari, M. T.; Melacini, G.; Britz-McKibbin, P., *Biochemistry* **2009,** *48*, 223.

35.   Myers, J. K.; Pace, C. N.; Scholtz, J. M., *Prot. Sci.* **1995,** *4*, 2138.

36.   Adams, E.; Norton, I. L., *J. Biol. Chem.* **1964,** *239*, 1525.

37.   Gryder, R. M.; Adams, E., *J. Bacteriol.* **1969,** *97*, 292.

38.   Finlay, T. H.; Adams, E., *J. Biol. Chem.* **1970,** *245*, 5248.

39.   Higgins, W.; Tardif, C.; Richaud, C.; Krivanek, M. A.; Cardin, A., *Eur. J. Biochem.* **1989,** *186*, 137.

40.   Pillai, B.; Moorthie, V. A.; van Belkum, M. J.; Marcus, S. L.; Cherney, M. M.; Diaper, C. M.; Vederas, J. C.; James, M. N. G., *J. Mol. Biol.* **2009,** *385*, 580.

41.   Eccleston, J. F.; Martin, S. R.; Schilstra, M. J., Rapid kinetic techniques. In *Biophysical Tools for Biologists: Vol 1 in Vitro Techniques*, Elsevier Academic Press Inc: San Diego, 2008; Vol. 84, pp 445.

42.   Pan, J. X.; Rintala-Dempsey, A. C.; Li, Y.; Shaw, G. S.; Konermann, L., *Biochemistry* **2006,** *45*, 3005.

43.   Stocks, B. B.; Konermann, L., *Anal. Chem.* **2009,** *81*, 20.

44.   Creighton, T. E., *Proteins: Structure and Molecular Properties*. 2nd ed.; W. H. Freeman and Company: New York, 1993.

45.   Smith, M., *Ann. Rev. Genet.* **1985,** *19*, 423.

46.   Botstein, D.; Shortle, D., *Science* **1985,** *229*, 1193.

47.   Arnold, U.; Ulbrich-Hofmann, R., *Biotechnol. Lett.* **2006,** *28*, 1615.

48.   Ramos, C. R. R.; Spisni, A.; Oyama, S.; Sforca, M. L.; Ramos, H. R.; Vilar, M. M.; Alves, A. C.; Figueredo, R. C. R.; Tendler, M.; Zanchin, N. I. T.; Pertinhez, T. A.; Ho, P. L., *Biochim. Biophys. Acta* **2009,** *1794*, 655.

49.   Lundqvist, T.; Fisher, S. L.; Kern, G.; Folmer, R. H. A.; Xue, Y. F.; Newton, D. T.; Keating, T. A.; Alm, R. A.; de Jonge, B. L. M., *Nature* **2007,** *447*, 817.

50.   Rubinstein, A.; Major, D. T., *JACS* **2009,** *131*, 8513.

51.   Nelson, D. L.; Cox, M. M., *Lehninger Priniples of Biochemistry*. Third ed.; Worth Publishers: New York, 2000.

52.   Puig, E.; Garcia-Viloca, M.; Gonzalez-Lafont, A.; Lluch, J. M., *J. Phys. Chem. A* **2006,** *110*, 717.

53.   Davoodi, J.; Wakarchuk, W. W.; Campbell, R. L.; Carey, P. R.; Surewicz, W. K., *Eur. J. Biochem.* **1995,** *232*, 839.

54.   Lederer, F., *Protein Sci.* **1992,** *1*, 540.

55.   Dobson, C. M., *Nature* **2003,** *426*, 884.

56.   Robinson, P. J.; Pinheiro, T. J. T., *Biochemistry* **2009,** *48*.

57.   Laskowski, R. A.; Gerick, F.; Thornton, J. M., *FEBS Lett.* **2009,** *583*, 1692.

(Intentionally Blank)

Chapter VI

Future Applications and Prospects

VI. Future Applications and Prospects

The work presented in this thesis has contributed novel approaches applicable to high-quality screening of drug candidates using CE as an integrative platform for characterizing the thermodynamics and kinetics of protein-small molecule interactions.   Several unique strategies have been developed to efficiently integrate labour-intensive sample pre-treatment steps during chemical analysis that are applicable to both proteins and metabolites, such as in-capillary *apo/holo*-protein generation with dynamic protein unfolding and on-line chemical derivatization with dynamic complexation of amino acid stereoisomers. Integration of these steps offers a more streamlined method for analysis which reduces the complicated sample handling and total analysis time that is often required for processing biological samples.   The framework developed in this thesis is particularly relevant towards improving drug development, notably for label-free screening of allosteric ligands to regulatory/receptor protein targets (*e.g.,* RIα, EPAC), as well as the unbiased assessment of inhibitors for enzymes with racemase and/or epimerase activity (*e.g.,* HyPRE, PRAC).   For instance, DLE-ACE in conjunction with multivariate analysis was introduced as a novel strategy for thermodynamic assessment of allosteric proteins based on multiple parameters associated with *holo*protein conformational stability, unfolding cooperativity and ligand binding affinity.   This approach allows for the determination of high affinity binding interactions over a wide dynamic range (K_d $\approx$ nM-mM) without chemical labelling, which also has promising applications for

differentiating orthosteric and allosteric binding events which is not feasible by conventional primary screening methods, such as competitive radiolabel assays. This thesis further demonstrated that CE offers a convenient method for characterizing mutants relative to wild-type enzymes based on the pH-dependence of protein unfolding. Deeper insight was achieved into relative conformational stability, specific function and catalytic mechanism of critical amino acid residues required for activity, such as the acidic/basic Cys dyad motif common to isomerases. Moreover, an unbiased assay was developed and validated for enzyme kinetic studies of amino acid isomerases using CE based on the resolution of various classes of enantiomers, stereoisomers and structural isomers which is relevant to the development of new classes of antibiotics. These examples highlight the versatility of CE as a unified platform for the characterization of proteins and their biomolecular interactions with small molecules for high-quality drug screening. Improved sample throughput, along with low-cost analyses and access to multiple thermodynamic/kinetic parameters will provide researchers with a better selection of parameters for characterization of putative drug candidates at early stages of screening.

6.1. Future Prospects of DLE-ACE

6.1.1. Osmolytes

The experiments within this thesis were performed *in-vitro* with buffers adjusted to physiological or optimal pH for maximum activity. However, in order

to better mimic intra-cellular conditions *in vivo*, osmolytes such as taurine, sorbitol, myoinositol or dilute polymer additives such as polyethylene oxide (PEO) can be used to determine the impact of a sterically-crowded environment on protein conformational stability and folding cooperativity. Since low molecular weight organic osmolytes present in cells are known to impact apparent protein conformational stability and folding cooperativity,[1-3] it is highly that ligand binding affinity is also sensitive to the local environment. It would be of interest to investigate whether changes to thermodynamic unfolding parameters in the presence of osmolytes can prevent the generation of intermediate unfolding states that are often observed for large multi-domain proteins and thereby improve the accuracy for direct K_d determination *in-vitro*. Such studies would be useful for high-quality screening of drugs to target specific cells such as cardiomyocytes for which osmolytes (*e.g.* taurine) have been shown to play critical roles in reducing osmotic stress.[4] Finally, the phenomena of osmolytes accumulation (*e.g.* glycine betaine) for protection of proteins also occurs naturally in bacteria such as *Sinorhizobium meliloti* for protection against osmotic stress suggesting that bacterial proteins may also be suitable model systems.[5]

6.1.2. Metabolite Screening and Evaluation of High-Affinity Interactions via *Holo*-protein Unfolding

DLE-ACE can be further expanded to characterize the unfolding of multimeric protein receptors that possess extremely high affinity interactions,

such as thyroxine binding globulin ($K_d \sim$ 100 pM for thyroxine)[6] and streptavidin ($K_d \sim$ 2 fM for biotin).[7] Indeed, thyroxine and biotin represent primary biomarkers for the diagnosis of metabolic disorders associated with congenital hyperthyroidism and biotinidase deficiency, which are currently analyzed via radioimmunoassay or enzymatic assays, respectively.[6, 8] The high stability of these particular protein-ligand complexes poses significant challenges to their assessment by DLE-ACE. Urea has been reported to function as an analogue of biotin therefore it is insufficient as a denaturant to induce complete unfolding of streptavidin even at high concentrations (> 8 M),[9] since it associates with the biotin binding site in the protein.[10, 11] In fact, successful denaturation has only been accomplished by use of excessive heating in the presence of the detergent SDS.[11] Successful unfolding of streptavidin by CE would represent a noteworthy feat since it represents one of the highest known affinity interactions which would be difficult to disrupt in a dynamic manner. Use of multiple denaturants (*e.g.* SDS and urea) as well as elevated temperature will likely be needed to induce dynamic unfolding during electromigration. Successful unfolding of these target proteins would permit direct quantification of thyroxine and biotin using calibration curves derived from the concentration-dependence of ligand-induced shifts in *holo*-protein unfolding. Earlier studies by DLE-ACE demonstrated a dependence of the unfolding thermodynamic parameters (*i.e.* C_M) on the concentration of ligand in the BGE. This observation could be exploited for the trace analysis of thyroxine and biotin without chemical labelling. By performing

DLE-ACE with thyroxin binding globulin and streptavidin, calibration curves can be established which correlate C_M and ligand concentration. This would provide an accurate, label-free assay for prognosis of congenital hypothyroidism and biotinidase deficiency.

6.1.3. Protein Allostery

In this thesis, the term allostery has been loosely used to describe conformational changes that occur during the allosteric regulation of proteins or enzymes. However, allosteric regulation can better defined as the response to modulator binding, coupling and mechanism.[12] Furthermore, protein allostery has been suggested to be considered only when a ternary complex is considered, such that changes induced by the binding of a modulator to a protein are only relevant when comparing modulation in the presence and absence of substrate.[13, 14] Evaluation of the ternary complex thereby reveals which conformational changes are induced by the binding of the modulator, which are related to allosteric regulation and which are associated solely with the binding event. There is also growing interest in quantifying the apparent free energy associated with allosteric coupling. In a two domain system, where binding of a modulator at one domain affects binding at a distant domain, allosteric coupling refers to the change in the free energy at the second site.[15] This phenomena is particularly important in the study of intrinsically disordered domains (IDs) which are associated with a wide variety of biological functions.[15, 16] Since folding of intrinsically disordered

proteins is often modulated through a distant binding event, IDs are gaining recognition as being critical components of protein regulation.

In this context, it would be of interest to use DLE-ACE to evaluate the conformational changes induced on larger multi-domain protein constructs as well as the multi-subunit protein complexes of the regulatory proteins examined in Chapters II and III. Here we have demonstrated the potential to identify inhibitors based on changes in unfolding thermodynamics and it would be of significant interest to validate this model against a full length, multimeric protein. Although conformational changes associated with allostery can be assessed with atomic resolution when using X-ray crystallography and NMR, there are cases where the conformation of an active and inactive protein show very few structural differences. One of the challenges associated with identification of ligand function is the ability to distinguish differences between the complex with the active modulator and the non-allosteric analogue. This was also observed experimentally, as shown in Chapter III by the PCA grouping of the weak competitive antagonists with the native and native-like modulators. Here, quantification of the free energy associated with allosteric events by dynamic unfolding of the ternary complex (*e.g.* full length Epac associated with its Rap protein target) by DLE-ACE may provide a more useful measurement of allostery since non-obvious structural changes may still have measureable effect on free energy of unfolding. Evaluation of changes at the ternary level, where conformational changes can propagate through other domains or subunits, may

yield additional information that may prove useful for identification of potential drug leads against allosterically regulated proteins and enzymes.

In order to advance DLE-ACE, careful selection of model systems will be necessary for step-wise validation of this technique. The technique should be first validated against a full length protein to ensure that changes observed for small allosteric domains are indicative of global changes on the whole protein. Progression to a multi-domain system will also require further validation against traditional biochemical assays and careful selection of the unfolding model to validate the absence of (or account for) partially unfolded intermediates. It would be of further value to develop or apply an allosteric cycle to describe the thermodynamic processes involved in regulation. Hilser and Thompson[15] describe a model used to quantify the free energy associate with site-to-site allosteric coupling. This model utilizes the unfolding free energy of the individual domains with and without the presence of substrate/modulator ($\Delta G_U +$ $\Delta G_{interaction}$) to evaluate the contribution of coupling energy. The results from theoretical modeling indicated that site-to-site coupling is not necessarily propagated by a physical mechanism, but by the overall free energy of the protein. Using a model protein with two-site allostery, it would be interesting to experimentally dissect the free energy of binding, unfolding and allostery. Success in this endeavour would aid in the fundamental understanding of allosteric regulation, which could further applied to more complex protein-protein or protein-DNA interactions.

6.2. Future Directions for Screening by CE

6.2.1 On-Column Enzyme Kinetics: Screening Cytochrome P450

Cytochrome P450 (CYP) enzymes are important for both metabolism and biosynthesis in many organisms ranging from bacteria to mammals.[17, 18] CYP enzymes are also important in the detoxification and metabolism of many drugs and environmental pollutants.[19, 20] The major role for CYP enzymes is to metabolize non-polar compounds by incorporation of a single oxygen atom from O_2 according to the following general scheme:

$$RH + NADPH + H^+ + O_2 \rightarrow ROH + NADP^+ + H_2O \qquad (6\text{-}1)$$
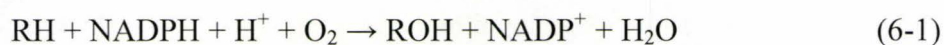
where the site of action on the RH substrate can range from aliphatic, double-bonded, aromatic carbons, heteroatoms, or a variety of functional groups such as esters, halides, nitro- and azo-groups.

Our CE platform developed for characterizing enzyme kinetics for HyPRE can be also applied to assess CYP activity while avoiding the need for synthetic substrates and probes. Conventional activity assays often involve monitoring the conversion of substrate to product using substrates that have been modified with chromophores, fluorophores or radiolabels. The most common fluorescent assay involves the detection of fluorescent end-products from resorufin, coumarin and/or fluorescein-based substrates in the presence of active enzyme similar to assays done by Uno et al.[21] Thus, for each compound for which activity is to be tested, a separate labelled analogue must be synthesized. This becomes costly since fluorogenic analogues are not available for all desired test substrates. The

development of a label-free method for CYP characterization will be realized based on the separation of membrane-bound enzyme, substrates/products and cofactors used in the assay by CE with UV detection based on the amount of NADH consumed and/or NAD^+ formed during the reaction. Freedom from use of fluorogenic substrates not only reduces the cost of performing the assay, but also removes bias associated with modified substrates since the bulky organic fluorophore can often lead to decreased binding and thereby an apparent decrease in enzyme activity. In addition, CE will also enable the characterization of CYP-active substrates based on the separation of various oxidized product(s) formed that is useful in predicting the impact of detoxification (*e.g.,* estradiol/drug metabolites).

Within the context of high-quality screening, the P450 family represents a class of enzymes that can metabolize xenobiotics, which affects the lifetime, bioavailability and activity of drugs.[22] In addition, it is desirable to know the biological fate of new drugs with respect to toxicity and potential drug interactions. It is therefore envisioned that use of a label-free CE-based method for screening potential CYP substrates would be highly advantageous in determining pharmacokinetics and pharmacodynamics of new potential drugs. This platform can also be used for fundamental studies of CYP enzymes where the range of metabolic substrates is still unknown such as with zebrafish species which possess unique CYP enzymes not found in other mammals. Within this context, the study of CYP enzymes is important in understanding the role the

aquatic organisms may play in the fate of many environmental pollutants such as polycyclic aromatic hydrocarbons. By studying the metabolism of such pollutants, the relation to biodegradations or conversely carcinogenesis can be better understood.

6.2.2. Pharmaceutical Chaperones

Enzyme enhancement therapy is a new therapeutic strategy based on improving the residual activity of mutant enzymes associated with inborn errors of metabolism (e.g., lysosomal storage disorders) through small molecules that bind and stabilize misfolded proteins. One direction, that is currently being pursued in our laboratory based on advances developed in this thesis, it is directed towards screening for allosteric modulators that serve as pharmaceutical chaperones. The target of this work has been the lysosomal enzyme β-glucosylceramidase (β-GC). Inherited mutations of this enzyme can result in cytosolic misfolding and proteolysis with reduced overall activity causing a severe accumulation of the substrate glucosylceramide which is associated with Gaucher's disease.[23-25] Preliminary kinetic characterization of putative active modulators identified by HTS has already identified the mechanism of a recently identified mixed inhibitor, bromhexine as shown in **Figure 6.1**. Further characterization will be undertaken to evaluate the both the thermodynamics and kinetics of drug interactions at both lysosomal and cytosolic pH values.
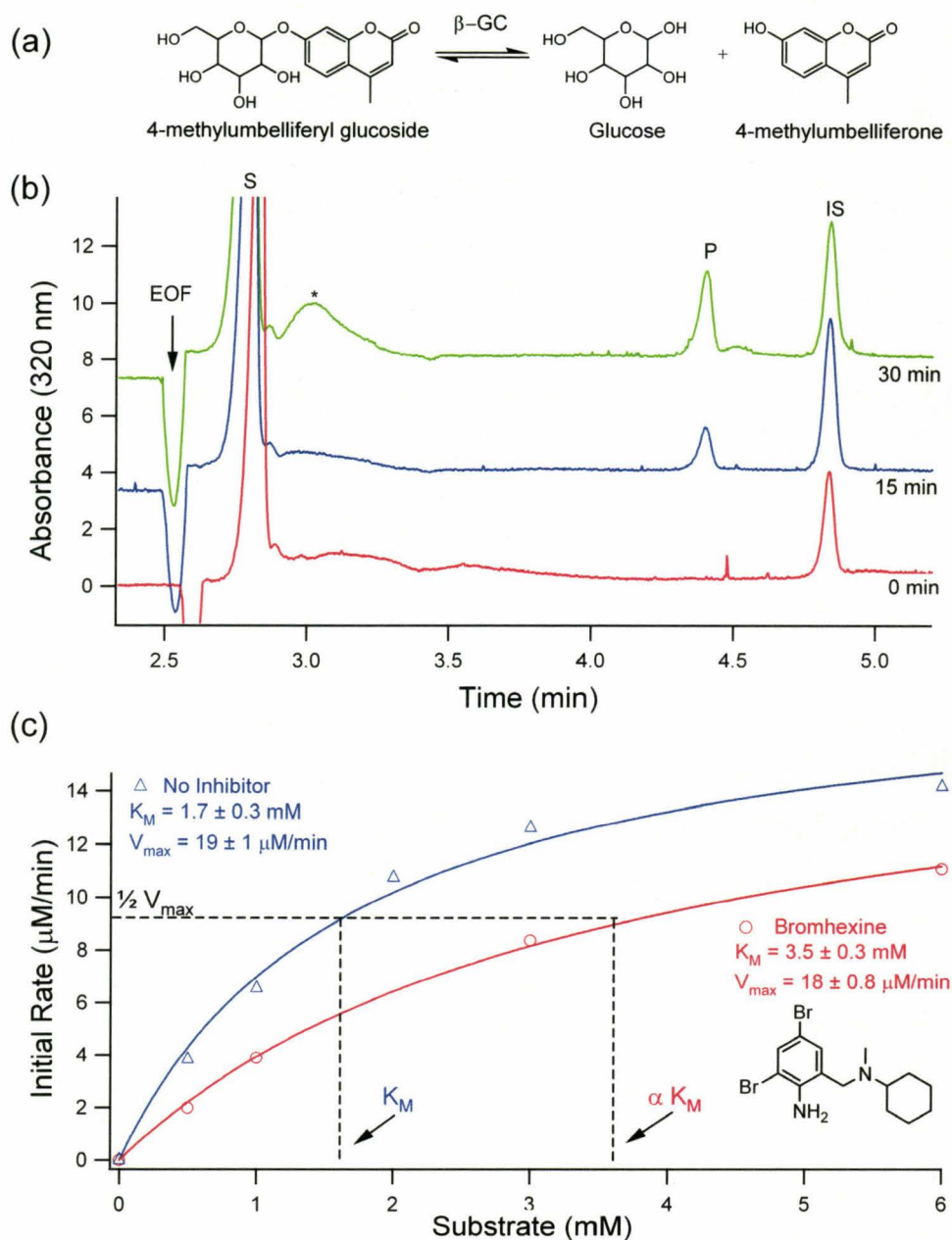
Figure 6.1. Enzyme kinetic studies of 25 nM β-glucoceramidase (β-GC) by CE. (a) Catalysis of methylumbelliferyl glucoside by β-GC. (b) Series of electropherograms depicting quantification of micromolar levels of product from 3mM 4-methylumbelliferyl β-D-glucoside as substrate as a function of time. (c) Non-linear regression of Michaelis-Menten kinetics highlighting inhibition of β-GC by 10 μM bromhexine. Assay Conditions: 0.1 M citrate, 0.2 M phosphate at pH 5.2 in 10 mM taurocholate assay buffer; 24.6 nM β-GC; 37°C; substrate initiated; samples quenched via heat (30 min at 90°C). CE Conditions: 150 mM borate pH 9.5 background electrolyte; injection, 50 mbar for 3.0 s; pressure assisted separation, 10 kV, 20 mbar; UV detection, 320 nm; capillary inner diameter, 50 μm; effective length, 30 cm; length to detector, 24.5 cm. * denotes noise associated with substrate hydrolysis over time.

Ultimately, the application of the developed CE methodology will aid in successful identification of allosteric modulators. These modulators can then serve as effective pharmaceutical chaperones for correcting misfolded proteins to ensure transport of the intact enzyme to its proper lysosomal compartment, while avoiding detrimental orthosteric competitive inhibition effects.[26]

6.2.3. Whole Cell Screening

In addition to screening proteins and enzymes for small effector molecules, a more holistic approach would be to extend the approaches developed in this thesis to the screening of intact cells. Development of whole cell screening methodologies based on CE would extend the *in-vitro* ligand screening methods for evaluation of the activity of a ligand *in-vivo*. Previous whole cell assays by CE have been driven by the need to rapidly detect and identify pathogenic bacteria. Modern CE-based methodologies involve the use of coated-capillaries[27] or polymer additives such as polyethylene oxide (PEO)[28, 29] and sodium alginate[30] as well as various methods of detection involving native chromophores, chemical labelling and complexation with optically active agents. Whole cell CE can be used to evaluate changes on a global level in response to model therapeutic ligands. Fundamental studies could potentially contribute to understanding of metabolic processes involved by bacterial drug uptake, since the native fluorescent properties of most cells are due predominantly due to metabolic co-factors such as flavins, NADH and NADPH. Also, direct susceptibility assays are

potentially possible by means of a CE approach by coupling LIVE/DEAD staining (Molecular Probes) and LIF, a method previously used by Armstrong,[29, 31] or can be accomplished by off-line plating of collected bacteria. This can then be used to screen cells for the effect of stressors, such as antibiotics or bactericidal agents, which can be evaluated by addition of the chemical stressor to the BGE or with online pre-incubation.

The advantages in applying this integrated approach to high-content drug screening is that sample handling would be reduced thereby improving assay reproducibility and automation, which will allow for pharmacokinetic properties to be assessed earlier in the screening process with model cell lines. Changes in the cell surface charge as a function of growth phase may affect the rate at which antibiotics are uptaken by bacteria. Conversely, uptake of an antibiotic may cause cellular changes that lead to a change in its surface or cell lysis which can be detected by CE as shown schematically in **Figure 6.2**. In addition, experiments can be performed to monitor the dynamics of ligand-binding to receptors on the cell surface.[32] Such studies would allow characterization of receptors in their native environments, thus eliminating difficulties associated with recombinant expression. It is envisioned that future studies could use DLE-ACE to screen for allosteric ligands and its net effect on the cell is evaluated by examining changes on the cell surface using fluorescent biomarkers by whole cell CE. The development of a sensitive and reproducible method to characterize
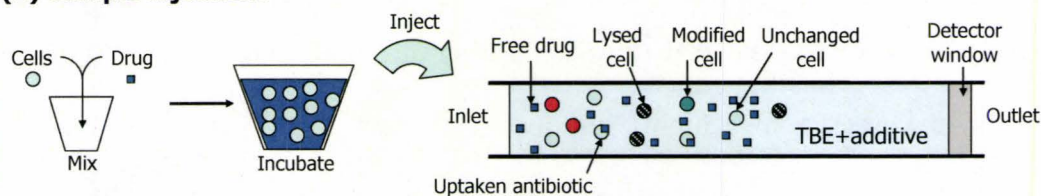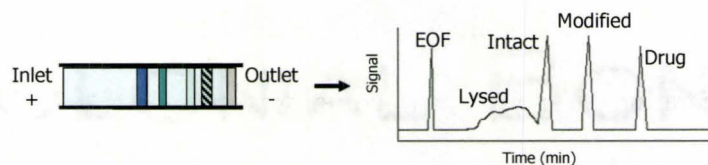
(A) Sample injection:

(B) Separation:

Figure 6.2. Schematic representation of the effect of a drug on bacterial cells as analysed by CE. (a) Cells are pre-mixed with drug and injected onto the capillary. TBE represents the Tris-Borate-EDTA BGE. (b) Zonal separation allows cells that are lysed or modified by the drug can be detected by CE. In addition the concentration of free drug and unmodified cells will also be detected allowing for quantification of uptake and drug lysis efficacy.

whole cells provides a better understanding of cell status under varying conditions and will provide a new method of studying the drug impact on a whole cell level. This is particularly relevant to high-content screening as it provides a label-free platform which can be used to determine the cellular impact of drug candidates without requiring the use of genetically modified cells expressing fluorescent or luminescent reporter genes. Thus a whole cell CE platform could potentially open high-quality screens to a wider variety of cellular targets.

6.3. Concluding Remarks

Research goals within this thesis have been focused on developing innovative methodols using CE as a unified platform for characterizing protein-small molecule interactions for high-quality screening. Initial work studied the

conformational and thermodynamic effect of binding of ligands to proteins and receptors. This was expanded from a construct of the regulatory subunit type Iα of protein kinase A to a highly allosteric construct of another cAMP-binding protein, Epac1. The ligand-induced increase in conformational stability was measured by novel methodology which incorporated preparation of the *apo*-protein, generation of new ligand-complexes using DLE-ACE and dynamic protein unfolding. In addition, a multivariate model for prediction of dissociation constants from unfolding thermodynamics was generated for EPAC1 based on a training set of cAMP-analogues. The significance of these projects include an improved approach to protein unfolding which allowed accurate prediction of dissociation constant and overcame some of the limitations of non-ideal conditions in a label-free manner. These new protocols permitted characterization of modulator-regulatory protein binding interactions and represent innovative tools for studying allosteric modulation. Some of the caveats to the developed methodologies such as limited study of small, two-state systems and the requirement of prior knowledge of modulator behaviour (Chapter II and III), were addressed in the studies with 4-hydroxyproline-2-epimerase (Chapter IV and V). Methodology developed for kinetic characterization demonstrated the versatility of CE for unbiased, sensitive quantitation as well as resolution of structural isomers and enantiomers. The ability to independently evaluate the activity of a small molecule against an enzyme target alleviates the reliance on cell-based assays, such as those which have been published for EPAC1. Use of the CE-

based platform offered improved detection over polarimetry-based assays and also removed the bias associated with the coupled-enzyme assays previously used to evaluate epimerase activity. Thermodynamic evaluation of HyPRE enzyme mutants demonstrated that dynamic protein unfolding by CE is a convenient platform for fundamental assessment of conformation, enzyme kinetics and catalysis. These studies contributed new understanding to the importance and contribution of Cys90 and Cys253 to catalytic function and conformational changes as well as highlighted similarities between HyPRE from two bacterial species. In summary, the methods discussed in this thesis represent new protocol that have the potential to make significant contributions to drug discovery. Analytical methods which integrate sample pre-treatment with chemical analysis were emphasized to encompass evaluation of binding affinity, stereoselective resolution of amino acid isomers for assessment of kinetic activity and determination of conformational stability for *apo/holo*-complexes and mutant proteins. The work in this thesis has demonstrated that screening, characterization and validation of potential therapeutics can be accomplished by using a CE platform. Nonetheless, application of these protocols towards drug development will require movement to a higher throughput platform which can be successfully accomplished by use of multiplexed CE instrumentation (*e.g.* 96 capillary array system). With the growing interest in microfluidic platforms, particularly for micro total analysis systems (μ-TAS), it is perhaps more probable that the principles and philosophies presented in this thesis will be suitable for integration

in a microchip CE format for future drug screening of biologically relevant targets.

6.10. References

1. Bell, L. N.; Hageman, M. J.; Muraoka, L. M., *J. Pharm. Sci.* **1995**, *84*, 707.

2. Garcia-Manyes, S.; Dougan, L.; Fernandez, J. M., *PNAS* **2009**, *106*, 10540.

3. Liu, Y. F.; Bolen, D. W., *Biochemistry* **1995**, *34*, 12884.

4. Galvez, A. S.; Ulloa, J. A.; Chiong, M.; Criollo, A.; Eisner, V.; Barros, L. F.; Lavandero, S., *J. Biol. Chem.* **2003**, *278*, 38484.

5. Talibart, R.; BJebbar, M.; Gouffi, K.; Pichereeau, V.; Gouesbet, G.; Blanco, C.; Bernard, T.; Pocard, J., *Appl. Environ. Microbiol.* **1997**, *63*, 4657.

6. Zhou, A.; Wei, Z.; Read, R. J.; Carrell, R. W., *PNAS* **2006**, *103*, 13321.

7. Diamandis, E. P.; Christopoulos, T. K., *Clin. Chem.* **1991**, *37*, 625.

8. Wolf, B., *J. Nutr. Biochem.* **2005**, *16*, 441.

9. Gonzalez, M.; Bagatolli, L. A.; Echabe, I.; Arrondo, J. L. R.; Argarana, C. E.; Cantor, C. R.; D. Fidelio, G. D., *J. Bio. Chem.* **1997**, *272*, 11288.

10. DeChancie, J.; Houk, K. N., *JACS* **2009**, *129*, 5419.

11. Kurzban, G. P.; Bayer, E. A.; Wilchek, M.; Horowitz, P. M., *J. Bio. Chem.* **1991**, *266*, 14470.

12.   Laskowski, R. A.; Gerick, F.; Thornton, J. M., *FEBS J.* **2009**, *583*, 1692.

13.   Fenton, A. W., *Trends Biochem. Sci.* **2008,** *33*, 420.

14.   Whitty, A., *Nat. Chem. Biol.* **2008,** *4*, 435.

15.   Hilser, V. J.; Thompson, E. B., *PNAS* **2007,** *104*, 8311.

16.   Wright, P. E.; Dyson, H. J., *Curr. Opin. Struct. Biol.* **2009,** *19*, 31.

17.   Zuber, R.; Anzenbacherova, E.; Anzenbacher, P., *J. Cell. Mol. Med.* **2002,**
        6, 189.

18.   Rewitz, K. F.; Styrishave, B.; Løbner-Olesen, A.; Andersen, O., *Comp.*
        Biochem. Physiol. C **2006,** *143*, 363.

19.   Miranda, C. L.; Chung, W. G.; Wang-Buhler, J.-L.; Musafia-Jeknic, T.;
        Baird, W. M.; Buhler, D. R., *Aquat. Toxicol.* **2006,** *80*, 101.

20.   Li, A. P.; Maurel, P.; Gomez-Lechon, M. J.; Cheng, L. C.; Jurima-Romet,
        M., *Chem. Biol. Interact.* **1997,** *107*, 5.

21.   Uno, T.; Okamoto, S.; Masuda, S.; Imaishi, H.; Nakamura, M.; Kanamaru,
        K.; Yamagata, H.; El-Kay, M. A. H.; Kaminishi, Y.; Itakura, T., *Comp.*
        Biochem. Physiol. A **2008,** *147*, 178.

22.   Harvey, R. A.; Champe, P. C., *Lippincott's Illustrated Reviews*
        Pharmacology. 3 ed.; Lippincott Williams & Wilkins: Baltimore, 2006.

23.   Beutler, E., *New England Journal of Medicine* **1991,** *325*, 1354.

24.   Kacher, Y.; Brumshtein, B.; Boldin-Adamsky, S.; Toker, L.; Shainskaya,
        A.; Silman, I.; Sussman, J. L.; Futerman, A. H., *Biological Chemistry*
        2008, *389*, 1361.

25.   Sawkar, A. R.; D'Haeze, W.; Kelly, J. W., *Cellular and Molecular Life Sciences* **2006,** *63*, 1179.

26.   Fan, J. Q., *Trends in Pharmacological Sciences* **2003,** *24*, 355.

27.   Szumski, M.; Klodzinska, E.; Buszewski, B., *Journal of Chromatography A* **2005,** *1084*, 186.

28.   Armstrong, D. W.; Schulte, G.; Schneiderheinze, J. M.; Westenberg, D. J., *Analytical Chemistry* **1999,** *71*, 5465.

29.   Desai, M. J.; Armstrong, D. W., *Microbiology and Molecular Biology Reviews* **2003,** *67*, 38.

30.   Shintani, T.; Yamada, K.; Torimura, M., *Fems Microbiology Letters* **2002,** *210*, 245.

31.   He, L. F.; Jepsen, R. J.; Evans, L. E.; Armstrong, D. W., *Analytical Chemistry* **2003,** *75*, 825.

32.   Berthod, A.; Rodriguez, M.; Armstrong, D. W., *Electrophoresis* **2002,** *23*, 847.